Turbulence and Heat Exchange under Ice

Cand. Scient. Thesis

in

Physical Oceanography

Anders Sirevaag

Geophysical Institute, University of Bergen

UNIS, University Centre on Svalbard

November 17th, 2003

Abstract

Turbulent fluxes of heat and salt were measured under sea ice at four different locations around Spitsbergen. In Kongsfjorden on West Spitsbergen additional measurements of heat fluxes in the ice and in the atmosphere were done and compared in an air/sea/ice heat budget. Ocean heat flux in Kongsfjorden is about 13 W/m^2 and comparison with the other heat fluxes at the ice/ocean interface shows a good agreement. From the heat budget at the ice/ocean interface, the ice growth during three subsequent days in March is calculated to be 4.4 cm. During the same three days the ice growth was measured to be 3.5 cm. The conductive heat flux in the ice is determined by the temperature gradient and the thermal conductivity of sea ice and the ice temperature is calculated from the measured convergence/divergence of conductive heat and absorption of short wave radiation. When the calculated ice temperature in Kongsfjorden is compared with the measured temperature, it shows that the best agreement occurs with a slight reduction of the thermal conductivity of sea ice ($\sim 10 - 15\%$).

Turbulent fluxes of heat are also measured in Van Mijenfjorden and in outer parts of Storfjorden. At both locations there are only small amounts of heat in the water column and measured heat fluxes are of order 1 W/m^2. Correspondingly, the turbulent fluxes of salt are small and of order -10^{-6} psu m/s, indicating small ice growth rates.

In the so called Whaler's Bay area north of Spitsbergen, the influence of the West Spitsbergen Current (WSC) is large. The WSC brings relatively warm water along the continental slope of Spitsbergen, resulting in large amounts of heat in the water column. In this area, heat fluxes of order 210 W/m^2 were measured 1 m below the ice. Comparison with the conductive heat flux in the ice indicates melting rates of order 5 cm/day. Also the measured turbulent salinity flux in this area shows large rates of melting, about 3.5 cm/day.

For all locations, a turbulent exchange coefficient for heat, the turbulent Stanton number, is calculated and the resulting Stanton numbers are in the range 0.006 – 0.007 for the locations Kongsfjorden, Van Mijenfjorden and Whaler's Bay.

Preface

The process of writing a thesis can often be tedious, frustrating and time-consuming. But for me, the number of highlights in this process has been closely linked to the amount of time spent at outdoor field work. So, thanks to my supervisor, Peter M. Haugan for including me in this project and for always providing valuable support and feedback. I am also very grateful to Miles McPhee for shearing his enthusiasm and knowledge, and most of all for including me in the WARPS project.

Also thanks to Frank Nilsen at UNIS for all practical help in Longyearbyen, to Tor-Villy Kangas and his experience in the Kongsfjorden work, to Dirk Notz and Grae Worster for providing ice core data and to all members of oceanographic group on the WARPS cruise who helped me fighting the ice.

Many thanks to the students at Geophysical Institute for helping me focussing on other things than this thesis and finally, thanks to Carita for being supportive and understanding throughout the last two years!

Anders Sirevaag
Bergen, November 17th, 2003

Contents

1 Introduction

In polar regions the ocean is a considerable source of heat and the interaction between ocean and atmosphere is an important part of the global climate system. In these polar regions sea ice often forms a barrier between the ocean and the atmosphere, blocking for direct exchange of heat. The role of this sea ice in heat budgets in polar regions is vital and has been subject of many studies (e.g. Maykut and Untersteiner, 1971; Doronin and Kheisin, 1977; Maykut, 1986; Ebert and Curry, 1993; Wadhams, 2000). Also properties of sea ice, both thermodynamic and dynamic, have been studied in detail in numerous experiments, first of all to understand the processes of the air/sea/ice interaction, but also to investigate the role of the sea ice cover in the climate system. For the last decades numerical modelling has been an important tool for predicting future climate and in this context a well working parameterization of the processes at the ocean/atmosphere interface in coupled numerical models is important.

Ice formation is a result of heat loss at the ocean surface and an existing ice cover acts as a buffer between the ocean and the atmosphere. A divergence/convergence of heat fluxes across the ocean/atmosphere interface results in ice freezing/melting, and for a specific location the equilibrium ice thickness is a balance between the heat fluxes in the ocean and in the air. At the underside of the ice the heat budget has three main components; the ocean heat flux, the conductive heat flux in the ice and a latent heat flux resulting from freezing/melting at the interface. The two last fluxes can easily be measured by monitoring the temperature gradients in the ice and the change in ice thicknesses, but the ocean heat flux is not so simple to measure. For early modelling this ocean heat flux was often assumed to be constant for a given geographical area, e.g. Maykut and Untersteiner (1971) assumed a constant value of 2 W/m^2 throughout the year in Arctic in their classic thermodynamic ice model. Ebert and Curry (1993) modified the same model and found that a value of the ocean heat flux of 1.8 W/m^2 was reasonable. However, the assumption of a constant ocean heat flux is rough, it might be justified as an average value for a large area for a long period of time, but it is clear that this heat flux is dependent on local conditions such as water temperatures and mixing in the water column. A method to estimate the ocean heat flux at a location is by measuring the ice temperatures and thicknesses. The ocean heat flux is then the remaining heat flux in the heat budget at the ice/ocean interface when the conductive heat flux in the ice and the latent heat flux from freezing/melting at the interface, are calculated. This so called residual method

is widely used in estimation of the ocean heat flux. E.g. Wettlaufer (1991) used this method during a drifting experiment in the areas north-east of Spitsbergen and estimated ocean heat fluxes in the range $0 - 37$ W/m^2. This method has also been implemented in numeric models to estimate the ocean heat flux (e.g. Holland *et al.*, 1997). But the method only captures a long term average of the heat flux of the order of days and does not resolve high frequency variations in the ocean heat flux (Omstedt and Wettlaufer, 1992).

The presence of turbulence in a flow affects the mixing processes significantly and the importance of turbulence on e.g. the exchange of heat with other water masses or across any boundary is well known. In earlier studies these turbulent effects have been parameterized by a turbulent exchange coefficient and the temperature gradient close to the boundary. But for the last couple of decades, methods and instruments have been developed for making high resolution measurements of temperature, salinity and three dimensional velocities close to the underside of the ice, in order to calculate turbulent fluxes of heat, salt and momentum. Measuring turbulent properties in the ocean is difficult and it requires a stable platform from which the measurements are performed. In this context sea ice is favourable, offering the possibility of doing these measurements from a stable platform at any location with ice thick enough to carry the equipment. These instrumentations consist of current meters with rapid sampling frequencies combined with fast response thermometers and conductivity sensors and often with the possibility of lowering the instruments to a preferable depth below the ice. This kind of instruments have been used at several different locations, both in the Arctic and Antarctic and from both drifting and land fast ice (e.g. McPhee *et al.*, 1987; McPhee, 1992; Shirasawa and Ingram, 1997; Shirasawa *et al.*, 1997; McPhee *et al.*, 1999). In these works, the methods have turned out to give reliable results compared to other methods for estimating the ocean heat flux. E.g. Shirasawa *et al.* (1997) compared the directly measured heat fluxes and the heat fluxes calculated using the residual method and found the offset to be about 20%. This offset is about the same as the inaccuracy in using the residual method, where uncertainties in measurements of ice growth and ice temperatures result in errors of this magnitude. When direct measurements of turbulent fluxes close to the ice exist, the flux magnitudes can be related to properties of the water masses in order to find a proper parameterization of the fluxes. Such a parameterization is made for the turbulent heat flux, relating it to the temperature of the mixed layer and mixing efficiency at the ice/ocean interface by a turbulent exchange coefficient, the turbulent Stanton number (e.g. McPhee, 1992; McPhee *et al.*, 1999).

The main purpose of this work has been to compare heat fluxes on small time scales and to investigate the air/sea/ice interactions under different conditions. This included use of several different methods in estimating heat fluxes below, in and above the ice, use of turbulent salinity flux in the estimation of the ice growth/melting rate and comparison of Stanton numbers under variable conditions. A special focus has been on the ocean heat flux, including measurement techniques, flux magnitudes and parameterization. The work has been performed in four different areas around Spitsbergen as a part of various projects and the four experimental sites are shown in figure 1.1. The common feature of all projects is the use of so called Turbulent Instrument Clusters (TICs) for measurements of turbulent fluxes close to the underside of the ice.
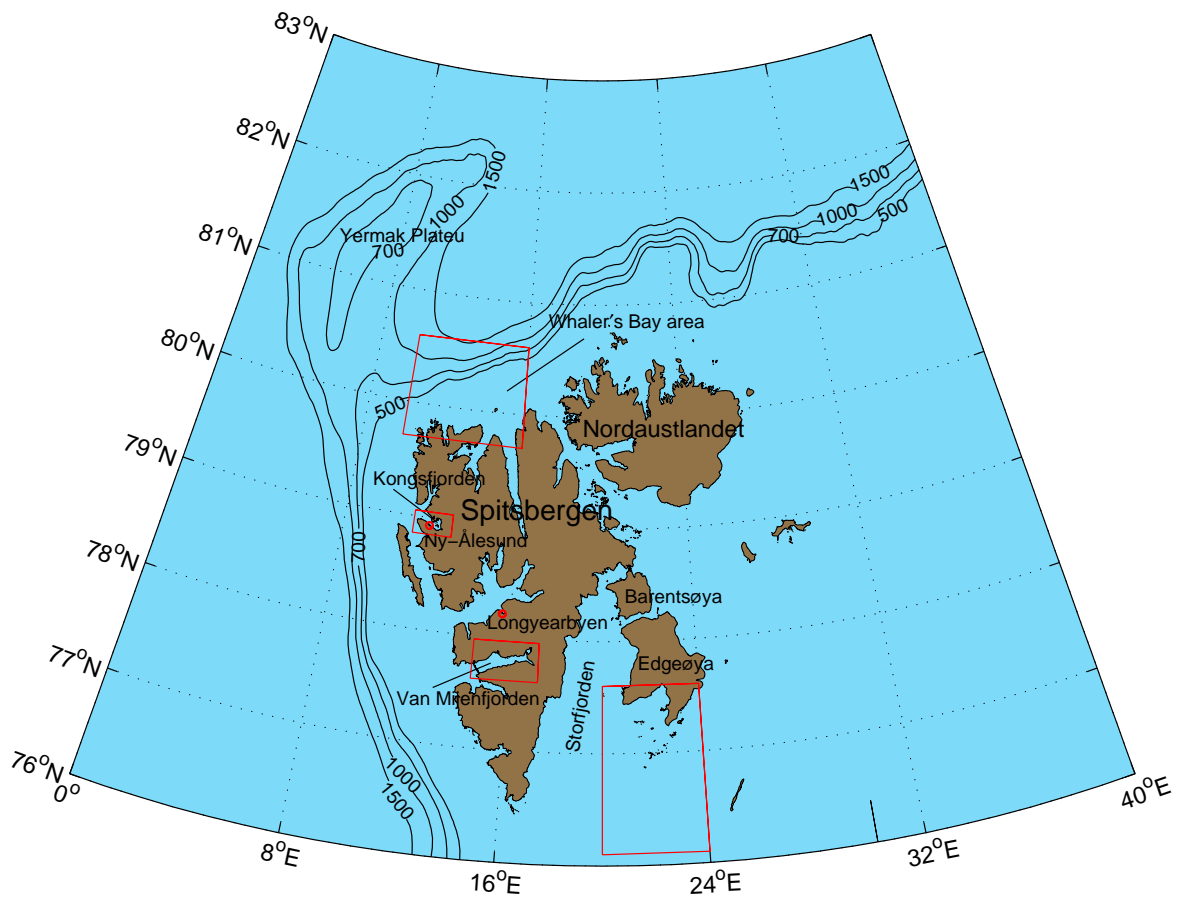

Figure 1.1 Map of Spitsbergen and the nearby areas. Depth contours are plotted to show the bathymetry of the area north-west of Spitsbergen. The four study areas of this thesis, Kongsfjorden, Van Mijenfjorden, outer part of Storfjorden and Whaler's Bay, are shown and the red squares indicate map sections used in later sections.

In winter 2002 field work was performed in Kongsfjorden and Van Mijenfjorden at Spitsbergen. The main focus of this project was small-scale physics of sea ice formation. High resolution measurements of turbulent heat fluxes under the ice and of the ice properties were extended by measurements of main water properties and measurements of atmospheric parameters such as wind, temperature, humidity and radiation. These measurements are used in comprehensive studies of the heat budget for the air/sea/ice system. In winter 2003, the TICs were used on a cruise with the German research ice breaker *FS Polarstern* in the areas around Spitsbergen. The aim of this cruise was to study the physical processes including ocean/atmosphere heat exchange and ice formation in connection with polynya formation in ice covered areas. During this cruise the instruments were used in the outer parts of Storfjorden and in Whaler's Bay (figure 1.1).

This thesis is presented in 7 sections. Section 2 gives a brief introduction to the theory regarding turbulence, properties of sea ice and air/sea/ice heat exchange. The results and discussions of the data from the different field work areas are then presented according to geographic location. This makes it easier to compare the heat fluxes at each location and to discuss the heat budget according to local conditions. The instrumental set up is also slightly different at each experimental site. In section 3 the results from Kongsfjorden are presented and discussed and in section 4 results and discussions from Van Mijenfjorden are presented. The data from the cruise in Storfjorden and Whaler's Bay are presented and discussed in section 5. Summary and conclusions are in section 6 and in the appendix, section 7, the eddy correlation method is described.

2 Theory

2.1 Turbulence

2.1.1 Turbulent flows

Although *turbulence* is an accepted notation used in several different situations, it is not easy to give a precise definition of turbulence. In 1937 Von Kármán and Taylor gave the following definition: "Turbulence is an irregular motion which in general make its appearance in fluids, gaseous or liquid, when they flow past solid surfaces or even when neighbouring streams of the same fluid flow past or over one another." (Hinze, 1959). Instead of trying to give a mathematical deterministic description of turbulence, a list of characteristic properties of a turbulent flow is helpful to identify such a flow (Hinze, 1959; Tennekes and Lumley, 1972; McPhee, 1990; Gade, 1996).

- Turbulent flows are always dissipative. Turbulent movement increases the internal energy on the expense of kinetic energy.
- Turbulence causes rapid mixing and increased transfer rates of e.g. salt, heat and momentum. This diffusivity is one of the most important features of turbulence and also a reason why turbulent processes are so important for example when it comes to the heat budget at an ice/ocean interface.
- A flow that is characterized as turbulent is always highly rotational in three dimensions.
- The movements are irregular and completely random, the process is stochastic.
- Turbulent properties are properties of the flow, not the fluid.
- Turbulence usually occurs in flows with a high Reynolds number, the Reynolds number is defined as $Re = \dfrac{u \cdot L}{\upsilon}$ where u is a characteristic velocity, L is a characteristic length and υ is the kinematic viscosity (Tennekes and Lumley, 1972). For flows in pipes or channels, turbulence can exist if the flow has a Reynolds number higher than 2000.

If a flow has quantitatively the same structure in all parts of the flow field, it is called *homogeneous* (Hinze, 1959) and if all moments (see definition in section below) of a turbulent

velocity are independent of time, the turbulence is said to be *stationary*. An *isotropic* turbulence is turbulence with no preferred direction, e.g. the statistical properties are of the same magnitude, independent of direction (Hinze, 1959).

The fact that a flow is irregular and random makes a deterministic approach to the turbulent problem quite difficult and it is easier to describe the process with statistical methods.

2.1.2 Statistical properties of a turbulent flow

In the following some statistical properties of a given scalar flow property is given.

The ensemble mean of the property, here a horizontal velocity component u, is calculated as

$$\langle u(t) \rangle = \frac{1}{N} \sum_{i=1}^{N} u(t)_i \tag{1}$$

which is also recognised as the first moment of the variable u(t). The second moment is

$$\langle u(t)^2 \rangle = \frac{1}{N} \sum_{i=1}^{N} \left(u(t)_i - \overline{u} \right)^2 , \overline{u} \equiv \langle u \rangle \tag{2}$$

also known as the variance of the variable u(t). The square root of the variance is the standard deviation of u(t).

Generally, velocities in a turbulent flow are divided into a mean and a fluctuating part, $u = \overline{u} + u'$, the fluctuating part having $\langle u' \rangle \equiv 0$.

A special property of a variable is the auto covariance, defined as the ensemble mean of the product of a variable and the same variable after a time delay τ.

$$C(\tau) = \langle u(t) \cdot u(t + \tau) \rangle \tag{3}$$

In the expression above the ensemble mean is assumed equal to zero, $\overline{u} = 0$, so u can be substituted by u'.

If C(τ) is Fourier transformed, the resulting expression is the spectral density of a variable u(t).

$$S(f) = \int_{-\infty}^{\infty} C(\tau) e^{i2\pi f\tau} d\tau \tag{4}$$

In the case of the velocity u(t), S(f) is the energy per unit mass as a function of frequency f and it is possible to use S(f) to obtain information at which frequencies the energy is distributed.

A common technique is also to find the auto correlation as a function of wave length, C(λ). The power spectral density is then a function of wave number, defined as $k = \dfrac{2\pi}{\lambda}$, and given as

$$S(k) = \int\limits_{-\infty}^{\infty} C(\lambda)e^{ik\lambda}d\lambda \qquad\qquad (5)$$

2.1.3 Spectral distribution of turbulence

According to Kolmogorov (1941), a turbulence that is stationary, isotropic and homogeneous has energy distributed on all wave numbers, ranging from a minimum limited by the available space and a maximum dependent on the dissipation process (Gade, 1996). Energy is supplied to the flow on relatively small wave numbers as large, energy containing eddies and the dissipation occurs on relatively large wave numbers where the eddies are broken down and the energy is dissipated into heat. The process where large eddies are broken down into smaller and smaller eddies and kinetic energy is transferred from small to large wave numbers, is called the *turbulent cascade*. In stationary turbulence, with energy supply on small and dissipation on large wave numbers, there must be an area where the energy transfer through the wave number spectrum is constant (Kolmogorov, 1941). This area is called the *inertial sub range* and in this area the energy distribution is a function of wave number k and dissipation ε only and given as

$$S(k) = \alpha\varepsilon^{\frac{2}{3}}k^{-\frac{5}{3}} \qquad\qquad (6)$$

α is a dimensionless constant set to 1.5 for three dimensional turbulence (Gade, 1996) and ε is the dissipation of energy in the turbulent eddies.

Taylor's hypothesis

To calculate a reasonable energy spectrum from measurements, it is necessary to measure turbulent properties in a space domain. This is a much more complex experiment than to measure turbulent properties as a time series at a given position. The most common technique is then to invoke Taylor's hypothesis (frozen-turbulence approximation) which concludes that if a turbulent flow is advected past a point with a mean velocity U and this mean velocity is much larger than the turbulent fluctuations u′, then the time series can be transformed to a series of a spatial distribution, $t = \dfrac{x}{U}$. This gives the relation between wave number and

frequency $k = \dfrac{2\pi}{U} f$ and the possibility to find the spectral density as a function of wave number from a time series. If $\dfrac{|U|}{|u'|} >> 1$ (Hinze, 1959) holds and Taylor's hypothesis is accepted, then it is possible to use the calculated spectral density to find a typical time scale (from frequency) and a typical length scale (λ) for the energy containing eddies (e.g. McPhee, 1992).

2.1.4 Turbulent exchange of properties

In a small control volume in a flow, the time development of a scalar property is dependent on any sources/sinks inside the volume and the flux of the scalar property into or out of the volume. The conservation equation for a given scalar property ε is then

$$\frac{\partial \varepsilon}{\partial t} = Q_\varepsilon - \nabla \cdot \vec{F}_\varepsilon \tag{7}$$

where Q_ε is an internal source of ε and F_ε is a flux out of the control volume. F_ε is the sum of an advective term and a diffusive term

$$\vec{F}_\varepsilon = \vec{v}\varepsilon + \eta \nabla \varepsilon \tag{8}$$

where $\vec{v}$ is the velocity and η is a molecular diffusion coefficient. Under natural conditions in the ocean there is usually a background current which makes the advection term considerably larger than molecular diffusion, therefore the approximation

$$\vec{F}_\varepsilon \cong \vec{v}\varepsilon \tag{9}$$

is used. The equation can then be written as

$$\frac{\partial \varepsilon}{\partial t} = Q_\varepsilon - \nabla \cdot \vec{v}\varepsilon \tag{10}$$

All properties are divided into a mean and a fluctuating part e.g. $\vec{v} = \bar{\vec{v}} + \vec{v}'$, defined by $\langle v' \rangle = 0$ and inserted in the equation.

$$\begin{aligned}
\frac{\partial}{\partial t}\left(\bar{\varepsilon} + \varepsilon'\right) &= Q_\varepsilon - \nabla \cdot \left(\bar{\vec{v}} + \vec{v}'\right)\left(\bar{\varepsilon} + \varepsilon'\right) \\
\frac{\partial \bar{\varepsilon}}{\partial t} + \frac{\partial \varepsilon'}{\partial t} &= Q_\varepsilon - \nabla \cdot \left(\bar{\vec{v}}\bar{\varepsilon} + \bar{\vec{v}}\varepsilon' + \vec{v}'\bar{\varepsilon} + \vec{v}'\varepsilon'\right)
\end{aligned} \tag{11}$$

When the mean value of the whole equation is taken and $\bar{\varepsilon}' = \bar{\vec{v}}' = \bar{0}$ is used, the conservation equation is reduced to the expression

$$\frac{\partial \bar{\varepsilon}}{\partial t} = \overline{Q_\varepsilon} - \nabla \cdot \left(\bar{\vec{v}}\bar{\varepsilon} + \overline{\vec{v}'\varepsilon'}\right) \tag{12}$$

The term $\overline{\varepsilon \vec{v}'}$ is called the mean turbulent Reynolds flux. In the rest of the thesis, focus will be on the ice, atmosphere and ocean system and at the ice/ocean interface the vertical fluxes of heat and salt will be of main interest. So in the following, vertical Reynolds fluxes and parameterization of these, will be given special attention.

According to Tennekes and Lumley (1972), the vertical turbulent flux of heat is given as

$$H = \rho c_p \overline{w'T'} \tag{13}$$

where ρ and c_p is the density and specific heat of sea water, respectively, and w' and T' are the fluctuating parts of vertical velocity and temperature. This is the Reynolds flux of heat, but it requires quite complicated instrumentation to measure these heat fluxes directly. Such instrumentation has only been in use from the 80's and later, (e.g. McPhee, 1992; Shirasawa *et al.*, 1997), parameterization for estimating turbulent fluxes from the properties of the mean flow has therefore always been necessary.

The mixing length theory, proposed by Prandtl in 1925, suggest that the vertical flux of a scalar property ε is dependent on three factors; A vertical gradient of ε, a characteristic velocity of the turbulent eddies, u_ε, and a typical length scale of the turbulent eddies, λ. (e.g. Hinze, 1959; Tennekes and Lumley, 1972; McPhee, 1990)

$$F_\varepsilon = -k u_\varepsilon \lambda \frac{\partial \varepsilon}{\partial z} \tag{14}$$

where k is the Von Kármán constant. And as an analogy to the kinetic theory of an ideal gas, an eddy viscosity for the property ε, dependent on the characteristic velocity and length, is defined as

$$K_\varepsilon = k u_\varepsilon \lambda \tag{15}$$

This creates a parameterization for the vertical flux of ε

$$F_\varepsilon = -K_\varepsilon \frac{\partial \varepsilon}{\partial z} \tag{16}$$

which is an often used parameterization of turbulent heat flux (e.g. Maykut and Untersteiner, 1971). In case of the turbulent heat flux, the parameterization is given

$$H = -\rho c_p K_H \frac{\partial T}{\partial z} \tag{17}$$

This relates the vertical heat fluxes to the mean properties of the flow, represented by the vertical temperature gradient and the turbulent properties of the flow included in the eddy diffusivity.

When water is flowing along an ice boundary, heat flux towards the ice/ocean boundary will as a first approximation be dependent on the available heat in the surrounding water masses, normally in the mixed layer, and the mixing efficiency at the boundary. The available heat can be given as $\delta T = T_{ml} - T_f(S_{ml})$ where T_{ml} is the mixed layer temperature and T_f is the freezing temperature of the mixed layer with salinity S_{ml}. Mixing efficiency can be indicated by u_{*0}, the friction velocity at the ice/ocean interface, and this characteristic velocity is given as

$$u_{*0} = \left(\langle u'w' \rangle_0^2 + \langle v'w' \rangle_0^2 \right)^{1/4} \tag{18}$$

where u', v' and w' represent the turbulent velocity components in a three dimensional coordinate system. The vertical heat flux is then given as

$$H = \rho c_p c_H u_{*0} \delta T \tag{19}$$

where c_H is a turbulent exchange coefficient for heat, the turbulent Stanton number.

Usually, when the flow is along a smooth wall, molecular effects in a thin layer close to the boundary are important when it comes to exchange of properties. But if the wall is rough and the flow is fully turbulent, such molecular effects are usually ignored. This transition between a smooth and rough flow under ice is assumed to appear at low turbulent Reynolds numbers, $Re_* < 100$ (McPhee, 1987).

$$Re_* = \frac{u_{*0}h}{\upsilon} \tag{20}$$

In this calculation of the Reynolds number the thickness of the transition layer is used as a length scale, $h=30z_0$, where z_0 is a characteristic size of the roughness elements under the ice and υ is the eddy viscosity.

A comprehensive laboratory study by Yaglom and Kader (1974) attempted to show the importance of these effects in turbulent transfer also across a rough boundary and to incorporate these in the Stanton number. This study was followed up by McPhee (1987), also finding a Stanton number dependent on molecular effects in the viscous boundary layer

$$c_H \propto Re_*^{-1/2} Pr^{-2/3} \tag{21}$$

Pr is the Prandtl number defined as $Pr = \dfrac{\upsilon}{\upsilon_T}$, where υ is the molecular viscosity and υ_T is the molecular diffusivity for heat. Typical values of υ and υ_T are 10^{-6} m^2/s and 10^{-7} m^2/s, respectively, which indicate a Prandtl number of order 10. But, comparisons of these expressions with measured data from several ice drift experiments, suggest that the Reynolds number dependency is not as strong as suggested earlier, it is more likely that the Stanton

number is more or less constant, even under different under ice roughness conditions (McPhee *et al.*, 1999) (figure 2.1).
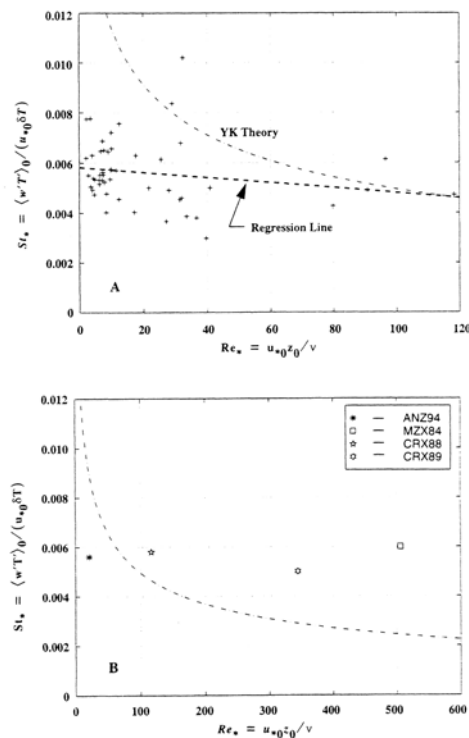

Figure 2.1 (A) Stanton numbers plotted versus turbulent Reynolds numbers from data obtained during two drift periods during the ANZFLUX experiment (McPhee *et al.*, 1996). The dashed curve labelled "YK Theory" is the Stanton number calculated from the theory of Yaglom and Kader (1974). (B) Average Stanton numbers from four different drifting experiments, dashed curve is the "YK Theory" curve from (A). Figure from McPhee *et al.* (1999).

2.2   Sea ice

2.2.1   Sea ice formation

Sea ice is formed as a reaction to cooling of sea water. When sea water at its freezing temperature is cooled further, it solidifies and usually forms a solid boundary between water and air. The freezing temperature of sea water is almost linearly dependent on its salinity content and for sea water with a salinity of 35 psu (practical salinity units) the freezing temperature is approximately -1.9°C. The temperature of maximum density of sea water is

also decreasing according to increasing sea water salinity and for salinities higher than 24.7 psu the temperature of maximum density is lower than the freezing temperature (Ono, 1965).

After lowering the sea water temperature to the freezing temperature, ice crystals start to form in the water column and these crystals grow into tiny horizontal discs with a typical diameter of 2 – 3 mm. Growing larger than this, the ice crystals get unstable and start forming crystals with a hexagonal form. These crystals are very fragile and all movements at the ocean surface tends to break them and leave a mixture of discs and arm fragments, also called *frazil ice* or grease ice (Weeks and Ackley, 1986).

These frazil crystals/fragments soon freeze together and form a continuous sheet of thin ice only a few centimetres thick and fully transparent, called *dark nilas*. Continuous thickening and growth of this ice sheet is done by so called congelation growth which means that ice crystals form on the underside of the existing ice sheet. This process gives the ice at first a grey and after a while a white look, a type of ice called *grey nilas*.

The ice crystals have a three dimensional shape and three axes, a, b and c, can be defined. a and b are the axes in the basal plane, while the c axis is the vertical axis perpendicular to the basal plane. Because of the molecular structure of ice, new ice crystals form more easily in the basal plane than along the c-axis (Wadhams, 2000). This means that when sea ice forms in open, calm waters, ice crystals grow in the basal plane with the c-axis vertical. After the formation of the thin layer of dark or grey nilas continuous congelation growth downward will "favourize" crystals with the basal plane oriented vertical. Because of this, it is possible to find a transition layer of 10-20 cm where the structure is shifting from a horizontal orientation of the crystals close to the surface to a more vertical, platelet structure below the transition layer.

It is common to distinguish between two types of sea ice, first year ice and multi year ice. The first one is formed mostly during autumn and winter and melts again during spring or summer. Multi year ice is per definition ice that has survived one summer season and is a typical kind of ice to find e.g. in the central Arctic.

2.2.2   Brine

When sea water is freezing, sea ice with a much lower salinity than in the sea water is formed. The main reason that there is salt in sea ice at all is the open platelet structure of growing ice. Sea ice rejects salt as it grows, leading to columns of very high salinity in between the platelets. These columns, containing water with a high concentration of salt, are closed at the

bottom by growing "ice bridges". The highly saline water, called *brine*, can exist in the interior of sea ice with high concentration of salt preventing freezing at the boundaries. A typical size of these brine cells is 0.5 mm in diameter.

Brine cells encapsulated in the ice are responsible for the salinity of sea ice and a typical salinity for newly formed ice is about 10 psu. In figure 2.2a salinities from an ice core obtained in Kongsfjorden are shown together with the ice temperatures measured at the same time. This shows the typical salinity structure of first year ice, with "high" salinities at the top and at the bottom (e.g. Perovich *et al.*, 1998).
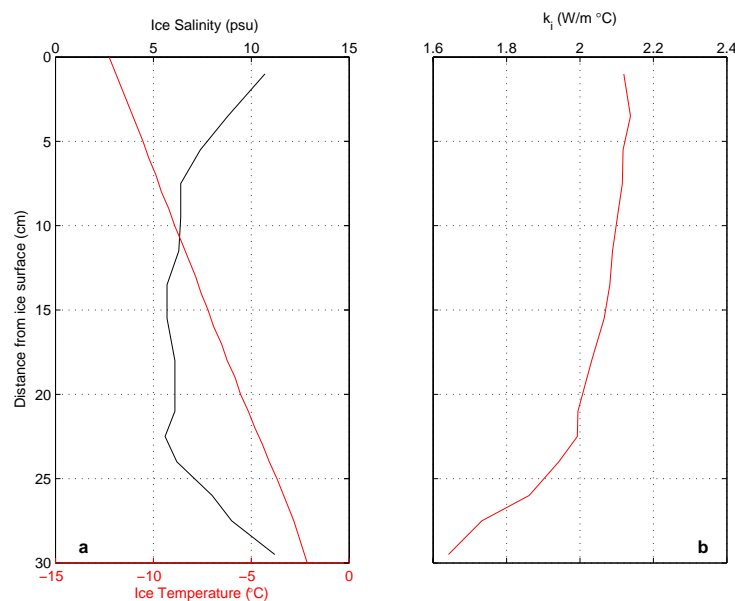

Figure 2.2 (a) Salinity of sea ice measured in an ice core in Kongsfjorden. The temperature profile is from thermistor data at the same time as the ice core was taken. (b) Thermal conductivity of sea ice, calculated using equation 22 and values of temperature and salinity in (a).

During ice growth the ice thickness reaches a critical value where the brine starts to drain from the ice. The most dominant mechanism responsible for this behaviour is believed to be gravity drainage, a mechanism based on the brine cells being a part of an interconnected system of fine pores. When the ice is growing thicker and the brine cells are lifted above the sea surface level, there will be a pressure force on the brine, forcing it to drain through the system of channels. Due to the negative temperature gradient in the ice in winter, an unstable density gradient exists in the brine cells in the whole ice column, forcing downward drainage of brine in the ice (Wadhams, 2000). The impact of brine cell migration on the heat conduction in the ice is discussed by McGuinness *et al.* (1998).

2.2.3 Thermodynamic properties of sea ice

In winter, sea ice normally forms the border between a relatively warm ocean and a cold atmosphere. This makes sea ice and the thermodynamic properties of sea ice the largest limitation in heat exchange between ocean and atmosphere.

Sea ice normally consists of four components; pure ice, brine, air bubbles and solid salt. The thermodynamic properties of sea ice are therefore dependent on the ratio of the different factors and the properties of every component. For example, heat conduction in air is much less than in pure ice, so a large air bubble content will result in lower capacity of heat transport in sea ice. Brine content is also important. Since brine has a high salinity it will always have a lower freezing temperature than the surrounding ice. This means that when the surrounding ice temperature is decreasing, some of the brine will freeze, release heat to the brine and give the remaining brine a higher salinity and even lower freezing temperature. If the temperature is rising, heat from the brine is used to melt some of the surrounding ice and the remaining brine will have a lower salinity, but still high enough to avoid freezing. This process leaves brine as a kind of thermal reservoir, reducing the internal cooling or heating of the ice (Wadhams, 2000).

In the following sections a brief introduction to the most important properties of sea ice regarding heat transport will be given.

Thermal conductivity

In sea ice there is usually a temperature gradient due to a temperature difference between ocean and atmosphere. This leads to a flux of conductive heat toward the area with lowest temperature. This heat flux is dependent on the ability of the ice to conduct heat; the thermal conductivity of sea ice. Thermal conductivity is given by Untersteiner (1961) as

$$k_i = k_0 + \beta \frac{S_i}{T_i} \tag{22}$$

where k_i is the thermal conductivity (W/m°K), k_0 is the conductivity of pure ice, T_i is the ice temperature in °C, S_i is the salinity of the ice (psu) and β is a constant given as 0.13 W/m. This is a rough approximation because k_i also is dependent on the air bubble content, as described above. The thermal conductivity of pure ice is found by Yen (1981) to be

$$k_0 = 9.828 e^{-0.0057T} \tag{23}$$

where T is the temperature in ˚K. This is a relation found empirically by several different groups of scientists (Wadhams, 2000).
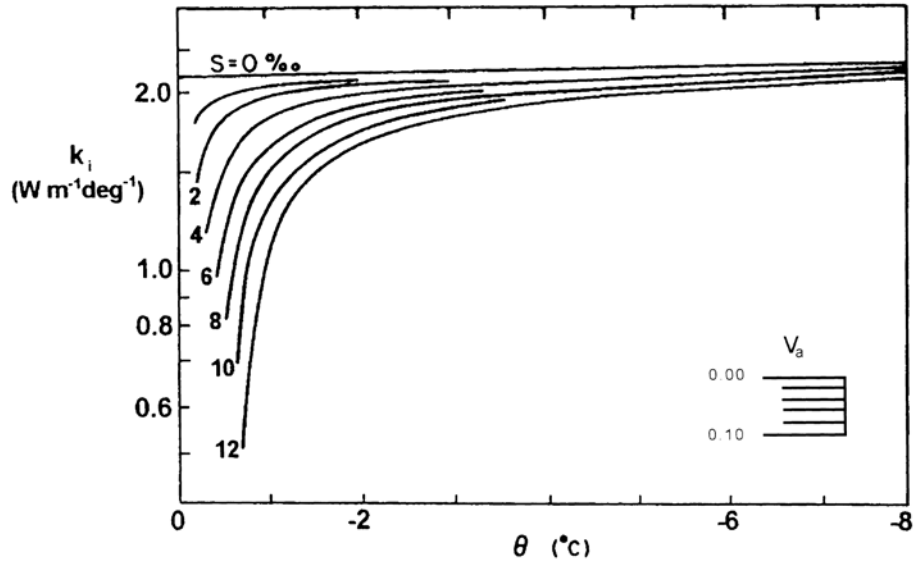

Figure 2.3 Thermal conductivity k_i of sea ice as a function of ice temperature θ and salinity S. The volume fraction of air V_a in the ice and its impact on the conductivity are shown in the lower right corner. Figure from Ono (1968).

The thermal conductivity of sea ice corrected for salinity and air bubble content, is calculated by Ono (1968) and shown in figure 2.3. As shown in the figure, salinity content has a large impact on the conductivity and a given volume fraction of air in the ice will lower the thermal conductivity for all temperatures. The thermal conductivity calculated from the salinity and temperature profiles in figure 2.2a from Kongsfjorden is shown in figure 2.2b. Later experimental programmes by e.g. McGuinness *et al.* (1998) and Trodahl *et al.* (2001) have tried to compute the thermal conductivity from comprehensive ice temperature and salinity investigations. Trodahl *et al.* (2001) calculated values generally ~10% lower than assumed according to previous studies, and the impact of this will be discussed later (section 3.3.6). But in the initial calculations the formula from Untersteiner (1961) is used (equation 22).

Specific heat

The specific heat of sea ice, c_i (J/kg˚C) is given as

$$c_i = c_0 + aT_i + b\frac{S_i}{T_i^2} \qquad (24)$$

15

c_0 is the specific heat capacity of pure ice with a value of 2113 J/kg˚C, T_i and S_i is the ice temperature and salinity in ˚C and psu, respectively. a and b are constants, a=7.53 J/kg ˚C^2 and b=0.018 MJ˚C/kg (Ono, 1967). This formula is assumed to be accurate for the range of temperatures and salinities that are encountered in connection with the work presented in this thesis. As evident in the formula, specific heat is decreasing with decreasing temperature and salinity.

Latent heat of fusion

As pointed out by Doronin and Kheisin (1977), fusion and crystallization of sea ice take place not at any fixed temperature, as in case of freshwater ice, but continuously, from the freezing point of sea water to the temperature at which the whole of the brine freezes. This implicates that for e.g. melting sea ice the heat needed is the heat required to melt the fraction of pure ice plus the heat required to raise the temperature of the brine to its freezing point. This means that the latent heat of fusion is indeed dependent on the fraction of brine in the ice. Ono (1968) produced a formula to calculate the latent heat of fusion in J/kg from given salinity and temperature

$$L = 333394 - 2113T_i - 114.2S_i + 18040\left(\frac{S_i}{T_i}\right) \tag{25}$$

where T_i is ice temperature in ˚C and S_i ice salinity.

Doronin and Kheisin (1977) also computed some values for the latent heat of fusion, which correspond well with the use of Ono's formula.

Radiation properties of sea ice

At the ice surface, radiation fluxes are an important part of the energy budget. It is common to distinguish between two types of radiation, solar radiation (short wave) emitted by the sun and long wave radiation emitted by the atmosphere and clouds. These two types of radiation affect the ice cover in different ways and the ice surface conditions are also very important when it comes to absorbing, reflecting and emitting radiation.

Long wave radiation does not penetrate into the ice cover, but is assumed to be absorbed at the ice surface (Doronin and Kheisin, 1977). It is also assumed that the long wave radiation emitted from the ice, $F_{long,out}$ (W/m^2), is described by Stefan-Boltzman's law

$$F_{long,out} = e_L \sigma T_0^4 \tag{26}$$

16

where T_0 is the surface absolute temperature (˚K), σ is the Stefan-Boltzman constant $5.671 \cdot 10^8$ W/m$^2 K^4$ and e_L is the long wave emissivity. The emissivity is a factor which describes how the emission from a surface differs from the emission from a black body and is usually dependent on the conditions of the ice surface (e.g. Maykut and Church, 1973; Wadhams, 2000).

A large fraction of the incoming short wave radiation is reflected at the ice/snow surface and the ratio between reflected and incoming radiation is called the albedo. New snow has an albedo very close to 1, which means that nearly all incoming radiation is reflected, while bare ice usually has an albedo in the range 0.4 - 0.6. The amount of radiation that is not reflected penetrates into the ice cover and this transfer is dependent upon the optical properties of the ice. Brine content and amount of air bubbles in the ice are both factors that affect the optical properties and the backscattering of solar radiation in the interior of the ice.

First of all, a fraction of the radiation is usually absorbed in the upper 5 - 10 cm of the ice, a fraction that is larger for multi year ice than for thin first year ice. This is due to a distinct surface layer which can be found in multi year ice and not in thin, newly formed ice. Grenfell (1979) defines the fraction that is transmitted through the surface layer, i_0 and calculates different values of i_0 for different ice and weather conditions. Below the surface layer, the absorption of solar radiation is assumed to follow Beer's law

$$I(\lambda, z) = I_0(\lambda) e^{\kappa(\lambda, z) z} \tag{27}$$

where I is the radiation flux at a given depth z and for a given wave length λ, I_0 is the radiation flux from the surface layer, κ is an extinction coefficient dependent of depth and wave length and z is the distance from the surface, positive z is up. The value of this extinction coefficient has been subject to many discussions (Doronin and Kheisin, 1977; Ebert *et al.*, 1995), but for simplicity a bulk coefficient for all wave lengths and independent of depth is normally used in calculations. However, it is important to be aware of the optical differences occurring in multi year ice and first year ice.

2.2.4   Heat fluxes in sea ice

The thermodynamic processes occurring in sea ice are well described by e.g. Maykut and Untersteiner (1971), who use a one dimensional model to describe the heat fluxes and the interaction between sea, ice and atmosphere in central Arctic. A sketch of the model is given in figure 2.4. A more comprehensive view of the model and especially the ice/atmosphere

interaction is given by Ebert and Curry (1993). In the following, all heat fluxes have the unit W/m^2 and the positive vertical direction is upward.
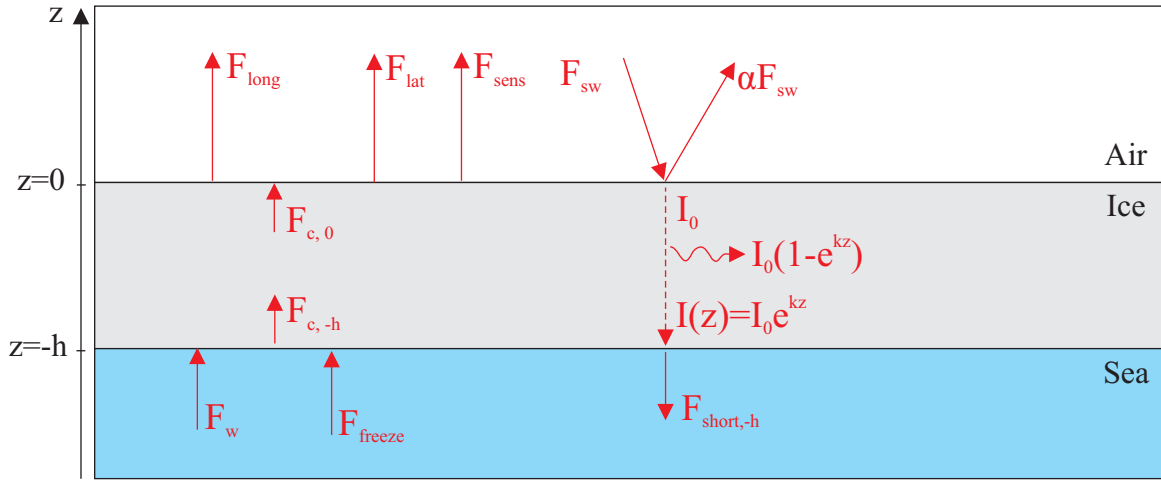

Figure 2.4 An overview of the heat fluxes affecting the heat balance at the air/ice and ice/ocean interfaces. All notations are explained in the text.

Using the notation in figure 2.4, the energy balance on the ice/air interface will be

$$F_{long} + F_{lat} + F_{sens} - F_{c,0} = 0 \qquad (28)$$

for $T_0 < 0°C$, which means no melting at the upper ice surface. F_{long} is the net long wave radiation, F_{lat} is the latent heat flux, F_{sens} is the sensible heat flux and $F_{c,0}$ is the conductive heat flux at the ice surface.

At the ice/ocean interface the balance will be:

$$F_w + F_{freeze} - F_{c,-h} = 0 \qquad (29)$$

where F_{freeze} represents the heat flux from melting/freezing at the ice bottom, F_w is the ocean heat flux and $F_{c,-h}$ is the conductive heat flux at the lower ice surface. Since the short wave radiation is assumed not to be absorbed at the interfaces, the net short wave radiation flux at each interface is zero and these contributions are not considered in the budget for the interfaces.

In the interior of the ice, there are only two fluxes that contribute to the energy balance at a given depth, the conductive heat flux and the short wave radiation. Looking at the whole ice column, a convergence or divergence of these fluxes is reflected in an increased or decreased mean ice temperature $\Delta \overline{T}$, respectively:

$$F_{c,-h} - F_{c,0} + I_0 - I(-h) = \frac{h_i c_i \rho_i \Delta \overline{T}}{\Delta t} \qquad (30)$$

18

where h_i, c_i, and ρ_i are the thickness, specific heat capacity and density of sea ice, respectively, and $\overline{T}$ and Δt are the mean temperature over the whole ice column and the time period, respectively. In the following sections a brief introduction in methods for calculation of the different fluxes is given.

Radiation fluxes

It is possible to parameterize the long wave radiation flux, but since the values used in this project are from direct measurements, no methods to do so will be presented here. The long wave radiation flux F_{long} in equation 28 is the net long wave balance given as

$$F_{long} = F_{long,out} - F_{long,in} \tag{31}$$

The short wave radiation flux at the ice surface is given as

$$F_{short} = (1-\alpha)F_{sw} \tag{32}$$

where F_{sw} is the incoming solar radiation flux and α is the albedo. Also in this case, values from direct measurements of flux in and flux out are used which exclude the problem of finding the correct albedo value. In the further flux calculations there is assumed to be a surface layer of the sea ice of 5 cm through which a fraction i_0 of F_{short} is transmitted. i_0 is calculated from Grenfell (1979) and has a value of 0.8 for first year ice with an ice thickness of 30 cm and no snow cover. Below the surface layer, the absorption is less and is described by Beer's law, using an extinction coefficient of $\kappa=1.8$ m^{-1} (Ebert *et al.*, 1995). This extinction coefficient is also calculated for first year ice. The short wave radiation flux at a given depth in the ice is then given as

$$I(z) = i_0 F_{short} e^{\kappa(z+0.05)} \tag{33}$$

where z is the distance (m) from the ice surface, positive direction is up and z = 0 is the ice surface. This formula is valid for $z \leq -0.05$ m

Sensible and latent heat

A temperature difference at the ice/atmosphere interface leads to a transfer of heat towards the coldest area. This heat is called sensible heat and the magnitude of this transfer is highly influenced by wind and small scale turbulence in the boundary layer close to the ice surface.

The latent heat flux is a heat transfer due to sublimation at the ice surface, a flux which is also influenced by turbulent activities in the atmospheric boundary layer.

To calculate values for both fluxes, a bulk aerodynamic parameterization is used (Ebert and Curry, 1993):

$$F_{sens} = \rho_a c_p C_T u_a (T_0 - T_a) \qquad (34)$$

$$F_{lat} = \rho_a L_v C_T u_a (q_{sat}(T_0) - q_a) \qquad (35)$$

In these formulas, ρ_a and c_p are the density and specific heat capacity of air, u_a is the wind speed 2 m above ice surface, T_0 and T_a is the air temperature at ice surface and at 2 m height above the surface, respectively. L_v is the latent heat of vaporization; q_{sat} is the saturation specific humidity at the ice surface and q_a the humidity 2 m above ice surface. C_T is a stability dependent transfer coefficient given by Louis (1979):

$$C_T = C_{T0}\left(1 - \frac{2b'Ri}{1 + c|Ri|^{1/2}}\right) \qquad Ri < 0 \qquad (36)$$

$$C_T = C_{T0}(1 + b'Ri)^{-2} \qquad Ri \geq 0 \qquad (37)$$

where Ri is the bulk Richardson number

$$Ri = \frac{g(T_a - T_0)\Delta z}{T_a u_a^2} \qquad (38)$$

and for a height Δz of 2 m, the parameter c has a value of

$$c = 1961b'C_{T0} \qquad (39)$$

for a roughness length of 1.6 x 10^{-4} m over ice (Leavitt, 1976). b' is a fitting parameter and the value b'=20 is used as a good approximation when $Ri \geq 0$ (Ebert and Curry, 1993). C_{T0} is a transfer coefficient for a neutral boundary layer and is assigned the value 1.3 x 10^{-3} for heat transfer over ice (Andreas, 1987). Humidity at 2 m height, q_a, is calculated from air temperature and relative humidity measured 2 m above the ice surface. Saturation specific humidity at ice surface, $q_{sat,}$, is calculated from the ice surface temperature.

Conductive heat flux

The conductive heat flux in the ice is parameterized as

$$F_c(z) = -k_i(z)\left(\frac{dT}{dz}\right)_z \qquad (40)$$

k_i is the thermal conductivity of sea ice defined in section 2.2.3. This formula gives the conductive heat flux at a given depth z, using the thermal conductivity calculated for the same depth. For simplicity, it is possible to calculate a bulk conductive heat flux, using the temperature difference between the ice surface and the ice bottom

$$F_c = -k_i \frac{\Delta T}{\Delta z} \qquad (41)$$

ΔT is here the temperature difference over the distance Δz and k_i is a bulk conductivity for the given ice column. In this case it is necessary to assume the conductive heat flux in the ice is constant and that the ice is homogenous. This method is useful in for example very thin ice where it is difficult to measure the temperature gradient and was used by e.g. Shirasawa et al. (1997) when calculating heat fluxes under thin, newly frozen ice.

Freezing and melting ice

When new ice is formed, latent heat is released to the surroundings. This creates an additional heat flux at the ice/ocean interface given as

$$F_{freeze} = \frac{L\rho_i \Delta h}{\Delta t}$$

(42)

Δh is the change in ice thickness (m) in the time interval Δt and L is the latent heat of fusion described in section 2.2.3. If melting of ice occurs, then Δh<0 and F_{freeze} has the opposite sign.

Ocean heat flux

The ocean heat flux is highly dominated by the turbulent activity in the boundary layer close to the ice. Earlier investigations with the aim of determining the ocean heat flux, have often used the so called residual method. This method simply combines equation 29 with measurements of conductive heat flux and freezing/melting of the ice (e.g. Wettlaufer *et al.*, 1990; Holland *et al.*, 1997). But with direct measurements of the turbulent fluctuations of vertical velocity and temperature, the ocean heat flux can be determined using the eddy correlation method (e.g. McPhee *et al.*, 1987; McPhee, 1992; McPhee and Stanton, 1996; Shirasawa *et al.*, 1997):

$$F_w = \rho c_p \langle w'T' \rangle$$

(43)

In equation 43 ρ and c_p are the density and specific heat of sea water, respectively and the angle brackets denote the average covariance of w' and T' over a given time period. The eddy correlation method is described in the Appendix, section 7.

2.2.5   Salinity flux

The heat budget equation at the ice/ocean interface (equation 29) is the result of conservation of heat in a control volume close to the ice. A similar conservation of salt can be assumed at the interface and the derived conservation equation is

$$w_0(S_0 - S_{ice}) = \langle w'S' \rangle_0$$

(44)

where w_0 is the interface velocity resulting from freezing/melting ($w_0 = -\dfrac{dh}{dt}$), S_0 is the sea water salinity at the interface, S_{ice} is the ice salinity and $\langle w'S' \rangle$ is the average covariance of the turbulent fluctuations of vertical velocity and salinity. Direct measurements of salinity fluxes combined with knowledge about the ocean and ice salinities make it possible to estimate the freezing/melting rate at the interface from this simple method.

3 Kongsfjorden

Field work in Kongsfjorden was performed in the period March 9th – 18th 2002. The main field work area was in the inner part of the fjord, approximately 12 km from Ny Ålesund, as shown on the map in figure 3.1, and the facilities of the Norwegian Polar Institute in Ny Ålesund served as a logistic base.

The main purpose of the Kongsfjorden project was to study processes at the ice/ocean interface, regarding freezing, melting and exchange of heat and salt. In addition, several parameters were monitored with the aim of making a complete survey of the air/sea/ice interactions.

In the following sections area and instruments (section 3.1), results (3.2) and discussion of the results (3.3) will be presented.

3.1 Material and methods

3.1.1 Area

Spitsbergen can offer a large variety of both ice and oceanographic conditions. The west coast, where Kongsfjorden is situated, is dominated by fjords and the influence of warm Atlantic Water flowing northward along the coast (Atlantic Water is normally defined as water with temperatures >3°C and salinity >35.0 psu (Loeng, 1991)).

Kongsfjorden is a fjord with depths of 200 - 300 m in the outer parts and 20 - 50 m in the inner parts and the fjord is surrounded by mountains up to 700 m high (figure 3.1). The drainage area around the fjord is approximately 140 km^2 (Svendsen *et al.*, 2002) of which about 77% is covered by glaciers. Several large glaciers are entering the fjord in the inner part, contributing with large amounts of fresh water due to melting, runoff and calving. The fjord does not have a typical sill in the outer part, but a trench following the fjord in to Lovènøyene. But south of Lovènøyene there is a kind of sill in north-south direction separating the fjord into two basins, one in the outer part and one in front of the Kongsvegen glacier. The inner basin has depths of about 50 m (figure 3.1). During winter calved icebergs from the glacier are often stranded on this sill, creating an even narrower passage between the inner and outer part of the fjord.

As on the rest of Spitsbergen, the winds in the Kongsfjorden area are following the valley direction and the prevailing wind direction in Kongsfjorden is out the fjord, 120° (Førland *et al.*, 1997).
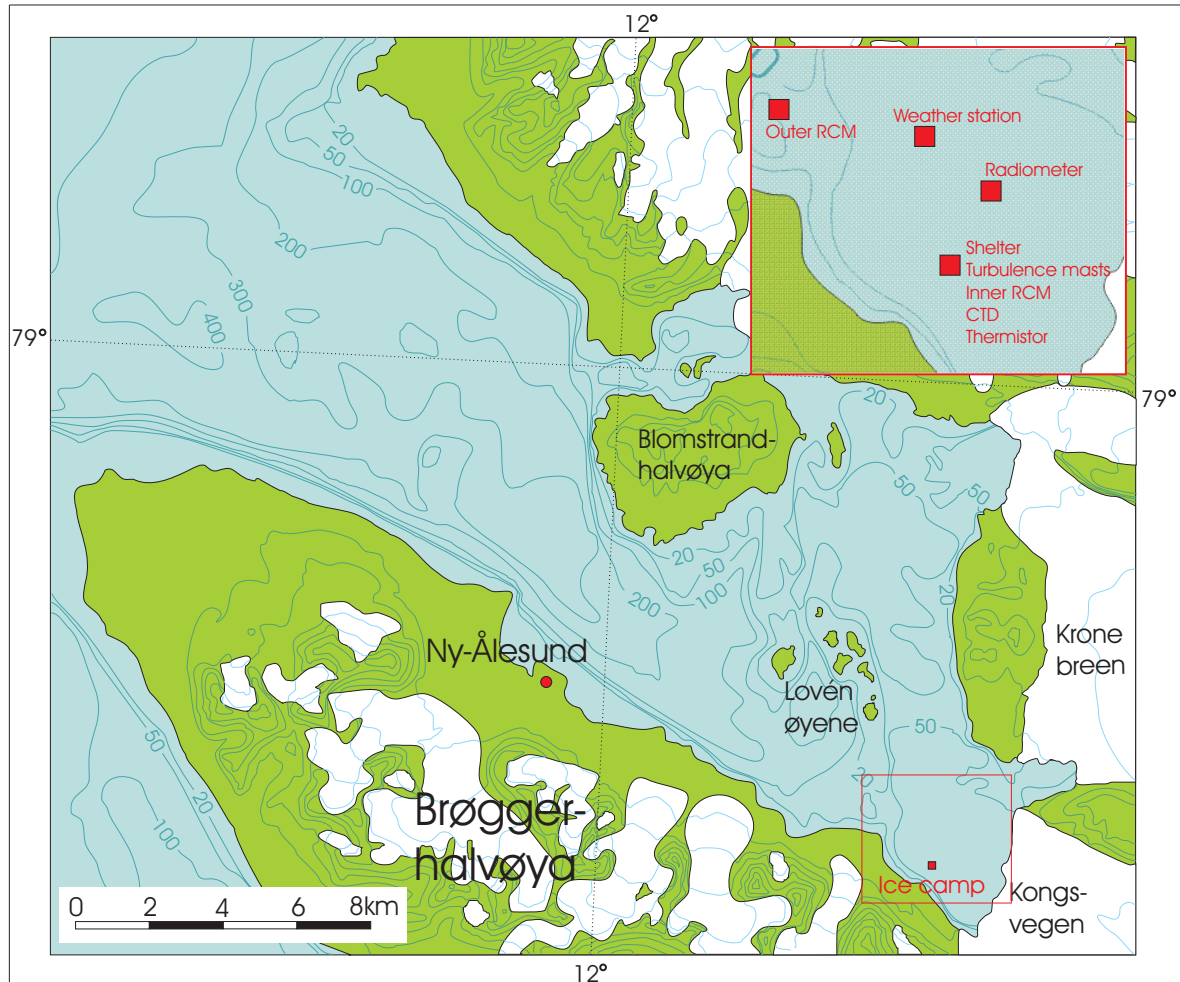

Figure 3.1 Map of the Kongsfjorden area and a detailed sketch of the field work site. For Kongsfjorden's location on Spitsbergen, see figure 1.1. The map is modified from Svendsen *et al.* (2002).

The total annual volume of fresh water supplied to Kongsfjorden is approximately 1.4 km^3 and about 90% of this is supplied during the summer season (Svendsen *et al.*, 2002). More than half the total volume is from glacier runoff, the rest is from river runoff, precipitation and calving.

Ice conditions in Kongsfjorden are highly variable and can change rapidly. Earlier ice observations, summed up in Svendsen *et al.* (2002), defines Lovènøyene as a western border for the area of fast ice, while the area west of this border is usually dominated by drifting ice. This was also the case in March 2002 when the extension of the ice covered area changed

considerably during the field work period. Typical ice thicknesses in the field work area were 20 - 40 cm with no snow on top of the ice.

The main driving forces for the water circulation in the fjord are wind, fresh water input and daily tidal variations (Svendsen *et al.*, 2002). In summer, the fresh water runoff in the inner part of the fjord results in a brackish surface layer of 2 - 3 m divided from the underlying water masses by a strong pycnocline. In this upper layer the circulation is controlled by the fresh water flux and the wind, normally resulting in an outflow on the northern side of the fjord and an inflow on the southern side. Measured velocities in the surface layer in summer 1999 are in the range 10 - 30 cm/s (Svendsen *et al.*, 2002). In 1999, a circulation in the deeper layers below the surface layer was also measured (Svendsen *et al.*, 2002). This is probably set up by the tide and winds at the Spitsbergen coast and results in a propagating Kelvin wave moving cyclonically around the Kongsfjorden basin. This circulation brings water from the West Spitsbergen Current into the deeper parts of Kongsfjorden with typical velocities of 8 - 10 cm/s.

In winter, the ice cover is preventing the wind to directly force the circulation, but the prevailing winds can transport surface water from the ice edge and westward. This results in a deeper return flow, bringing warmer water in under the ice and in turn slows down the ice grow rate (Svendsen *et al.*, 2002).

In the inner basin, in front of the Kongsvegen glacier, Svendsen *et al.* (2002) concludes that the circulation is cyclonic based on a measured decrease in water temperature northwards along the glacier margin.

The field work area was situated on the land-fast ice south-east of Lovènøyene (figure 3.1) and the approximate depth at the site was 40 m. Due to bad ice conditions, the area had to be accessed by snowmobile on the shore from Ny Ålesund, the ice was entered directly south of the field work site.

3.1.2 Instruments

In Kongsfjorden, several instruments to monitor the air/sea/ice interaction were used. Most important of these are the turbulence masts, designed to measure turbulent fluxes of heat, salt and momentum under the ice. In addition to these, two current meters, a CTD (Conductivity Temperature Depth), a weather station, a net radiometer and a thermistor chain were used to obtain data. Detailed investigations of the ice properties were also done, but these data are not

treated in this thesis. In the following section a brief introduction to each instrument and the use of it in Kongsfjorden is given, but a more technical description of the instruments is given in Sirevaag (2002).

Turbulence mast

Turbulent fluxes were measured by a so called Turbulent Instrument Cluster (TIC) which comprises an acoustic current meter (ADV) from Sontek/Ysi and a temperature sensor (SBE3), a conductivity sensor (SBE4) and a micro conductivity sensor (SBE7) from SeaBird Electronics. The compilation of the TIC is shown in figure 3.2. The ADV is mounted with the transducers pointing upward with the sampling volume 18 cm above the tip of the probe, while the other sensors are mounted on a plastic bracket rotated 90 degrees clockwise from the ADV sampling volume. All instruments are mounted on a stainless metal rod with a total length of 2 m and aligned so that they all measure at the same vertical level. Excepted from this is the SBE4 conductivity sensor which is mounted with the intake towards the control volume approximately 10 cm above the sampling plane.

To the ADVs there belongs an underwater processing module (UPM), which processes the signals from the ADV-probe.
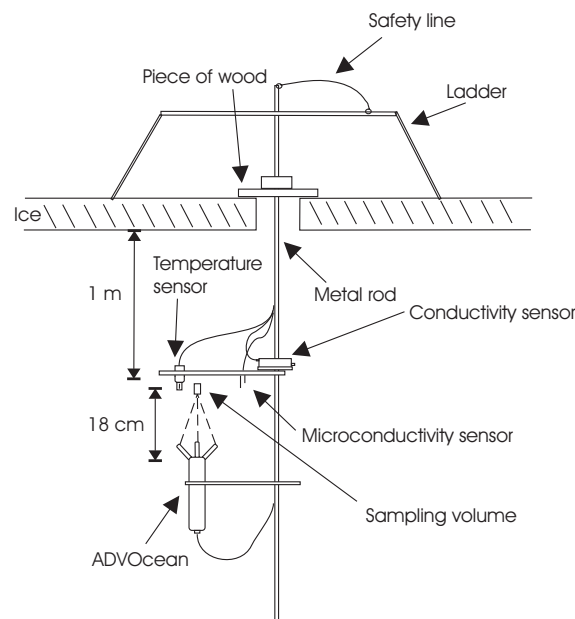
Figure 3.2 A schematic sketch of the compilation of the turbulence masts. Note that the proportions on the sketch are not correct.

In Kongsfjorden, two separate turbulence masts were used, deployed approximately 1.4 m apart horizontally. Both were equipped as shown in figure 3.2, except that only mast #1

26

included a micro conductivity sensor. Both masts were lowered through the ice, levelled with the sampling plane 1 m below the underside of the ice. Data from all Sea-Bird sensors and the ADV on mast #1 were processed through a SBE9+ processing unit and synchronized in a SBE11 deck unit and recorded on a laptop. The ADV on mast #2 transferred data through the UPM and recorded directly on a separate laptop, using DOS-based Sontek software. Therefore the synchronization of the ADV data and SBE data from mast #2 had to be done manually after recording, by synchronizing the CPU clocks on both laptops. The TIC system sampled once per second (1 Hz) and the sampling frequency was the same for all sensors except for the ADV on mast#2 which operated independently and sampled at 2 Hz. The SBE9+ and the UPMs were all situated on the ice with only the instruments in the water and the deck unit and laptop were situated inside a heated shelter 2 - 3 m away from the deployment site.

To run this system it is necessary with a continuous power supply provided by a Honda generator, which must be running to obtain data. This is the largest limitation of the system and responsible for the gaps in the data during the field work period.

Current meters

In addition to the turbulence mast, two Aanderaa Recording Current Meters (RCM7) were deployed from the ice, one was deployed in the inner basin (inner RCM) while the other one was deployed approximately at the sill (outer RCM) (figure 3.1). Both RCMs were attached to the ice with a rope, chains and ice screws, positioning the RCM's 12 m below the underside of the ice. The RCMs were equipped with a battery pack and all data were stored in an internal data storage unit (DSU 2990) and downloaded after recovery. Current velocity and direction were measured and both RCMs had a temperature sensor to monitor the water temperature. In addition, the inner RCM had a pressure sensor and the outer RCM had a conductivity sensor. But since the inner RCM was deployed at a known depth and the conductivity data from the outer RCM were drifting during the field work period, these data were not used. Both RCMs were set to record at 10 minutes intervals. The inner RCM was deployed from March 11th 12.30 to March 16th 11.00 and the outer RCM was deployed from March 13th 14.15 to March 16th 09.00

CTD

A Sea-Bird SEACAT SBE19*plus* CTD was used in Kongsfjorden to get profiles of salinity and temperature at the location where the other instruments were deployed. Before

deployment, the CTD was preheated inside the shelter to prevent freezing of the sensors and then lowered rapidly into the water down to a depth of 10 m. After one or two minutes the CTD was raised to a level just below the surface and the temperature/salinity profile was obtained. For lowering the CTD, a hand winch attached to a snowmobile sledge was used and the lowering speed was approximately 1 m/s. During the field work period, 11 CTD profiles were made.

Radiometer

A CNR1 Net Radiometer from Kipp & Zonen was used to obtain measurements of the radiation balance at the ice surface. The CNR1 consists of five sensors, 2 CM3 pyranometers, 2 CG3 pyrgeometers and an internal temperature sensor. It measured both incoming and outgoing longwave and shortwave radiation and was set to record at 10 minutes intervals. The radiometer was attached to a metal rod with the sensors levelled 1 m above the ice surface. The instrument was placed on the ice approximately 150 m north of the ice camp (figure 3.1).

Weather station

Approximately 300 m north of the ice camp, an Aanderaa Automatic Weather Station (AWS) was placed on the ice (figure 3.1). This AWS was equipped with sensors for temperature, pressure, relative humidity, wind speed and wind direction, all instruments measuring 2 m above the ice surface. The wind speed sensors had two output signals, one for average wind and one for wind gust which is the maximum speed over a 2 second interval. The AWS was also equipped with an Aanderaa Data Logger 3660 which read signals from the sensors at 10 minutes intervals and stored them on a DSU 2990.

3.2   Results

3.2.1   CTD

The deployment site of the instruments is in a typical enclosed basin, trapped between a glacier margin in southeast and a sill in northwest (figure 3.1). Two of the CTD profiles taken in this basin are shown in figure 3.3, the first taken on March 13th 12.04 and the other one taken on March 16th 09.25. The first profile reveals a two layer system, with a water column divided at approximately 20 m depth, which corresponds to the sill depth. The water column consists of a rather quiescent lower layer with water close to the freezing temperature and

relatively high salinities and a tidally active upper layer, always warmer and less saline than the lower layer. The mean temperature and salinity in the upper layer during the whole period are -1.62˚C and 34.67 psu, while the corresponding values for the lower layer are -1.79˚C and 34.73 psu. This two layer system remains until a mixing event occurs between March 15th and 16th, homogenizing the whole water column, except the lower 2 – 3 m (figure 3.3). After the mixing event the mean values of salinity and temperature are 34.70 psu and -1.68ºC.
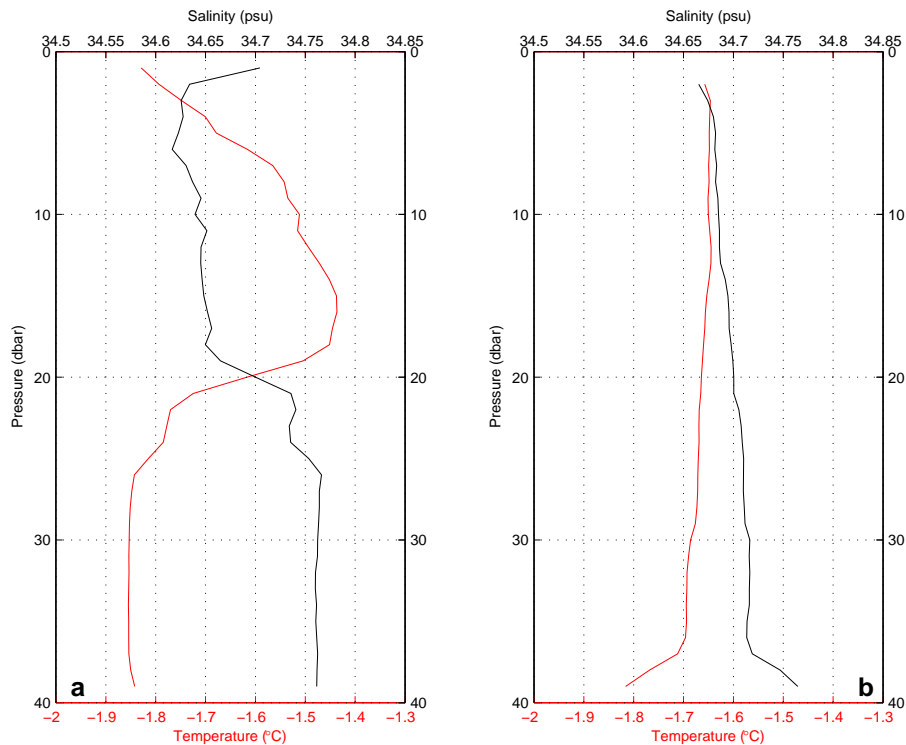
Figure 3.3 CTD profiles taken in the inner basin in Kongsfjorden on (a) March 13th 12.04 and (b) March 16th 09.25.

3.2.2   RCM

Current speeds and directions from the inner RCM and the outer RCM are plotted in figure 3.4 and figure 3.5, respectively. Plots show 40 minutes mean values of both horizontal speed and direction and the y-axis is oriented south-north. The RCM7 has a threshold value of 1.1 cm/s and in the data from the inner RCM about one of five values are below this threshold value. This means that all recorded speeds that are smaller than 1.1 cm/s are recorded as 1.1 cm/s and in the calculation of the mean speed, half this threshold value, 0.55 cm/s, is used instead of 1.1 cm/s to get a more correct distribution of speeds below 1.1 cm/s.

Low speeds seem to occur only when the current is changing direction from inflow to outflow and visa versa. In the outer RCM only a small number of speeds lower than the threshold value were recorded.

Temperatures obtained from the temperature sensors on the RCMs are plotted in figure 3.6, also here as average values over 40 minutes.

3.2.3   Weather station

Weather conditions in Kongsfjorden, recorded by the weather station at the ice are shown in Sirevaag (2002). However, wind speed and direction are plotted in figure 3.7 and air temperature is plotted in figure 3.8. The main wind direction in Kongsfjorden is from the glaciers in the inner part and along the fjord towards northwest, an angle of about 125˚. This corresponds well with the investigations of Førland *et al.* (1997) which concludes that the prevailing wind directions at Spitsbergen in general are from the inland, along the valleys and towards the sea. During the whole period of field work in Kongsfjorden, the wind direction was more or less constant 122˚. Mean wind speed during the period was 5.4 m/s, but wind gusts of 20 m/s were measured during the period of low air pressure around noon on March 14th (figure 3.7).
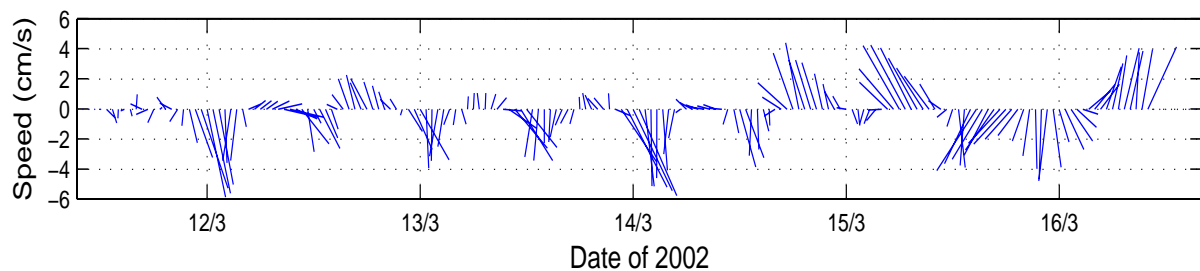
Figure 3.4 Stick plot of current speed and direction measured at the inner RCM. Values are averaged over 40 minutes and the y-axis is oriented south-north. Date labels indicate midnight, 00.00 a.m.
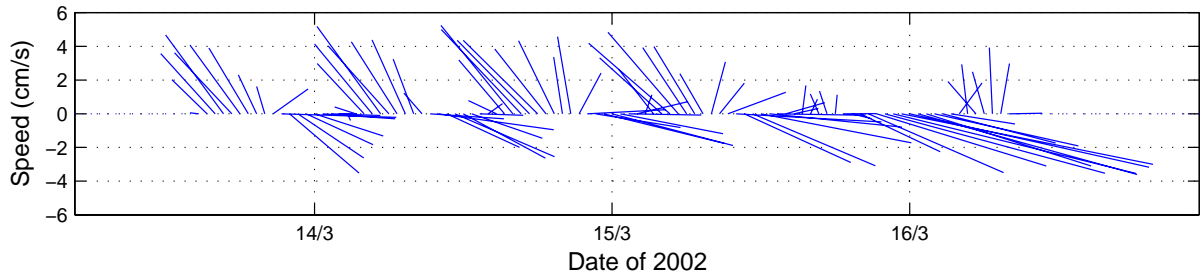
Figure 3.5 Stick plot of current speed and direction measured at the outer RCM. Values are averaged over 40 minutes and the y-axis is oriented south-north. Date labels indicate midnight, 00.00 a.m.
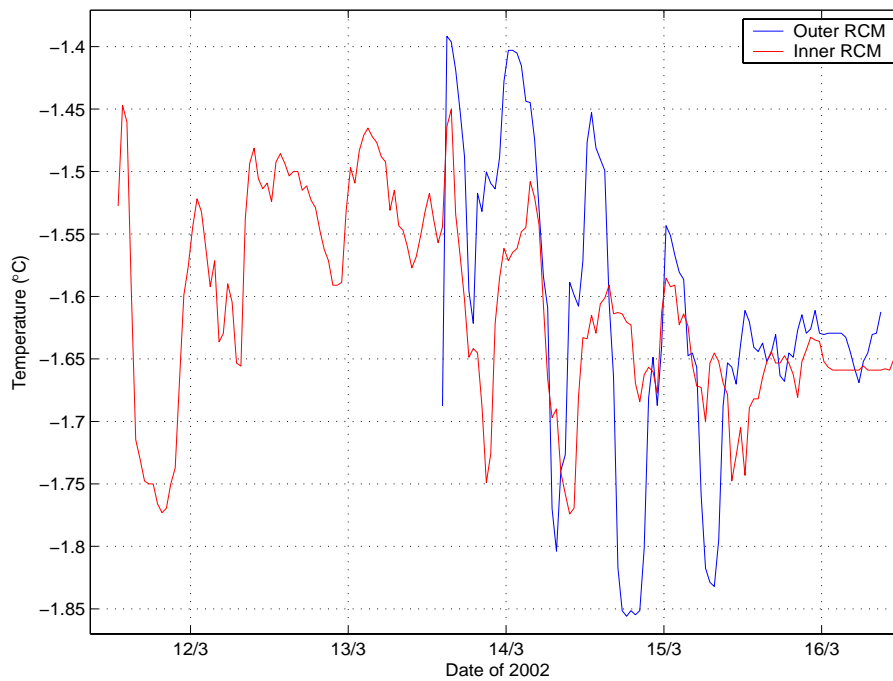

Figure 3.6 Water temperatures measured at the inner and outer RCM, 12 m below the ice. Values are averaged over 40 minutes. Date labels indicate midnight, 00.00 a.m.
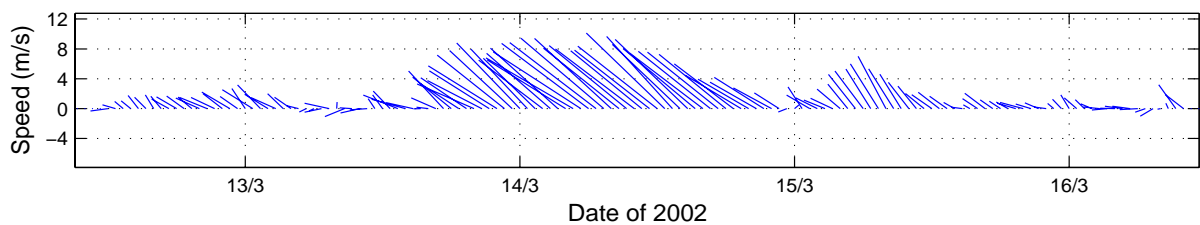

Figure 3.7 Wind speed and direction in Kongsfjorden measured at the weather station, values are 40 minutes averages and y-axis is oriented north-south. Date labels indicate midnight, 00.00 a.m

Air temperatures varied from a maximum of -8.9˚C, which coincided with the passing of a low pressure system, to a minimum of -22.6˚C (figure 3.8). The mean temperature in the period was -14.3˚C.
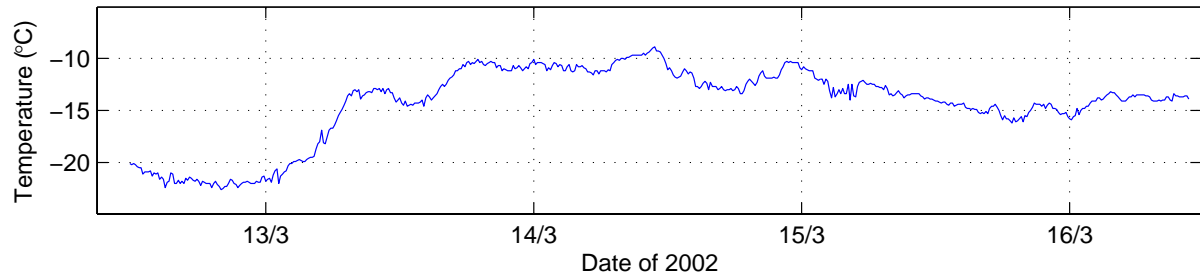
Figure 3.8 Air temperature in Kongsfjorden during the field work period, measured at the weather station. Temperature data are averaged over 40 minutes and date labels indicate midnight, 00.00 a.m.

3.2.4 Thermistor chain

The temperature development in the ice is shown in figure 3.9, data are from a thermistor chain deployed in the ice. The uppermost thermistor is situated at the surface. Then there is a thermistor for every cm from 5 cm to 25 cm depth and a thermistor every 2.5 cm in the depth interval 25 - 35 cm. Theoretically, it should be possible to determine the ice thickness from the thermistor data, the lower ice surface is below a given thermistor depth once the temperature is below the freezing temperature. The ice thickness varied from 23 cm to 31 cm during the period the thermistor chain was in the ice, but it is difficult to determine the lower ice edge from the thermistor data. Both because the spacing between each thermistors gets larger in the given range and because there might be errors connected with large water content in the lower layer of newly formed ice corrupting the temperature data.

3.2.5 Radiometer

In figure 3.10 data from the net radiometer are shown, represented by the balances of long wave and short wave radiation, positive fluxes are up. The plotted values are 40 minutes averages. In the short wave radiation data it sometimes occurs during the night that the balance showed small, positive values, which indicate a negative albedo. This is not possible and might be explained by a small instrumental inaccuracy. These positive values are artificially set to zero in the following.
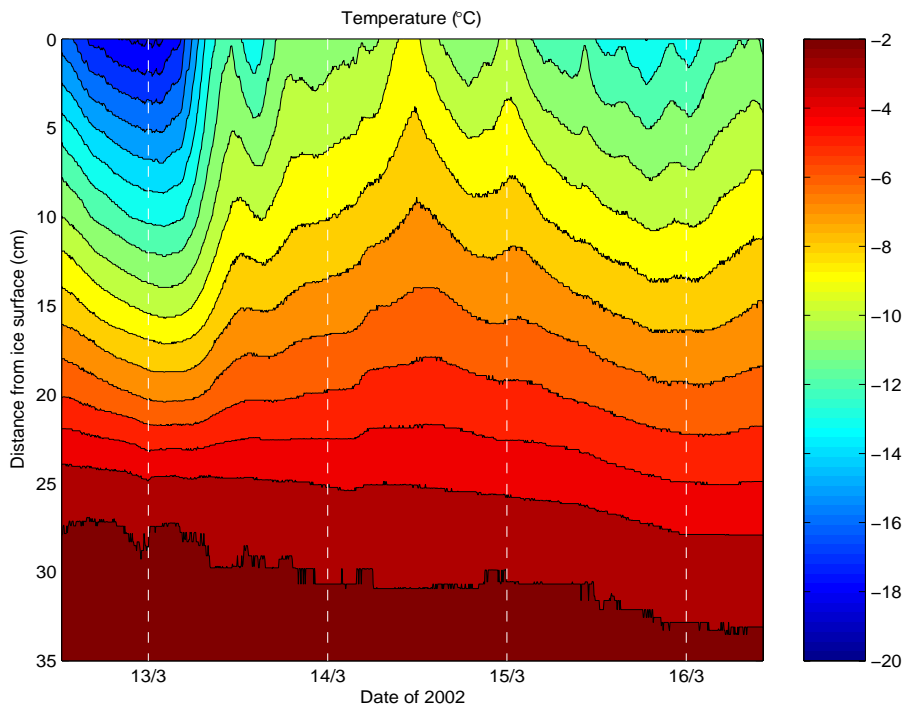
Figure 3.9 Ice temperature at different depths from data obtained from the thermistor chain frozen in the ice. Date labels indicate midnight, 00.00 a.m.
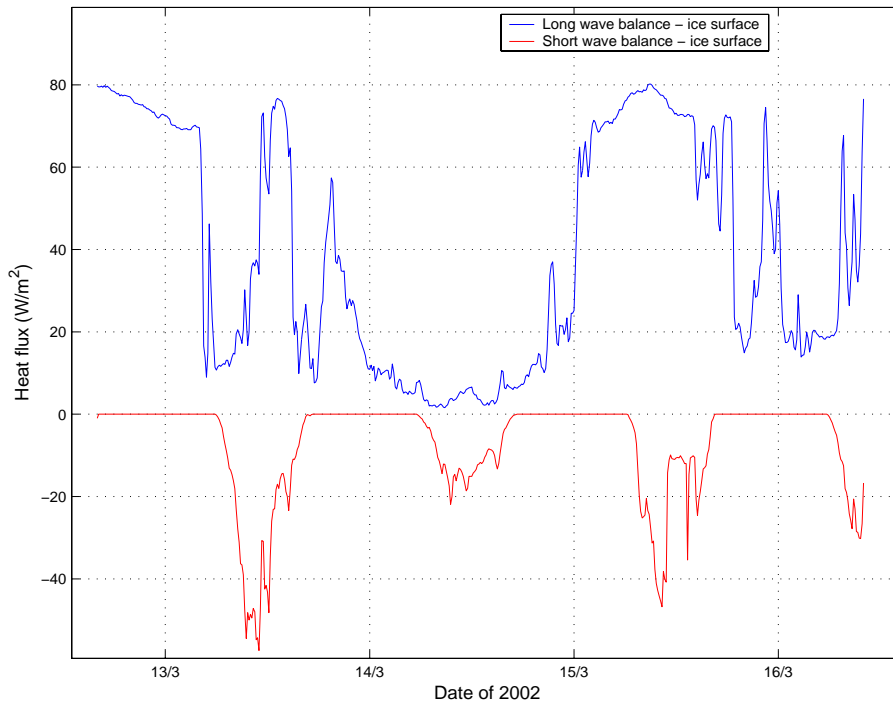

Figure 3.10 Balances of short wave and long wave radiation at the ice surface, positive fluxes are upward. During night, the short wave radiation flux is artificially set to zero (see text). Date labels indicate midnight, 00.00 a.m.

During the whole period the ice surface was more or less snow free, only some drifting snow covered the surface for shorter periods. This drifting snow on the ice surface was wet in daytime during the field work period.

3.2.6 Turbulence masts

On the turbulence masts, one of the ADVs was new and after data recording some problems with the synchronization of the ADV on mast #2 occurred. Due to this, the velocities from this current meter are not considered in the following discussion of the results. The turbulence mast data are divided in 15 minutes realizations where the mean temperature and absolute horizontal speed are calculated. After this all the 15 minutes values are averaged over 2 hours and plotted in figure 3.11 and figure 3.12. The error bars indicate ±1 standard deviation of the 15 minutes values. This data presentation is identical to the one used for the turbulent fluxes presented in section 3.3.6 and gives an indication of the variability of speeds and temperatures vs. turbulent fluxes, described and discussed later.
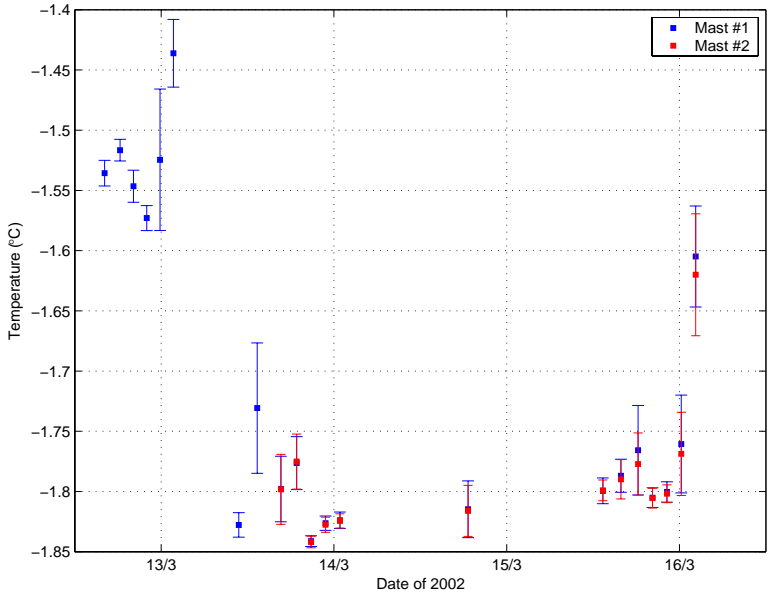
Figure 3.11 Water temperatures measured at 1 m depth by the temperature sensors at the turbulence masts. Temperatures shown are average values over 2 hours and errorbars indicate ±1 standard deviation. Date labels indicate midnight, 00.00 a.m.
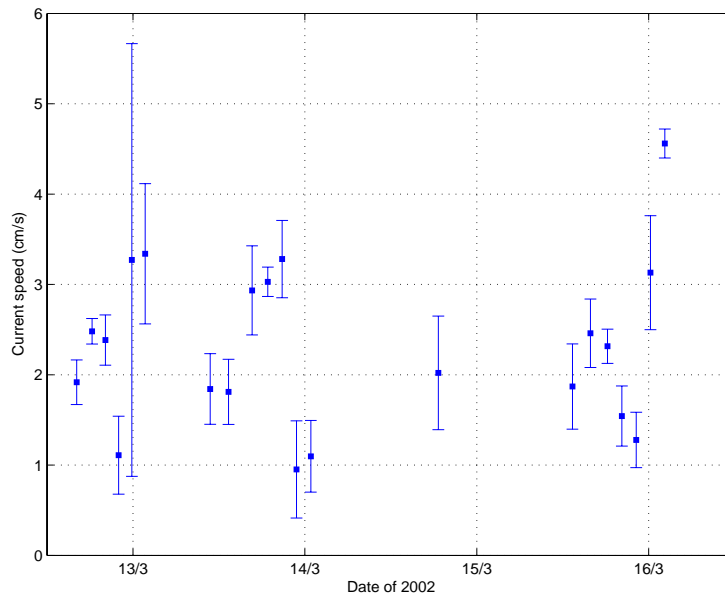
34

Figure 3.12 Mean horizontal speed averaged over 1 hour measured by the ADV on turbulence mast#1. Error bars indicate ±1 standard deviation and date labels indicate midnight, 00.00 a.m.

3.3 Discussion

3.3.1 CTD

The revealed two layer system in the inner basin of the fjord (figure 3.3a) is not typical of an Arctic fjord in winter. According to Svendsen *et al.* (2002) Kongsfjorden should have a weak stratification in winter, but the CTD profile shows the effect of the protecting sill northwest of the inner basin. The upper layer has a mean temperature 0.2°C higher and a mean salinity 0.1 psu lower than the lower layer. The lower layer is more or less unchanged throughout the different profiles, but the depth of the border between upper and lower layer is changing. When water is flowing over the sill, mixing will occur and the efficiency of this mixing is dependent of the current velocity at the sill (e.g. McClimans, 1978; Gade and Edwards, 1980). This might explain the changes in the depth of the upper layer.

The upper layer is dominated by tidal inflow of warmer water and the amount of heat in the upper layer is dependent on when in the tidal cycle the profile is taken. But the upper layer also has a typical surface layer dominated by the interaction with ice and atmosphere; hence one observes lower temperatures in the upper 2 m, due to heat loss to the ice. The salinities are also higher in this surface layer, which might be a natural result of ice freezing and release of salt to the surrounding water. This process would create an unstable stratification which

can not be permanent and these measurements in the upper 2 m are most likely corrupted by movements of the CTD.

The mixing event between March 15th and 16th homogenized the whole water column except the lowest 2 - 3 m where one still observes water close to the freezing temperature and with high salinities after the mixing (figure 3.3b). The reason for this mixing might be found in the velocities measured by the outer RCM situated at the sill, which show a strong inflow around midnight on March 16th (figure 3.5). Mean current velocity between March 15th 22.00 and March 16th 02.00 was 13.9 cm/s, which might be high enough to mix the whole water column except the very lowest 2 - 3 m.

The water masses in Kongsfjorden are, as mentioned in section 3.1.1, affected by the West Spitsbergen Current (WSC) carrying relatively warm Atlantic Water north along the Spitsbergen coast (Svendsen *et al.*, 2002). Even in the inner part of the fjord this exchange is noticeable. After the mentioned mixing event, almost the whole water column in the inner basin has a temperature about 0.2˚C above freezing.

3.3.2 RCM

Both RCMs were deployed at 12 m depth, in the middle of the tidally active upper layer. In the inner RCM, generally small velocities are measured. Average speed during the whole period was 2.3 cm/s, but larger velocities on maximum inflow/outflow are measured. There is a clear semi diurnal signal in the inner RCM (figure 3.4), confirming that the semi diurnal lunar component (M_2) is the most dominant tidal component as stated by Svendsen *et al.* (2002). The tidal variation is also clear in the temperatures from the inner RCM, with higher temperatures on inflow than on outflow (figure 3.6). The temperature differences are in the range 0.1 - 0.3˚C from outflow to inflow. But even though the tidal signal is clear, the current directions in the inner basin are not as distinct as on the sill, indicating a more complex current pattern inside the inner basin.

In the outer RCM the directions are much more distinct, either in or out of the inner basin (figure 3.5). The average current speed is 5.0 cm/s, but with much larger speeds around the maxima in the tidal cycle, maximum speed from the outer RCM is 17.2 cm/s. Temperatures from the outer RCM reveals the same pattern as inside the basin, with inflowing water considerably warmer than the outflowing water. The temperature difference is about 0.2 - 0.4˚C, slightly larger than in the inner RCM (figure 3.6).

Svendsen *et al.* (2002) found clear evidence of a counter clockwise circulation in the inner basin in summer, with water flowing north along the glacier margin of Kongsvegen (figure 3.1). Volume transport calculations from the outer RCM show that there was a net transport of water over the sill and into the basin which also indicate a counter clockwise circulation in the inner basin in winter.

Svendsen *et al.* (2002) suggest that wind along the fjord can transport surface water away from the ice edge and set up a deeper return flow of warmer water in under the ice. It is not possible to see an increased volume transport of water as a result of the increased wind speed on March 14th from the RCMs (figure 3.4 and figure 3.5), but a return flow can be deeper or only noticeable further out in the fjord.

Data from both RCMs show the large influence of the WSC on the water masses in Kongsfjorden, and give an indication of a significant transport of heat into the inner part of the fjord. Calculations from the outer RCM indicate a net heat transport of order 10^9 J into the inner basin during the period of deployment. During summer the large glaciers entering the inner part of the fjord and the large amount of melt water runoff contribute to cool down the "warm" water. This is not the case in winter when all the inflowing water has sub-zero temperatures and it will not be further cooled by the melt water. This leaves interaction with the atmosphere as the most important factor for cooling of the fjord water in winter.

3.3.3 Ice temperatures and salinity

As known, the sea ice cover works as a kind of buffer between the warm ocean and the cold winter atmosphere. From the plot of ice temperatures in figure 3.9 it is clear that temperatures at the ice surface varies over a much larger range than temperatures at the bottom. Comparison with the air temperature in figure 3.8 shows that the ice surface temperature varies almost as the air temperature, while the temperature at the underside of the ice is more or less constant. This adjustment of the ice surface temperature to the air temperature results in large variations in the temperature gradient in the ice and subsequently also in the conductive heat flux. It is often assumed that the temperature gradient is close to constant throughout the ice column, but with the temperature adjustment to the air temperature this can not be the case. After the adjustment of the surface layer it will take time before the rest of the column is adjusted and in these periods there will always be a convergence/divergence of conductive heat flux in the ice.

The salinity profile from the first year ice in Kongsfjorden has a typical C-shape as known from other studies (e.g. Perovich *et al.*, 1998; Gerland *et al.*, 1999), with relatively high salinity at the top and at the bottom (figure 2.2a). Mean value of the ice salinity is 7.3 psu, while the values at bottom and top are about 11 psu.

Both temperature and salinity are important parameters in determining the thermodynamic properties of the sea ice and important for the heat budget of the air/sea/ice system, calculated in section 3.3.6.

3.3.4   Radiation

The radiation balances presented in figure 3.10 show how the weather conditions affect the radiation balance at the ice surface. While the upward long wave flux from the ice is relatively constant, the downward flux of long wave radiation is strongly dependent on the cloud fraction. As shown in figure 3.10, on March 14th, a day of bad weather, the cloud cover is considerable and the net long wave balance is close to zero. On other days with clear weather, the downward flux is small and the resulting net balance has a relatively large, positive value. The short wave radiation is also controlled by the cloud cover, due to blocking of direct radiation from the sun. The effect of this can be seen on March 14th (figure 3.10), where it is also clear that the peaks of the short wave radiation are concentrated to small time intervals around noon every day due to low solar angle and small amounts of direct solar radiation this early in winter.

Alfred Wegener Institue (AWI) has a meteorological station in Ny Ålesund measuring both long wave and short wave radiation and it is possible to compare the radiation data from the ice in the inner part of the fjord with radiation measured at the Koldewey station[1] (figure 3.13). This comparison shows that the agreement is ok, but the magnitudes measured on the ice are a bit larger than measured at the Koldewey station. On days with a small cloud cover it seems that the long wave radiation from the ice covered ocean is larger than from the snow covered ground, which also is natural according to the Stefan-Boltzmans law (equation 26). The flux of short wave radiation is always larger on the ice than measured at the Koldewey station. This might be due to the location of the Koldewey station right north of the Zeppelin mountain (554 masl.), which might block for some of the direct radiation, especially early in winter.

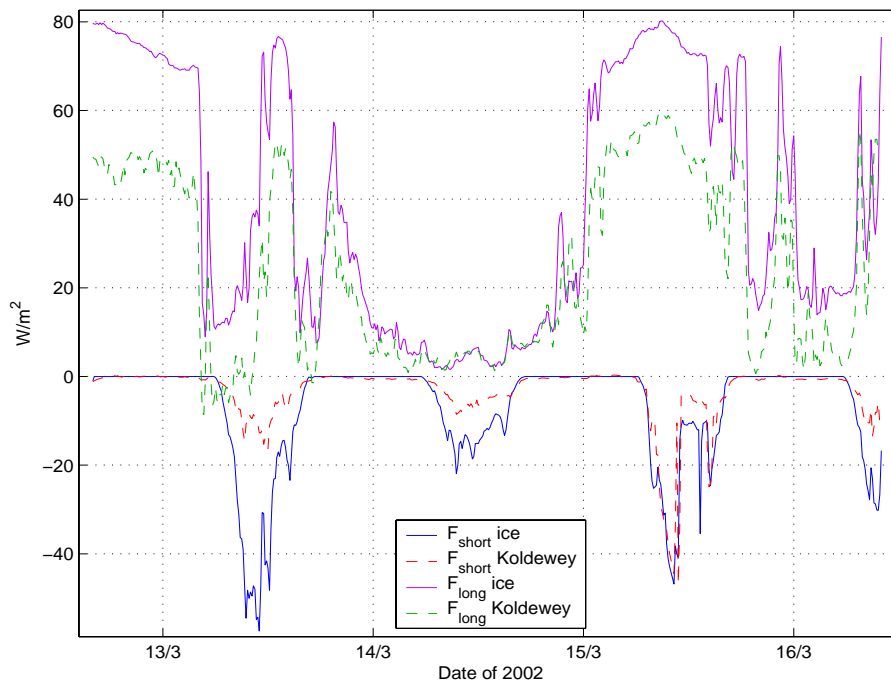[1] Data from http://www.awi-bremerhaven.de/MET/NyAlesund/obsequery2.html

Figure 3.13 Short wave and long wave radiation balances measured on the ice compared with the balances measured at the Koldewey station. Date labels indicate midnight, 00.00 a.m.

3.3.5   Turbulence masts

Water temperatures measured during the field period with the TICs at 1 m depth (figure 3.11) are generally lower and closer to the freezing point than the temperatures measured by the inner RCM at 12 m depth (figure 3.6). The variation in temperature is also smaller close to the underside of the ice than in the middle of the tidally active upper layer where the inner RCM was deployed. But the temperature sensor on the RCM may not be as good calibrated as the SeaBird temperature sensors to show the correct absolute temperatures.

Measured speeds at mast#1 (figure 3.12) are of the same order as speeds from the inner RCM. Mean value from the mast is 2.3 cm/s, the same as measured with the current meter (figure 3.4) at 12 m depth. Even though the velocities measured by the ADV on mast#1 are small, the quality of the data should be good using the Doppler shift technique in velocity estimation (ADV manual from Sontek). The standard deviations in the ADV horizontal velocity calculations are relatively large and might reflect the "noisy" current regime in the inner basin with periods of small velocities and rapidly changing directions.

To transform the data from the time domain to the wave number domain the mean velocity has to be sufficiently larger than the turbulent fluctuations in velocity. Data from mast#1 indicate that U is 5 - 10 times larger than u'. To fulfil the requirement of Hinze (1959), this

ratio should be >>1 and an attempt to calculate any typical length or time scale from the power spectrum of these data may include too large uncertainty.

The velocity data from the turbulence mast are divided into 15 minutes realizations and the friction velocities are calculated by the eddy correlation method (Appendix, section 7). Friction velocities calculated from mast#1 data (figure 3.14) have a mean value of 0.15 cm/s, which is quite large considering the small measured velocities. However, it is not certain how the current conditions affect the turbulent fluctuations.
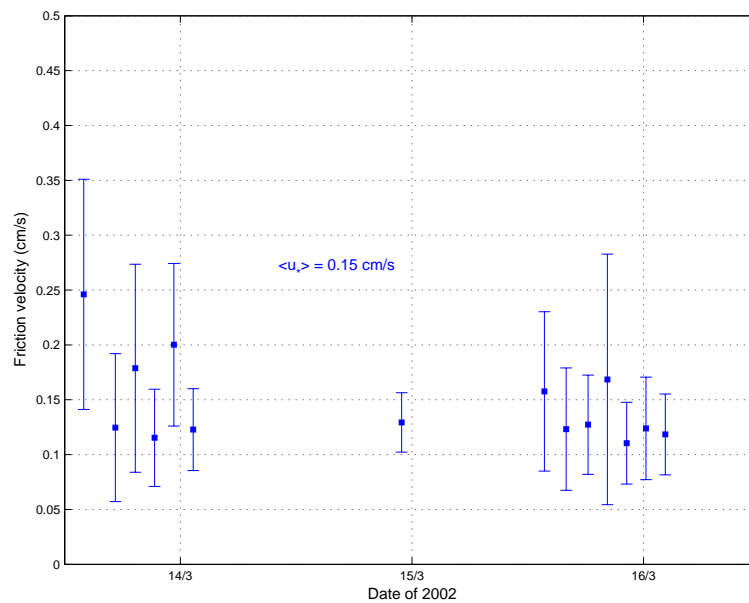
Figure 3.14 Calculated friction velocities from the ADV on mast#1. Error bars are ±1 standard deviation and date labels indicate midnight, 00.00 a.m.

3.3.6   Heat budget

Results presented in the previous section give the possibility to set up a heat budget for the air/sea/ice system in Kongsfjorden. Most of the measurements cover the same period of time and it is therefore possible to compare the fluxes at the different interfaces. The chosen period for the heat budget comparison is from March 13th 12.00 to March 16th 10.00. At the start of this period the thermistor chain has been deployed for 24 hours and that should be sufficient for the chain to freeze in and the thermistors to be in equilibrium with the ice temperatures.

Atmospheric fluxes

The radiation fluxes come directly from the radiometer and no further treatment of these data is done except adjusting them to the correct time period. The short wave balance during night is also set to zero, as described in section 3.2.5.

Fluxes of latent and sensible heat are calculated from the weather data according to the parameterization in section 2.2.4. In these calculations, the values $\rho_a = 1.275$ kg/m^3, $L_v = 2.5 \cdot 10^6$ J/kg and $c_p = 1005$ J/kg $^\circ$C are used. Temperatures from the uppermost thermistor in the thermistor chain situated at the surface are used as surface temperatures. Fluxes are plotted in figure 3.15 and the mean values of the latent and sensible heat fluxes are 18.1 W/m^2 and 14.6 W/m^2, respectively. It is obvious, both from figure 3.15 and from the parameterization of the fluxes, that the wind speed has a large influence on these atmospheric heat exchanges, with a clearly visible peak in both fluxes around noon on March 14th. The direction of the fluxes is always from the ice to the atmosphere, except for some shorter periods on March 13th and very early on March 14th.
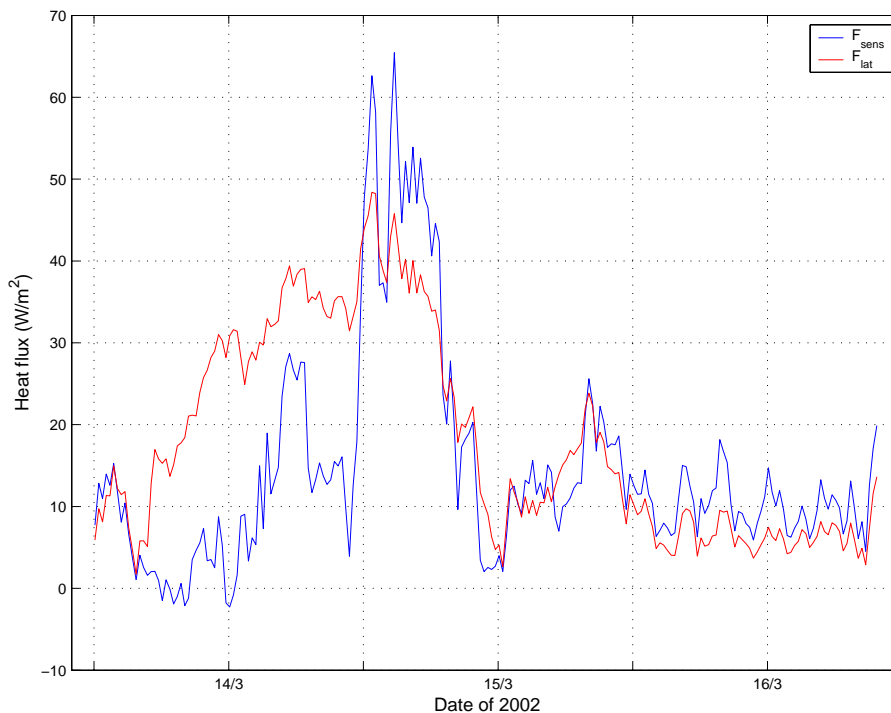
Figure 3.15 Turbulent fluxes of latent and sensible heat at the ice surface calculated from data from the weather station and ice surface temperatures. Date labels indicate midnight, 00.00 a.m.

Conductive heat flux

The conductive heat flux in the ice is a function of the temperature gradient in the ice and thermal conductivity of the ice, again determined by the ice temperature and salinity (equation 22). A common approach to calculate the conductive heat flux in ice is to use a bulk value determined from the temperature difference over the whole ice column and common ice salinity for first year ice. But the main interest in Kongsfjorden is to set up a budget on both the ice surface and bottom and therefore local temperature gradients are used. The surface conductive heat flux is calculated using the temperature values at surface and at 5 cm depth.

$$F_{c,0} = k_i \frac{T(0\,cm) - T(5\,cm)}{0.05} \tag{45}$$

The thermal conductivity, k_i, is determined using the mean temperature in the 0 - 5 cm depth interval and the salinity in the same interval obtained from the ice core presented in figure 2.2. $F_{c,0}$ is plotted in figure 3.16.

Ice thicknesses were measured once a day and the measurements were done manually by drilling a hole and measure the thickness. According to these measurements, the ice thickness increased from 28 cm to 31.5 cm during the period from 13th to 16th of March. This makes it difficult to choose what thermistors to use to calculate the conductive heat flux in the lower part of the ice. The temperature difference between 25 cm and 27.5 cm is used to calculate the temperature gradient in the beginning of the period. Once the ice thickness has passed 30 cm, this interval should ideally be changed to 27.5 – 30 cm. But this creates an artificial jump in the heat flux because the temperature gradient is lower closer to the water and therefore the flux is calculated as

$$F_{c,-h} = k_i \frac{T(25\,cm) - T(27.5\,cm)}{0.025} \tag{46}$$

for the whole period. $F_{c,-h}$ is also plotted in figure 3.16 and the mean values of $F_{c,0}$ and $F_{c,-h}$ are 59.7 W/m^2 and 57.5 W/m^2, respectively.

Variations in $F_{c,0}$ are large, much larger than the variations in $F_{c,-h}$, which is relatively constant during the period (figure 3.16). The adjustment of the ice surface temperature to the air temperature is more rapid than the adjustment of temperature at 5 cm depth in the ice, which make the temperature gradient and consequently $F_{c,0}$ vary largely during the period.

Calculations of fluxes at other depths in the ice show that larger mean values can be found in the interior of the ice, and using the temperature difference between surface and bottom gives a conductive heat flux with a mean value of 62 W/m^2. This discrepancy might be linked to

interior temperature changes. The heat budget for the interior of the ice column is treated separately in a later section.
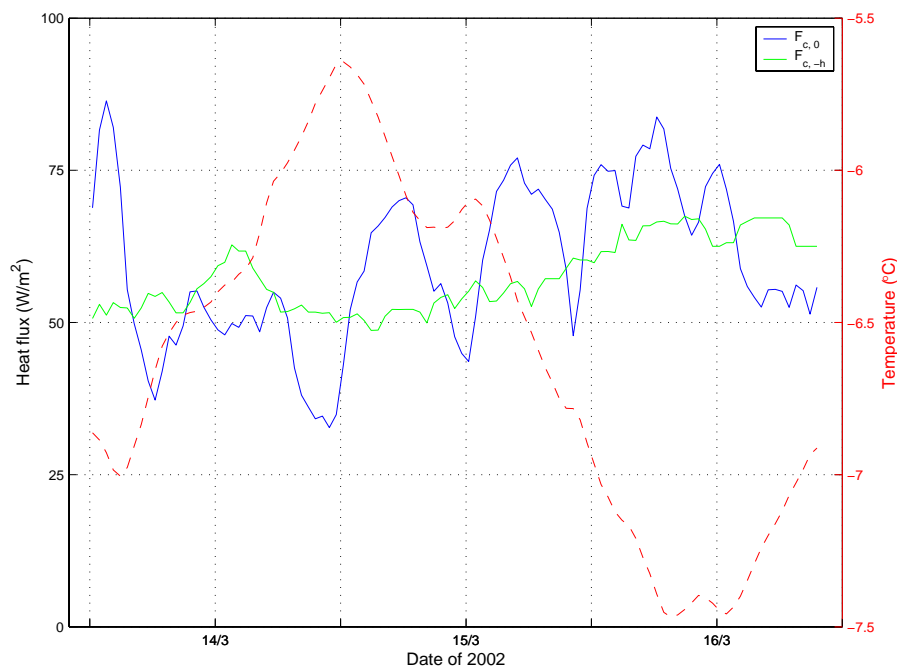

Figure 3.16 Conductive heat flux at the ice bottom ($F_{c,-h}$) and ice surface ($F_{c,0}$). Red dotted line shows the mean ice temperature in the same period. Date labels indicate midnight, 00.00 a.m.

Ocean heat flux

The turbulent heat fluxes measured by the TIC on mast#1 are calculated using the eddy correlation method and values are obtained from 15 minutes realizations as for the velocities and temperatures in section 3.2.6. Heat fluxes are plotted in figure 3.17. A more detailed explanation of the flux calculations is given in the Appendix, section 7. Due to bad weather no data from the turbulent masts were obtained on March 14th. The mean value over the period is 12.7 W/m^2, but the standard deviations indicate large variations within the time intervals (figure 3.17).

Published results of directly measured ocean heat fluxes are sparse and most of the experimentation is performed in the deep ocean, not in fjord conditions as in Kongsfjorden. But Shirasawa *et al.* (1997) performed an experiment measuring fluxes under thin ice in Saroma-ko Lagoon in Japan with a similar instrumental setup. They measured an ocean heat flux with a mean value of 57.9 W/m^2 over a period of two days. Measured velocities in Saroma-ko Lagoon were also larger than in Kongsfjorden, with a mean of 4.5 cm/s, but the calculated friction velocity, 0.13 cm/s, is comparable to the one calculated in Kongsfjorden. In

Saroma-ko Lagoon the large fluxes might be the result of a relative high water temperature; measured temperatures were around -1˚C, which imply that large amounts of heat are available for mixing towards the surface, in contrast to Kongsfjorden where temperatures were about -1.6˚C.

McPhee (1992) related measured ocean heat fluxes to the properties of the mixed layer, temperature elevation above freezing, and properties of the turbulent flow close to the surface represented by the friction velocity. From these parameters he found a turbulent Stanton number used to parameterize the heat flux from the mixed layer properties (equation 19).

The mixed layer in Kongsfjorden had a mean temperature of -1.61˚C, measured with the inner RCM and a mean salinity of 34.7 psu, which is the mean of all the CTD profiles at 12 m depth during the period. That means that the mixed layer has a temperature elevation of

$$\delta T = T_{ml} - T_f(S_{ml}) = 0.3˚C \tag{47}$$

which together with the friction velocity of 0.15 cm/s indicate a Stanton number $c_H = 0.0069$ from equation 19.

McPhee (1992) analysed data from three different ice drift experiments and ended up with Stanton numbers in the range 0.005 – 0.006 for the measured heat fluxes.

Velocities measured in Kongsfjorden are generally small and variable in both magnitude and direction. This lack of a "uniform" background current makes it more difficult to separate the turbulent fluctuations from the mean properties of velocity, temperature and salinity, which introduces another uncertainty into the calculation of heat flux, salinity flux and the Stanton number.

Ice/atmosphere interface

Comparing the fluxes at the ice/atmosphere interface makes it possible to set up a heat budget for the ice/atmosphere interaction, plotted in figure 3.18. F_{up} is the sum of fluxes away from the interface, in this case the sum of sensible heat flux, latent heat flux and net long wave radiation. F_{down} is the fluxes towards the interface, in this case the conductive heat flux, $F_{c,0}$. Since the short wave radiation is not absorbed at the interface, this flux is not considered in the interface budget.

As visible in figure 3.18, the mean value of F_{up} is slightly larger than F_{down}, the difference is plotted as the dashed green line in figure 3.18 and has mean value of 7.3 W/m². From the plotted lines it seems like F_{down} is trying to adjust to F_{up}, which means that the ice temperatures and the heat fluxes in the upper part of the ice are trying to adjust to the

atmospheric forcing. The discrepancy in the mean value over the whole period is assumed to be a result of inaccuracy in the atmospheric heat flux calculations and measurements. On shorter time scales, the large deviations from zero in the difference between F_{up} and F_{down} are assumed to be due to a longer response time in the ice than in the air. From figure 3.18 it seems that the response time of the air is on the order of tenths of minutes while the response time in the ice is on the order of hours.

Ice/ocean interface

At the underside of the ice, measurements of the turbulent ocean heat flux and the conductive heat flux in the lower part of the ice are available. But observations of ice thicknesses and ice growth are sparse, usually limited to one thickness measurement per day. This and the fact that ice thickness might vary within a small horizontal area create a large uncertainty in the calculations of the balance at the underside of the ice. The method is here to turn everything around and assume balance between the fluxes at the underside and let the ice growth be the unknown. Then one can compare the calculated ice growth rate with actual measurements. In figure 3.17 the fluxes are plotted for the given period. If it is assumed that there is balance between the fluxes at the ice/ocean interface, a flux resulting from freezing/melting of new ice must "cover up" the difference between F_c and F_w. F_{freeze} then has a mean value of 44.9 W/m^2 and the variation of this flux through time is also plotted in figure 3.17. The dotted area of F_{freeze} is due to lack of measurements of ocean heat flux in this period.

Ice thicknesses were measured once a day and measured ice thickness on March 13th 08.25 was 28 cm. From this initial thickness, the growth of new ice is calculated using equation 42 and the calculated F_{freeze} from figure 3.17. This gives an ice thickness development shown in figure 3.19 with a mean calculated ice growth in the given period of 4.4 cm. In the "dashed area" of F_{freeze} in figure 3.17 the turbulent ocean heat flux is assumed to be constant and equal to the mean of the last measurement before and the first measurement after the data "gap". The standard deviations of F_w are used to calculate an upper and a lower limit of F_{freeze} giving the upper and lower limit of the calculated ice growth shown in figure 3.19. For comparison, the measured ice thicknesses are also plotted.

The measured thicknesses are within the limits of the calculated ice thickness, but ice growth calculated from $F_c - F_w$ seems to overestimate freezing at the underside of the ice. Especially in the second half of the time period, this calculation overestimates the ice growth.
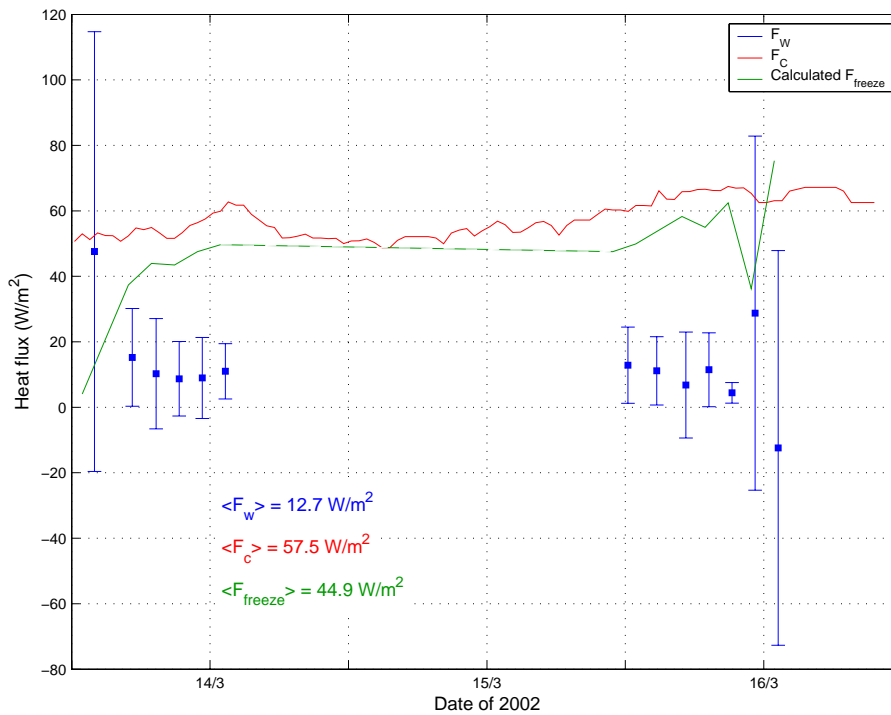
Figure 3.17 Heat balance at the underside of the ice. Error bars on F_w indicate ±1 standard deviation and date labels indicate midnight, 00.00 a.m.
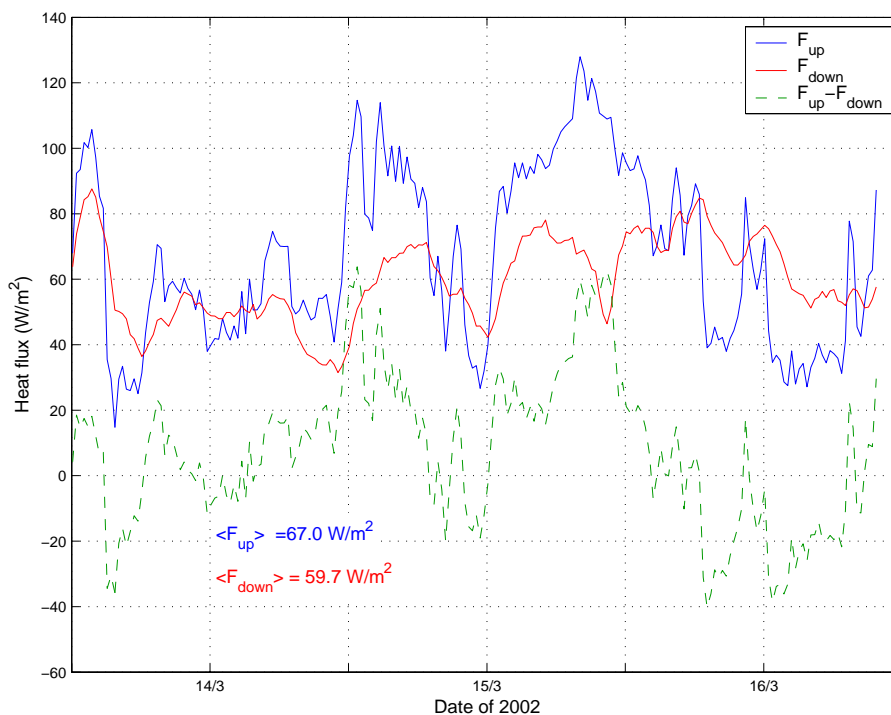

Figure 3.18 Comparison of heat fluxes at the ice/atmosphere interface. F_{up} is the sum of fluxes away from the interface; latent heat flux, sensible heat flux and long wave radiation and F_{down} is the fluxes toward the interface, the conductive heat flux $F_{c,0}$. Date labels indicate midnight, 00.00 a.m.

Using the residual method (see section 2.2.4) in determining the ocean heat flux from the measured ice thicknesses, suggest a larger F_w than measured, with values around 25 W/m^2, about twice the measured ocean heat flux. But there are uncertainties concerning the heat flux measurements. First of all there is a variation in the measured ocean heat flux within every time interval, visible in the end as "wide" limits for the calculated ice growth. Second, the ocean heat flux is assumed to be constant in the period of March 14th – 15th, when there is a lack of measurement from the turbulence mast. This period was dominated with large wind speeds, which may induce more mixing in the water column and an enhanced heat flux, which would give a smaller F_{freeze} and ice growth in this period. A third uncertainty is the conductive heat flux. Early in the period the temperature gradient was measured close to the lower ice edge and the measured values give a good indication of the temperature gradient at the interface. But during the period the ice grew thicker and the temperature gradient was measured further away from the ice boundary. In addition, newly formed ice contains more water and temperature gradients are lower compared to the more solid ice closer to the interior of the ice column. The value of F_c is increasing slightly during the period and the mean measured value is probably larger than the actual F_c at the interface. This leads to an overestimation of F_{freeze}.
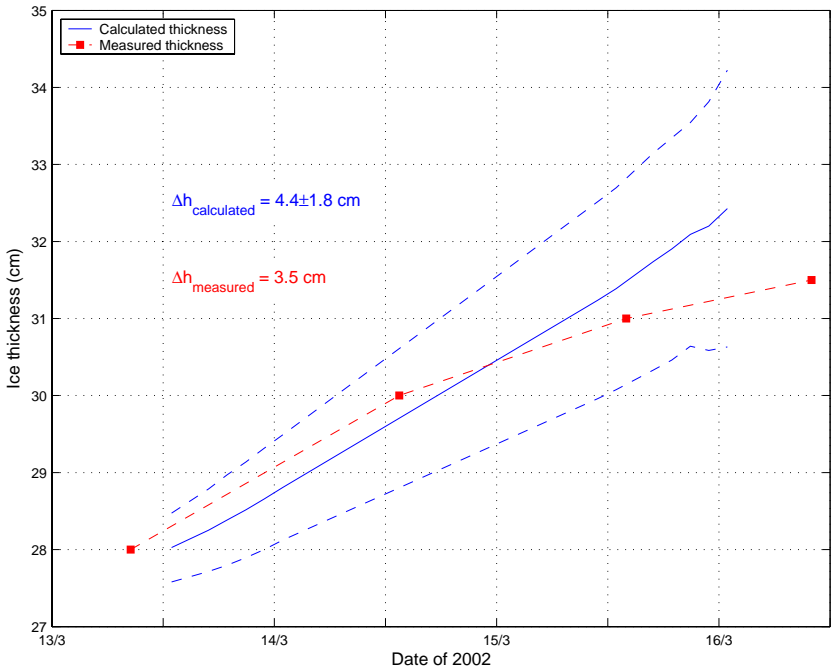

Figure 3.19 Ice thicknesses measured in Kongsfjorden (red squares) together with calculated time development of the ice thickness from F_{freeze} in figure 3.17. Dashed lines are the upper and lower limit of the ice thickness calculated from the standard deviations of F_w Date labels indicate midnight, 00.00 a.m.

Also Shirasawa *et al.* (1997) compared directly measured ocean heat fluxes with fluxes obtained using the residual method. They found that the difference in the two methods was of size ± 20 – 30 W/m² during the days of their field experiment. They also pointed out that the difficulty of estimating the "correct" flux value using the residual method increased with decreasing ice thicknesses.

The growth rate of new ice could be verified by the turbulent salinity flux close to the underside of the ice. But although the calculated salinity flux combined with equation 44 indicates ice growth in the same range as measured, the large standard deviation of the salinity fluxes makes the uncertainty in this method too large. This results in an uncertainty in ice growth rate of about ±3 cm over the whole period and calculated salinity flux in Kongsfjorden can therefore not be used to verify neither the measured nor the calculated ice growth rate.

Interior of the ice

In the interior of the ice, the conductive heat flux is often assumed to be constant throughout an ice column with a constant temperature gradient. If that is correct, the ice temperature will always be determined by the temperatures at the upper and lower interface. As shown previously, $F_{c,0}$ has a mean value of 2.2 W/m² larger than $F_{c,-h}$, and the variation in the flux at the ice surface is much larger than at the ice bottom (figure 3.16). This divergence/convergence in conductive heat flux should be possible to observe as a decreased/increased ice temperature. In figure 3.16 the mean ice temperature is plotted together with $F_{c,0}$ and $F_{c,-h}$, and it is clearly visible that the temperature is increasing in the periods where $F_{c,-h}$ is larger than $F_{c,0}$ and decreasing when the situation is opposite.

To investigate these changes more closely, changes in temperature gradients in the whole ice column have to be studied and as shown in figure 3.20 temperature gradients throughout the ice column are not constant. As mentioned in section 3.2.4, there is one thermistor at the ice surface and then one thermistor every cm from 5 cm to 25 cm depth. Below 25 cm there is one thermistor every 2.5 cm. There seems to be different thermal properties in different layers, leading to a difference in temperature gradient and consequently a difference in conductive heat flux.

Theoretically, if all horizontal temperature gradients are ignored, the temperature variation in a given volume of sea ice has two contributions; absorption of short wave radiation and a

divergence/convergence of conductive heat flux in the ice volume. Knowing these parameters would make it possible to calculate the temperature changes in the ice volume. To check if the temperature variations can be determined from only these contributions, a simple calculation is made. At every level in the ice between 6 and 24 cm depth a small volume of height 2 cm is constructed and the fluxes into and out of this volume are calculated according to equation 48 (figure 3.21).

$$F_{in} - F_{out} = \left[F_{c,z-1} + I(z+1)\right] - \left[F_{c,z+1} + I(z-1)\right]$$
$$= \frac{h_i c_i \rho_i \Delta T}{\Delta t} \tag{48}$$
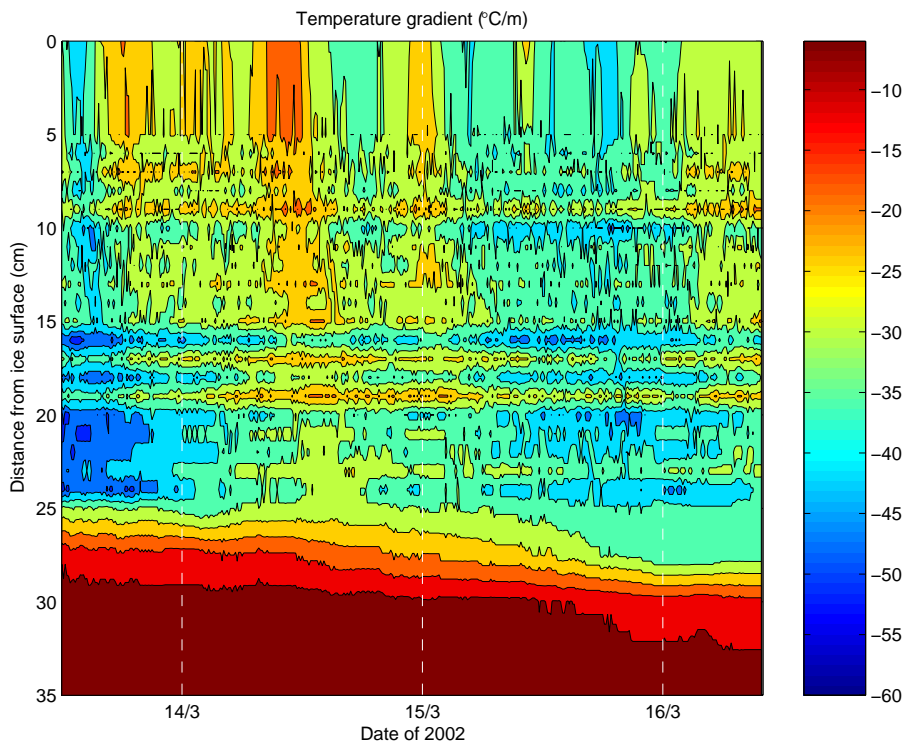
Figure 3.20 Temperature gradients at different depths in the ice calculated from the thermistor data. Date labels indicate midnight, 00.00 a.m.

ΔT is here the change in temperature in the ice volume, Δt is the time in seconds between the measurements, h_i is the height of the ice volume and c_i and ρ_i are the specific heat and density of sea ice, respectively. To determine the actual thermal conductivity at every level in the ice, the temperature at the given level and the ice salinity at the same level determined from an ice core are used together with equation 22. The difference between F_{in} and F_{out} will result in a temperature increase or decrease as described in equation 48. After calculating the temperature variation at each level, the contributions from every level from 6 to 24 cm depth

are summed up and the mean temperature development through time is calculated with the measured mean ice temperature at March 13th 12.00 used as a start value. This calculated temperature development compared to the measured temperature is shown in figure 3.22. In the calculations different parameters are adjusted and the best correlation between calculated and measured ice temperature occurs with a slight modification of the thermal conductivity:

$$k_i = k_0 + \beta \frac{S_i}{T_i} - 0.22 \qquad (49)$$

The constants k_0 and β are given in section 2.2.3. This 10 – 15% lowering of the thermal conductivity agrees well with the result of Trodahl *et al.* (2001) where they calculated the thermal conductivity from measurements to be ~10% lower than assumed by most models. Without the modification of k_i, the convergence of conductive heat in the ice is overestimated, resulting in a mean ice temperature about 1˚C above the measured temperature at the end of the period.
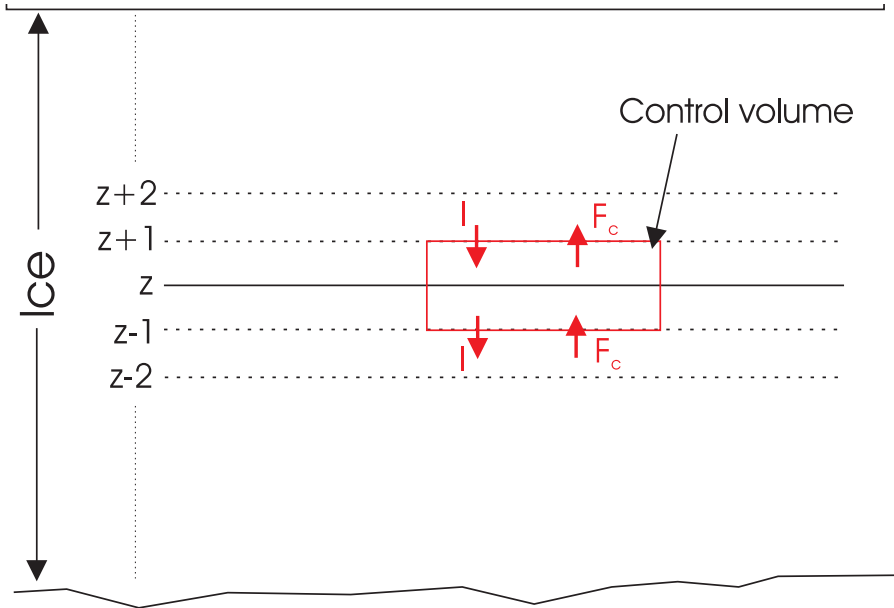
Figure 3.21 The temperature development in a small volume of ice is calculated from the convergence/divergence of conductive heat flux (F_c) and absorption of short wave radiation (I).

A modified k_i would also affect the heat budgets at the interfaces. At the ice/atmosphere interface, a reduced k_i will reduce $F_{c,0}$, which will double the mean divergence from 7 W/m^2 to about 14 W/m^2 at the interface. The opposite effect will be experienced at the ice/ocean interface, where a reduced k_i will reduce the calculated ice growth to 3.7 cm over the whole period. This is close to the measured ice growth of 3.5 cm. However, it is important to

remember that the modification of the thermal conductivity is calculated for the ice column at 6 - 24 cm depth and is therefore not automatically valid for the ice adjacent to the surface and bottom.
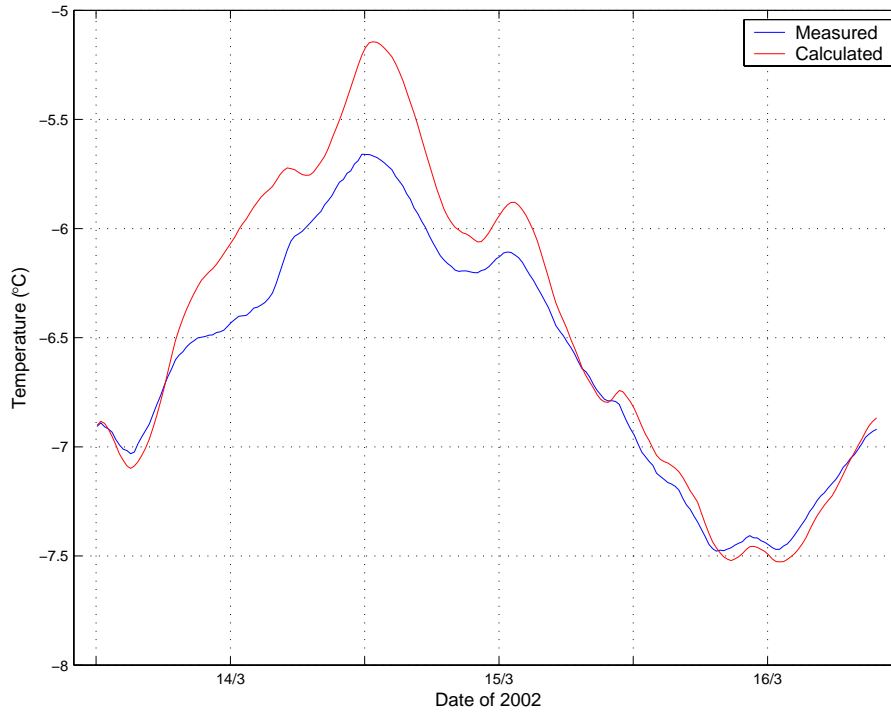

Figure 3.22 Mean measured ice temperature and mean calculated ice temperature. Date labels indicate midnight, 00.00 a.m.

4 Van Mijenfjorden

4.1 Material and methods

Field work in Van Mijenfjorden was carried out as a part of the course AGF 211 "Air, Sea, Ice Interaction" at the University courses on Svalbard (UNIS). It took place in the period March 19th to March 22nd 2002 close to Svartodden in Van Mijenfjorden (figure 4.1).

4.1.1 Area

Van Mijenfjorden is a 70 km long fjord stretching north east from the western coast of Spitsbergen (for location, see figure 1.1). The mouth of the fjord is 10 km wide but it is blocked by Akseløya, a 8.5 km long island. This leaves a 1 km wide passage on the northern side and two small passages of 200 m and 500 m on the southern side (Kangas, 2000) and all passages around Akseløya can be dominated by strong tidal currents. The mean depth in the outer part of the fjord is about 70 m, while mean depth in the inner part is about 30 m. Mean circulation in the fjord is cyclonic and mainly controlled by the tide in winter, when the fjord is ice covered, and by tide, modified by wind and fresh water runoff in summer (Kangas, 2000). Kangas (2000) measured mean current speed of 3.1 cm/s in mid April 1999 at 2 m depth, at a location close to Svartodden.

During winter ice freezing modifies the water masses in the fjord and in late winter the fjord is basically homogenous with temperatures close to freezing and salinities about 34.5 psu for the whole water column (34.3 psu in March 1998, measured by Kangas (2000)).

Measured ice thicknesses in Van Mijenfjorden are normally in the range 80 – 110 cm, dependent on the time of year and location in the fjord (Kangas, 2000; Nilsen, 2001).

Ice conditions in Van Mijenfjorden are quite stable, except close to the mouth of the fjord where stronger currents commonly lead to break up of ice. During the days of field work the ice thickness was about 80 cm with a 10-20 cm thick layer of wind packed snow on top. Air temperatures in the same period were low, ranging from -28˚C to -13˚C, with a mean value of -19˚C (figure 4.2).
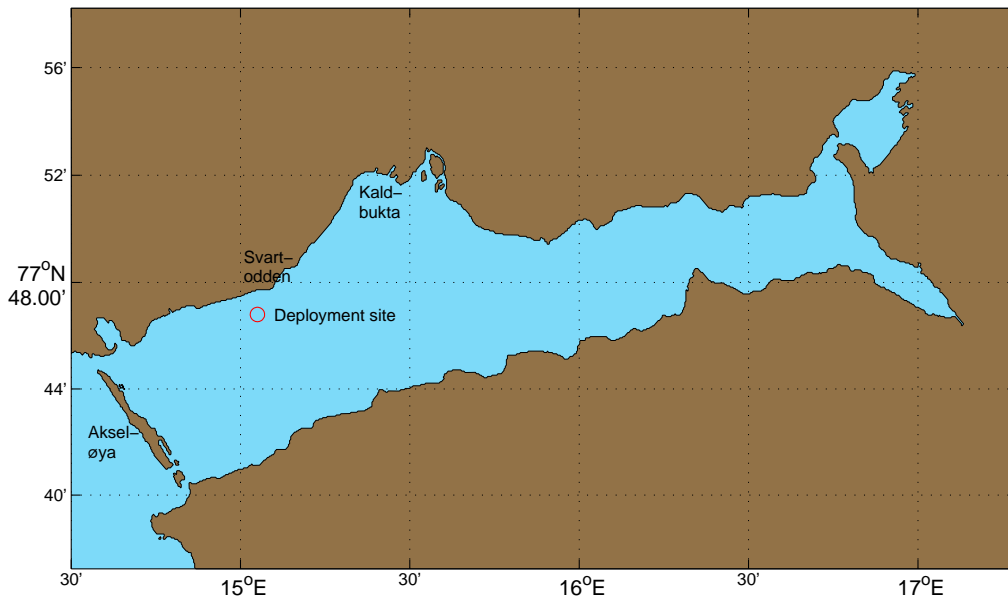
Figure 4.1 Map of Van Mijenfjorden showing the deployment site close to Svartodden.

4.1.2 Instruments

In Van Mijenfjorden, two turbulence masts were used with the same configuration as in Kongsfjorden (figure 3.2). Sampling frequencies were also the same; 1Hz for mast #1 and 2Hz for the ADV on mast #2 (section 3.1.2). The masts were deployed as in Kongsfjorden, about 1.5 m apart horizontally, both with the measuring level 1 m below the underside of the ice.

In addition to the measurements of turbulent fluxes, UNIS made measurements with other instruments, including current meters, a weather station, thermistors in the ice and in the snow and an ultrasonic current meter (UCM). The UCM was situated only 5 m from the turbulence masts while the other instruments were spread out over a larger area in the fjord. Ice cores were also taken to examine temperature and salinity profiles in the ice at different locations. More details about the Van Mijen work and results are found in Nilsen (2002).

In this Van Mijenfjorden section, results from the turbulence mast are used together with temperature data from the weather station, in addition to results presented in the data report from UNIS (Nilsen, 2002).

4.2 Results

4.2.1 Weather station

Air temperatures from the actual time period are plotted in figure 4.2. Data are from the weather station situated about 100 m from the deployment site of the turbulence masts. Temperatures are measured at two levels, 0.45 m and 1.45 m above the snow surface.
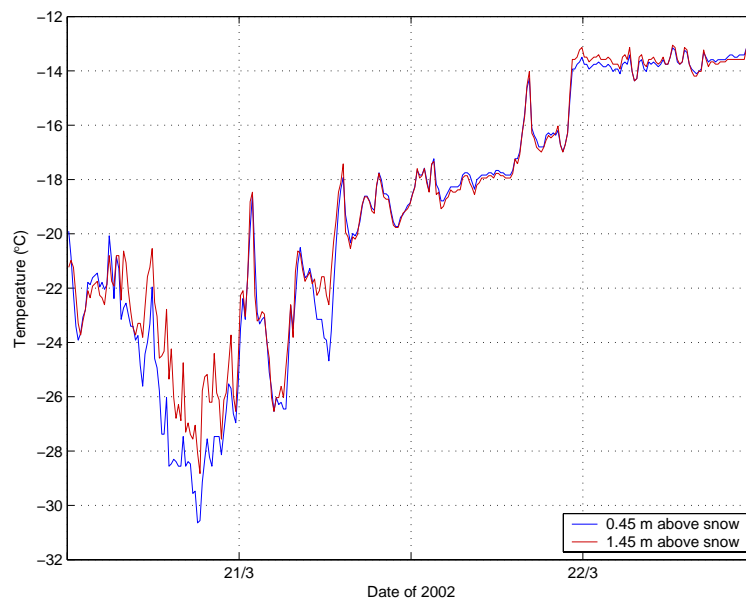

Figure 4.2 Air temperatures in Van Mijenfjorden. Temperatures are measured at two levels above the snow surface. Date labels indicate midnight, 00.00 a.m.

4.2.2 Turbulence masts

In figure 4.3 horizontal speeds from mast#1 are shown, both speed and temperature data are grouped in 15 minutes intervals and then averaged over 1 hour, the same method as used in Kongsfjorden. Speeds are generally higher than in Kongsfjorden, mean speed from mast#1 in Van Mijenfjorden is 6.6 cm/s, but the variation in measured speed are of the same order as in Kongsfjorden.

The same problems regarding synchronization of mast#2 data were present in Van Mijenfjorden, so the velocities from this mast are not used in further calculations. But the current speeds from this mast are of the same order as mast#1, with a mean value of 7.2 cm/s, as also shown in figure 4.3.

The turbulent fluctuations in velocity and the mean velocity in Van Mijenfjorden is of the same order as in Kongsfjorden (section 3.3.5), the ratio $\frac{|U|}{|u'|}$ is about 7 for the data from mast#1.

Variations in water temperatures are small, the mean standard deviation is only 0.001˚C and temperatures are always close to freezing, which is visible in data from both masts (figure 4.4). Also the temperatures are averaged over 1 hour and mean temperatures are -1.9˚C from both mast#1 and mast#2.

4.2.3 Ice cores and thermistors

Data from ice cores taken in the same time period as the turbulence mast data are not available, but salinity data from ice cores taken later (April 7th – April 10th) are used to find a typical salinity value of the first year ice in Van Mijenfjorden. These data show higher salinities at bottom and surface, a typical salinity profile for first year ice, and mean salinities are in the range 4 – 5.5 psu (Nilsen, 2002).

A thermistor was deployed in the ice during the whole period of our field work and typical values of temperature gradients from this thermistor (Nilsen, 2002) are used in heat budget comparisons in later calculations.

4.3 Discussion

4.3.1 Turbulence masts

From the measured temperatures at the turbulence masts it is indicated that Van Mijenfjorden is a more typical Arctic winter fjord than Kongsfjorden, with temperatures close to the freezing point and small turbulent fluctuations in temperature. This is also confirmed by CTD measurements the same winter (Nilsen, 2002), and in results from earlier winter studies in Van Mijenfjorden (Kangas, 2000; Nilsen, 2001). As mentioned in section 2.1.4, the turbulent ocean heat fluxes at the underside of the ice are dependent on the available heat in the water column and the mixing efficiency at the ice/ocean interface. Friction velocities, u_*, calculated from data from mast#1, are shown in figure 4.5. The friction velocity has a mean value of 0.34 cm/s, a value about 2 times the values in Kongsfjorden (figure 3.14).
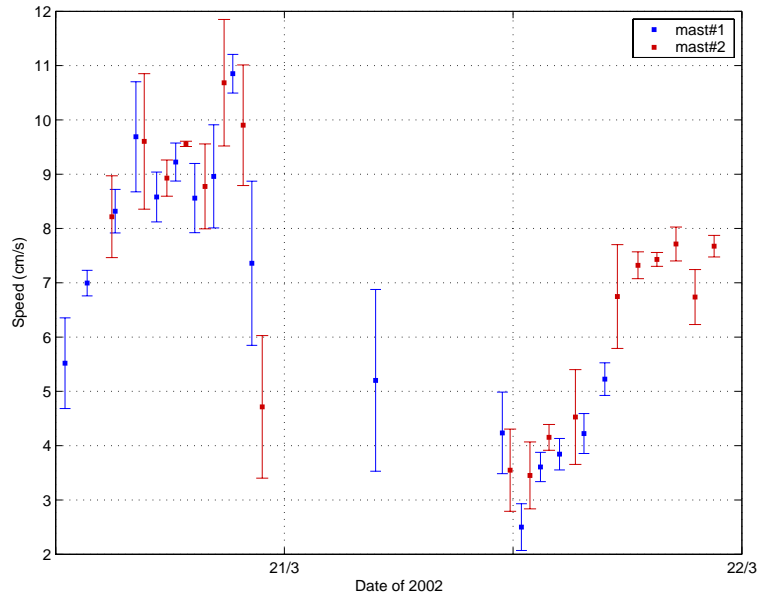
Figure 4.3 Horizontal speeds measured at turbulence mast#1 and #2 averaged over 1 hour. Error bars indicate ±1 standard deviation and date labels indicate midnight, 00.00 a.m.
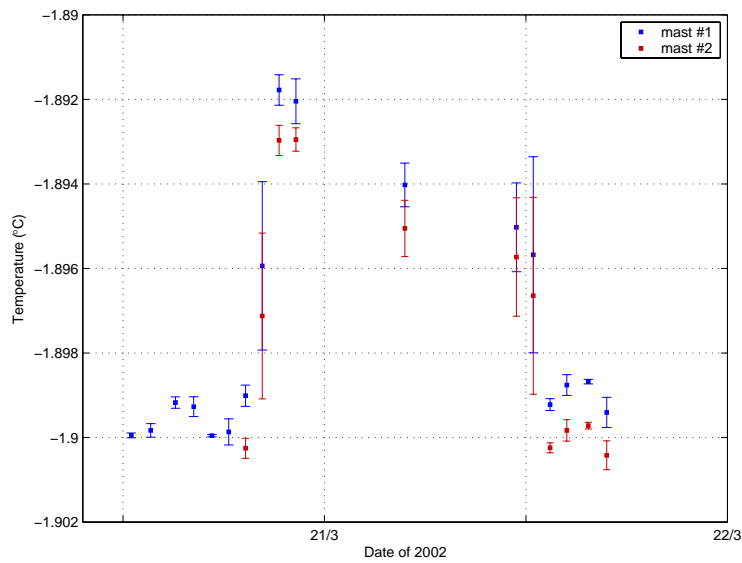

Figure 4.4 Temperatures measured at both turbulence masts, 1 m below the ice bottom. Values are averaged over 1 hour and error bars are ±1 standard deviation. Date labels indicate midnight, 00.00 a.m.

But, as the measured temperatures show (figure 4.4), the amount of available heat in Van Mijenfjorden is very small, indicating small heat fluxes. Heat fluxes, calculated using the eddy-correlation method, are shown in figure 4.6.
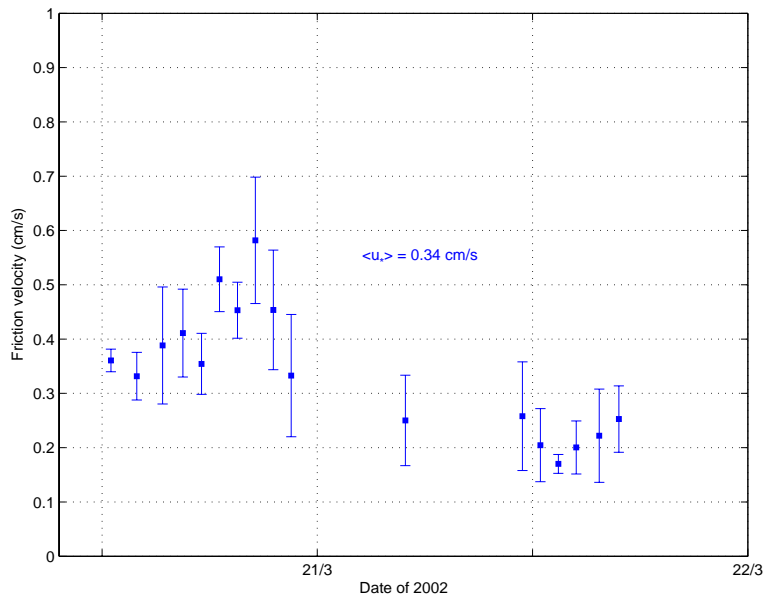
Figure 4.5 Friction velocities calculated from data from mast#1, values are averaged over 1 hour. Error bars are ±1 standard deviation and date labels indicate midnight, 00.00 a.m.
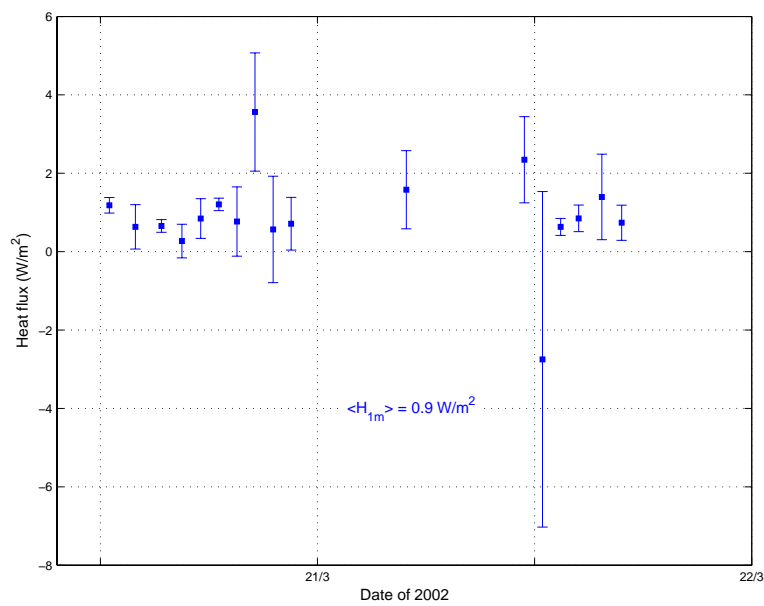
Figure 4.6 Vertical heat fluxes calculated from mast#1 in Van Mijenfjorden, averaged over 1 hour. Error bars are ±1 standard deviation and date labels indicate midnight, 00.00 a.m.

Mean value of the vertical heat flux is 0.9 W/m², a value much smaller than in Kongsfjorden (12.7 W/m²), but the standard deviations of the calculated heat fluxes are also of a much smaller range.

The small values of heat flux are comparable to fluxes measured in 2001, when a similar experiment was performed. In 2001, heat fluxes in the range $0.5 - 2$ W/m^2 were reported under similar conditions and at the same time of year (Nilsen, 2001).

From Nilsen (2002) CTD profiles show that in the given period typical temperatures in the mixed layer were about 0.01°C above freezing. Using this value as δT and assuming that u_* calculated at 1 m depth is valid as an interface value, a rough estimation of the Stanton number results in $c_H = 0.0065$ (equation 19). This value is in the same range as the corresponding value in Kongsfjorden (0.0069).

4.3.2 Heat budget

In Van Mijenfjorden, the instrumental set up does not allow a complete air/sea/ice heat budget comparison as in Kongsfjorden, but some factors can be evaluated to compare with and validate the calculated heat fluxes.

The turbulent salinity flux is an indication of freezing or melting of ice at the underside of the ice and the calculated fluxes are shown in figure 4.7. These fluxes are calculated as described in section 2.2.5. The mean salinity flux over our period of field work is $-1.14 \cdot 10^{-6}$ psu m/s. The negative sign and the magnitude of this flux indicate a net formation of new ice at a rate of 0.3 cm/day when the ice salinity, S_i, is assumed to be 4 psu (equation 44).
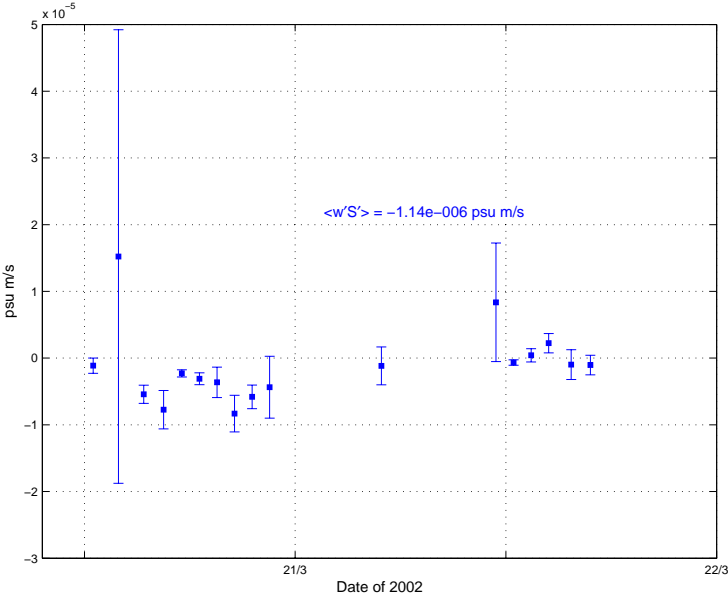

Figure 4.7 Vertical salinity flux measured at turbulence mast#1, 1 m below the ice. Data are averaged over 1 hour and error bars are ±1 standard deviation. Date labels indicate midnight, 00.00 a.m.

This is a very small ice growth, but can be reasonable since the ice is already close to what seems to be its equilibrium thickness of about 80 – 110 cm, as measured previous winters (Kangas, 2000; Nilsen, 2001). The ice salinity used in this calculation is from ice cores taken in the beginning of April and due to continuous brine drainage from the ice, the actual ice salinity might have been larger. If this is correct, the actual ice growth is smaller (equation 44). This ice growth together with the small ocean heat flux result in a net flux of heat towards the ice underside of ~11.5 W/m^2 and from heat conservation this implies that also $F_{c,-h} \approx 11.5$ W/m^2 (equation 29). From Nilsen (2002) thermistor data in the same time period show a temperature difference over the ice column of about 6°C, which gives a bulk value of F_c of about 15 W/m^2 for an ice thickness of 80 cm, an ice salinity of 4 psu and $k_i = 2$ W/m °C. These values are of the same order as the results above, but this is a very rough estimation, because the temperature gradient in the ice is determined visually from the report. The agreement is therefore no good validation of the values of the measured heat fluxes, but it can indicate that the measured fluxes are of the right order and also of an order as expected in these fjord settings with small amounts of heat available in the water column.

Another simple method to control the calculated values of turbulent heat fluxes is by the use of air temperature and water temperature. The air temperature is measured 0.45 m over the snow surface and with the reasonable assumptions $T_{snow\ surface} = T_{air}$, $T_{water} = -1.9$°C and conservation of heat flux at the ice/snow interface, it is possible to calculate the temperature gradients in the ice and the snow when both thicknesses are known (see sketch in figure 4.8).

The following parameters are used: $S_{ice} = 4$ psu, $h_i = 0.8$ m, $h_s = 0.2$ m, $k_i = 2$ W/m °C and $k_s = 0.17$ W/m °C (Massom et al., 2001), where h_i and h_s indicate thicknesses of ice and snow, respectively, and k_s is the thermal conductivity of snow. Using the mean value of T_{air} in the period March 19th – March 22nd, the conductive heat flux in the ice can be estimated to 11 W/m^2.

This also shows a good agreement with the calculated ocean heat flux, but it is necessary to be aware of the fact that the "real" turbulent heat flux can differ considerably from the calculated mean value without altering the roughly estimated heat budget significantly. Calculated mean value of the heat flux can be in the range 0.5 – 4.5 W/m^2 and still agree well with the other fluxes at the ice/ocean interface. But again, it gives an indication that the calculated heat fluxes are of the correct order compared to other measurements in the fjord and that the values are as expected in an Arctic fjord during winter.
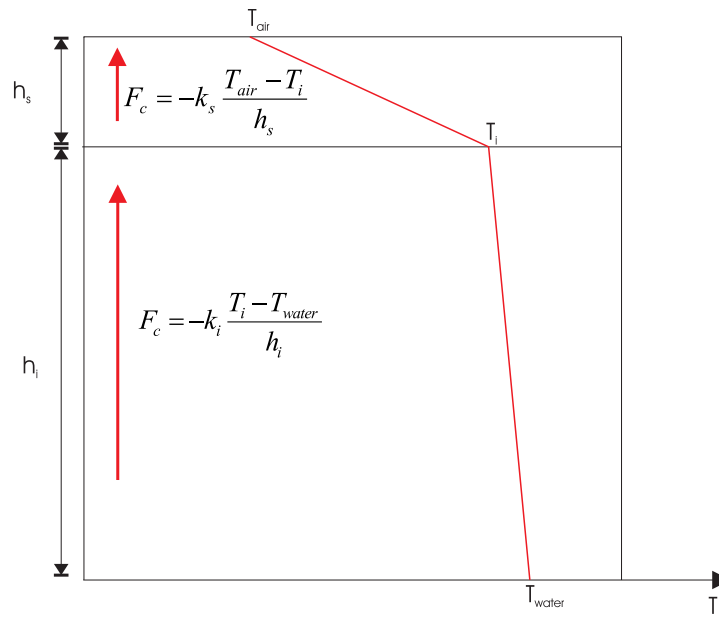
Figure 4.8 A sketch of the temperature gradients in the sea ice and in the snow cover. If T_{air}, T_{water}, k_i and k_s are known and heat conservation at the ice/snow interface is assumed, then T_i can be determined. Consequently the conductive heat fluxes in the ice and the snow can be determined.

5 Storfjorden and Whaler's Bay

5.1 Material and methods

During a cruise in March and April 2003 with the German ice breaker *FS Polarstern*, the TICs were used again at different locations in measurements of turbulent fluxes. The cruise was a part of the scientific programme WARPS (Winter ARctic Polynya Study) with the aim of investigating air/sea/ice interaction processes including both oceanography and meteorology studies. The cruise was carried out as a combination of measurements done from the ship, such as e.g. CTD measurements and measurements done from the ice during shorter periods. During these ice stations, the turbulence mast was deployed, normally at least 200 m away from the ship.

5.1.1 Areas

Over the period of the cruise, a total of five ice stations were carried out; three in Storfjorden and two in the area north of Spitsbergen (See map in figure 1.1). In this thesis, data from two of the stations in the outer part of Storfjorden and data from one station in the so called Whaler's Bay area are presented and discussed.

Storfjorden

Storfjorden is the area limited by Spitsbergen in the west and Barentsøya and Edgeøya in the east (figure 1.1). It covers an area of 13 - 14 000 km^2 and has a sill of 120 m depth approximately at the 77˚N latitude (Haarpaintner *et al.*, 2001). Inside, the maximum depth is about 190 m and the fjord has relatively wide shelf areas. Loeng (1991) assumes a cyclonic coastal current in Storfjorden, originating from the East Spitsbergen Current which flows southward on the eastern side of Barentsøya and Edgeøya.

The Barents Sea area and Storfjorden are assumed to be suitable sites for production of dense bottom water, due to shallow coast- and bank-areas (Midttun, 1985) and in Storfjorden observations of dense water produced and exported out of the fjord, have been done (e.g. Quadfasel *et al.*, 1988; Schauer and Fahrbach, 1999). Due to topographic conditions, the Storfjorden area is suited for polynya formation and the formation and existence of polynyas

result in increased ice formation, brine release and modification and densification of the water masses inside Storfjorden (Haarpaintner *et al.*, 2001).

Whaler's Bay

North of Spitsbergen there is a shallow, continental shelf area, called Whaler's Bay (figure 1.1). In the north-west, this area is connected to the Yermak Plateu, over which a branch of the West Spitsbergen Current (WSC) brings relatively warm water into this shallow area. When this warm, originally Atlantic Water, enters the area, large amounts of heat are available in the water column. This leads to large heat fluxes and subsequently large melting rates when this water encounters the ice from north and a very distinct mixed layer of ~100 m depth is formed (Meincke *et al.*, 1997).

In winter, this mixed layer stretches all the way down to the core of Atlantic Water, from which heat is transferred upward by turbulent mixing and double diffusive processes (Meincke *et al.*, 1997). The continental slope areas north and north-east of Spitsbergen are assumed to be important areas for heat exchange between ocean and atmosphere. E.g. Coachman and Barnes (1963) assumed that most of the latent heat in the WSC is lost while flowing eastward along the continental slope. Also other authors (e.g. Aagaard *et al.*, 1987; Dewey *et al.*, 1999) have calculated large heat fluxes from the WSC due to mixing processes along the continental slope.

5.1.2   Instruments

On the WARPS-cruise, the TICs were used in another configuration than in Kongsfjorden and Van Mijenfjorden. Both turbulence masts were put together to one long mast of 6 m length, where mast#1 was the upper mast and mast#2 the lower. In between the TIC-masts, an additional mast containing the SBE9+ "fish", a compass, a pressure sensor and a vane was attached (figure 5.1).

The upper end of the whole 6 m mast was attached to a wire which allowed it to rotate freely according to the mean current. On the ice, a metal frame attached to a wooden platform and covered with a tent was used as a shelter over the deployment hole and a hand winch attached to the frame was used to lower and raise the mast. All UPMs were attached to the mast and all data were transmitted to the deck unit through a 25 m or a 100 m cable. Sampling frequencies were 2 Hz for all instruments. The deck unit was situated in a plastic shelter, called "tomato", together with the laptop, and as before, power was supplied by a generator.

With this configuration the mast is measuring turbulent fluxes at two levels, 4 m vertically apart and on the WARPS cruise the upper cluster was usually situated 1 m below the ice. With the use of 30 kg ballast at the bottom, the mast remains vertical and the vane makes the ADVs point towards the mean current, avoiding disturbance from the mast itself.

In Storfjorden and Whaler's Bay the ice is drifting and to record the ice drift during the periods of deployment, a GPS was used and position data were recorded to the laptop at a frequency of 1 Hz.

The plastic "tomato" is constructed to be lifted by helicopter with all the equipment inside, making it very easy to transport the equipment from the ship and to a favourable deployment site nearby.

In addition to the turbulence mast, some CTD data acquired from the ship at the positions of the ice stations are used.
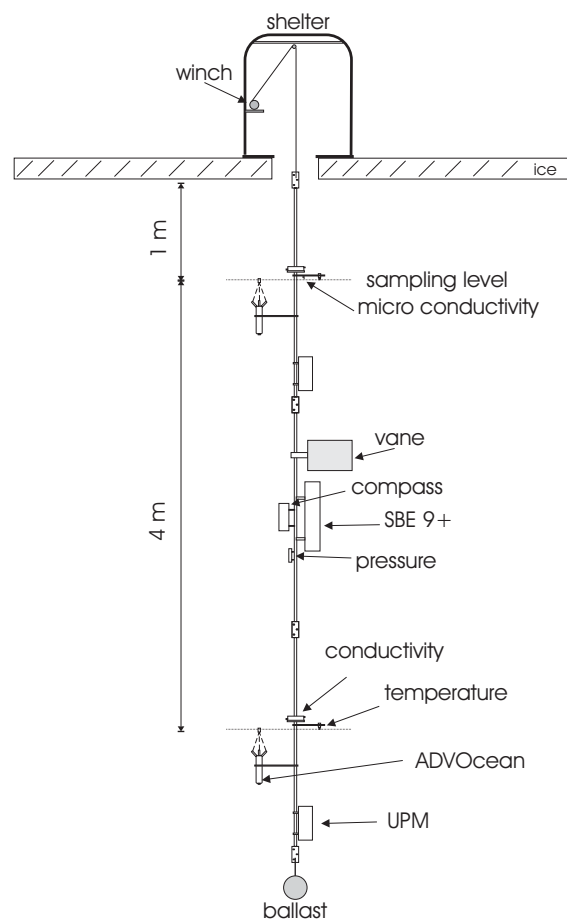
Figure 5.1 Compilation of the turbulence mast used during the WARPS cruise in Storfjorden and Whaler's Bay.

5.2 Storfjorden

Due to rough ice conditions, the cruise was performed mostly in the outer parts of Storfjorden. Ice conditions were a mix of multi year ice transported into Storfjorden by the East Spitsbergen Current and locally frozen first year ice. The ice cover contained a lot of ridges, rafted ice floes and open leads. A relatively large ice floe was needed to carry out the ice station work and on the two ice stations in Storfjorden floes of first year ice with thicknesses of 60 cm and 80 cm were chosen. The first station took place on March 16th -17th, while the other one took place on March 23rd.

Positions and drift tracks for the two stations, hereafter called station 1 and station 2, are shown in figure 5.2.
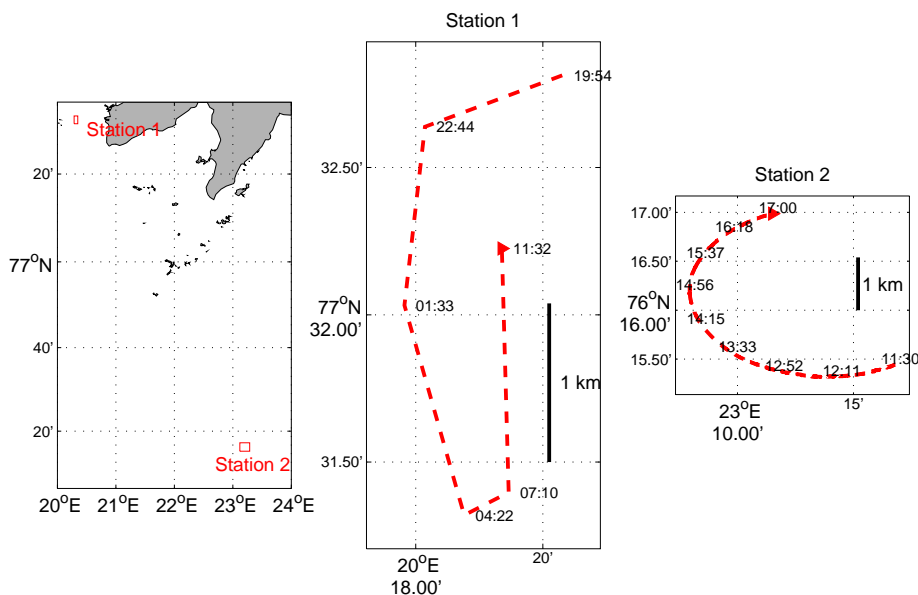
Figure 5.2 Locations and drift tracks for station 1 and station 2 in Storfjorden.

5.2.1 Results

The structure of the water column at station 1 and station 2 is revealed by the CTD profiles shown in figure 5.3. CTD profiles at station 1 and station 2 are obtained on March 17th 00.43 and March 23rd 06.34, respectively.

Data from the turbulence mast show that measured horizontal velocities in Storfjorden are in the range 5 – 11 cm/s, shown in figure 5.4 and figure 5.5. Velocity and temperature data are treated as in Kongsfjorden; grouped in 15 minutes intervals and then averaged over 1 hour. At

station 1 the mean speeds were 7.1 cm/s and 8.6 cm/s measured 1 m and 5 m below the ice, respectively. At station 2 the corresponding mean speeds were 7.3 cm/s and 5.3 cm/s. Water temperatures measured with the turbulence mast are close to freezing at both stations (figure 5.6 and figure 5.7), mean values are -1.9°C for station 1 and -1.89°C for station 2 and at both stations the same mean value was recorded at both levels. Differences between temperatures measured at 1 m and 5 m depth at both stations in Storfjorden are very small and differences are most likely caused by a difference in calibration between the two temperature sensors. Both temperature and horizontal velocity data are averaged over 1 hour.

5.2.2 Discussion

At station 1 the CTD profile reveals an upper layer of 40 m thickness with temperatures close to freezing, which again leaves small amounts of heat for mixing towards the surface. If data from the cluster at 1 m depth are used, a mean friction velocity of 0.41 cm/s is calculated, which is slightly higher than the value measured in Van Mijenfjorden (0.34 cm/s). Friction velocities from station 1 are shown in figure 5.8. But the temperature data from the same cluster show that even though mixing activity is present in the upper layer, there are only small fluctuations in the measured temperature and the mean standard deviation in temperature is only of order 10^{-4}°C, indicating that only small amounts of heat are "carried" by the turbulent eddies. Calculations of the heat fluxes from the first station are shown in figure 5.9, mean values are 0.4 W/m^2 and 0.7 W/m^2 at 1 m and 5 m depth, respectively. These values are small, but expected according to the CTD profile and the temperature measurements.
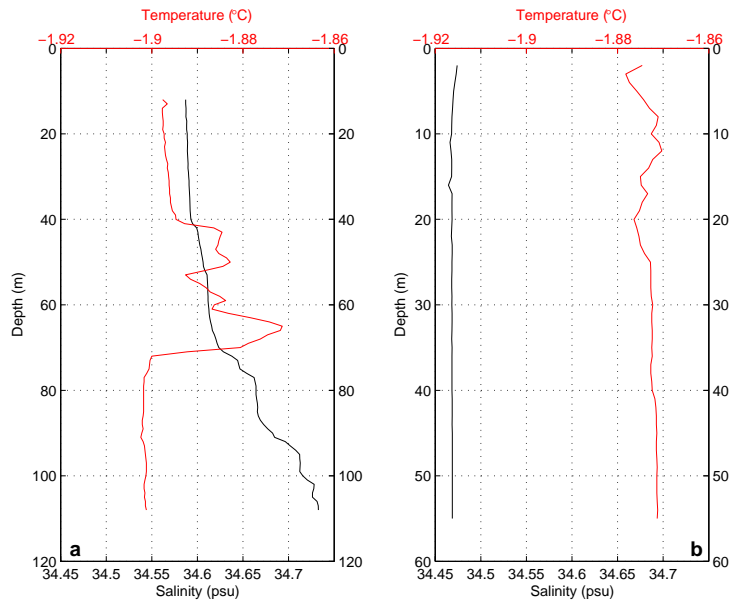
Figure 5.3 Profiles of temperature and salinity obtained at (a) station 1 on March 17th 00.43 and (b) station 2 on March 23rd 06:34.
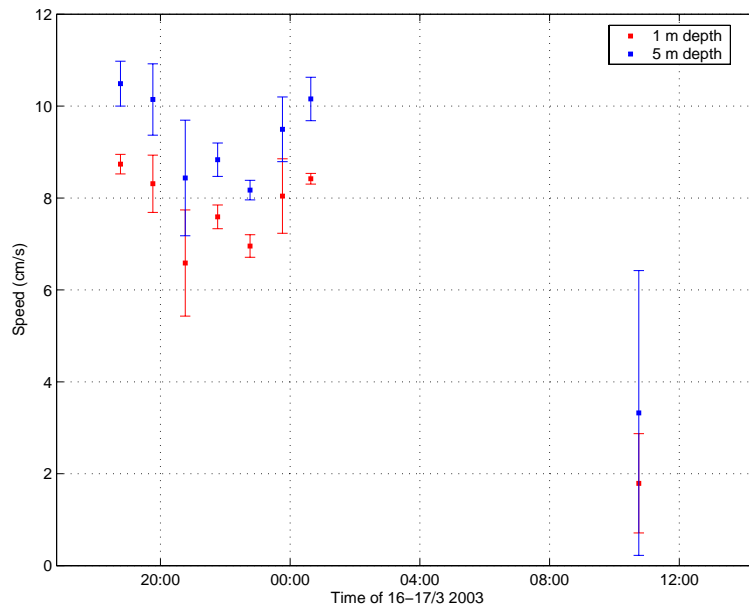

Figure 5.4 Horizontal speeds measured at two depths with the turbulence mast at station 1, data are averaged over 1 hour and error bars indicate ±1 standard deviation.
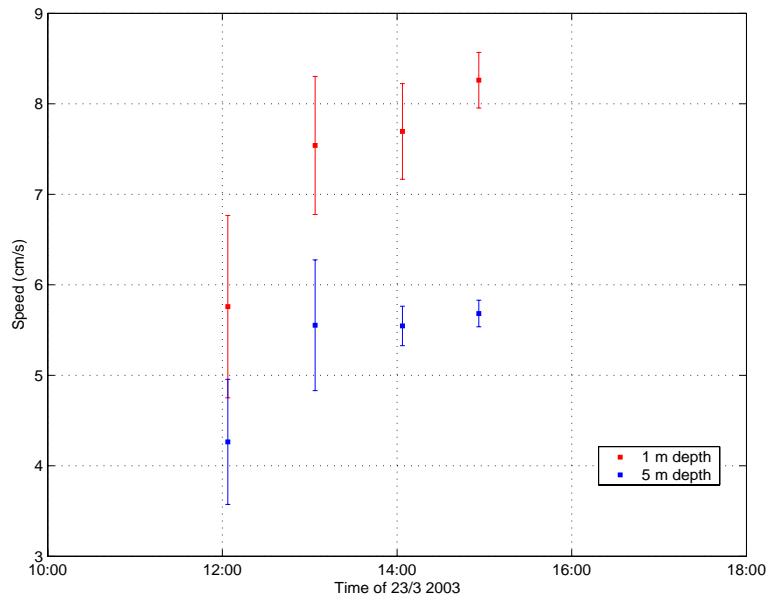
Figure 5.5 Horizontal speeds measured at station 2 at 1 m and 5 m depth. Error bars are ±1 standard deviation and data are averaged over 1 hour.
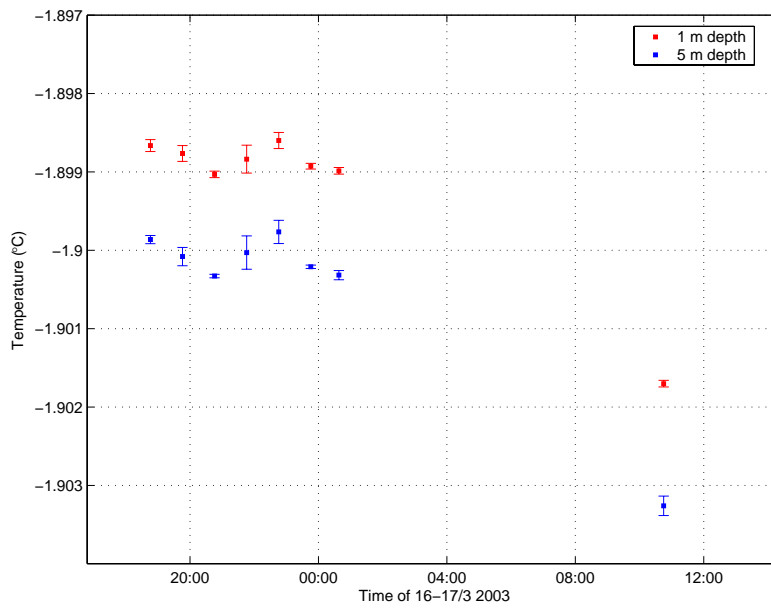

Figure 5.6 Temperatures measured with the turbulence mast at station 1, data are averaged over 1 hour. Error bars indicate ±1 standard deviation
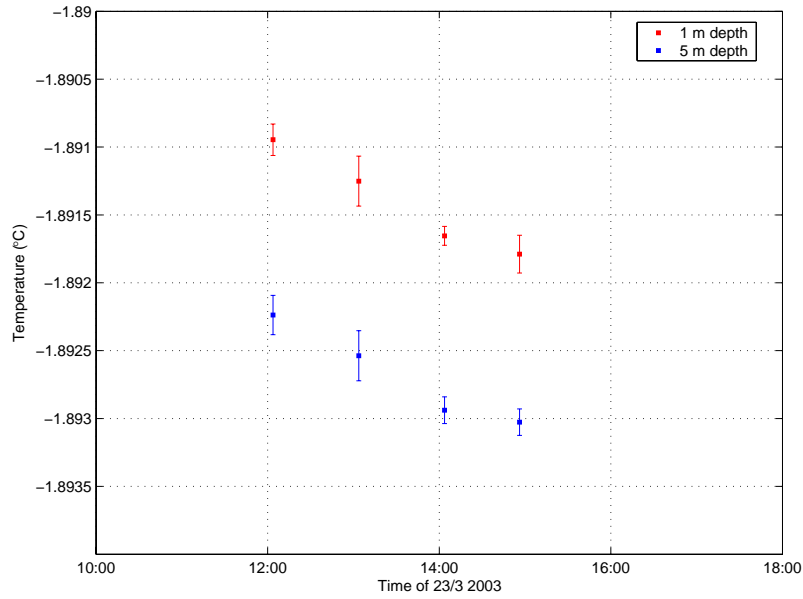
Figure 5.7 Water temperatures at two depths at station 2, measured with the turbulence mast. Error bars are ±1 standard deviation and data are averaged over 1 hour.
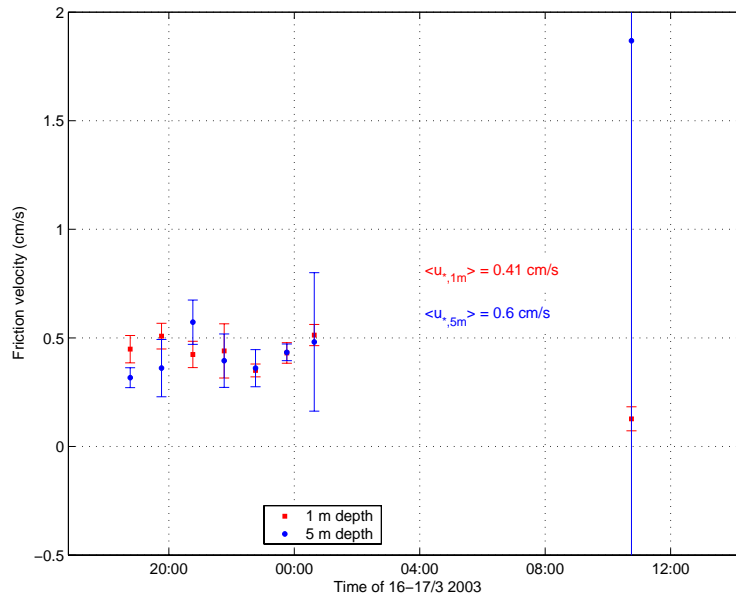

Figure 5.8 Calculated friction velocities from the data at station 1. Values are 1 hour averages and the error bars indicate ±1 standard deviation. The standard deviation on the last value of friction velocity on 5 m depth is somehow large and therefore cut by the axes to focus on the other values.

Calculated salinity fluxes at the same station show that these fluxes are negative during most of the period and the values of the fluxes are small, the mean value is $-2.7 \cdot 10^{-6}$ psu m/s (figure 5.10). This indicates formation of new ice, but at a very small rate, and it also

indicates that the net flux of heat at the ice/ocean interface should be relatively small. If this is correct, there should also only be a small flux of conductive heat in the ice to balance the fluxes at the lower surface. Unfortunately, there are no ice cores or temperature profiles from the ice to compare with, but the ice was covered with about 15 - 20 cm of snow which can reduce the heat conduction in the ice significantly, so a small conductive heat flux in the ice can be reasonable.
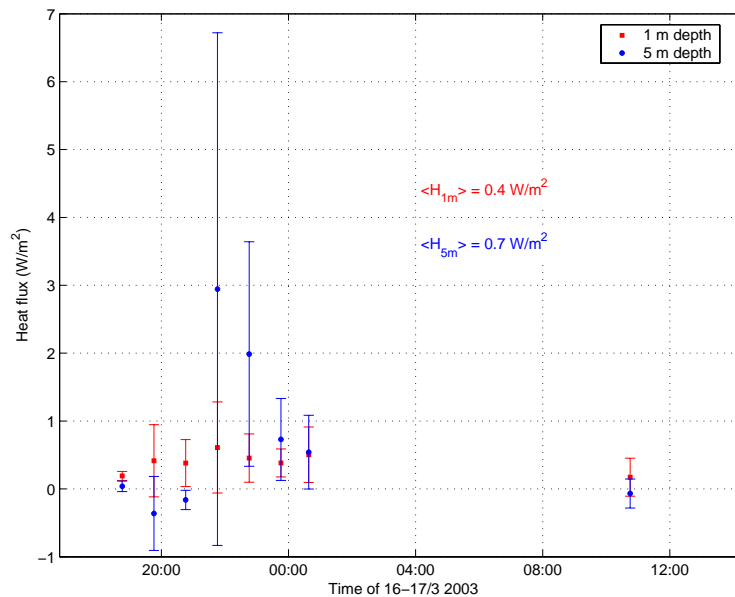

Figure 5.9 Calculated heat fluxes at two depths at station 1, values are averaged over 1 hour. Error bars indicate ±1 standard deviation.

Close to the position of the second ice station the CTD profile reveals a more homogenous water column than on the first station (figure 5.3). There are no distinct layers in the water column, neither defined by salinity or temperature, and the water column is slightly warmer (~0.02˚C) and slightly fresher (~0.15 psu) than at station 1.

Also at this station the fluctuations in measured temperatures at the turbulence mast are small, of the same order as on the first station (~10^{-4}˚C). And again the calculated heat fluxes are small; mean values are 1.0 W/m² and 0.5 W/m², measured at 1 m and 5 m depth, respectively (figure 5.11). The calculated friction velocities are also of the same order as at station 1, with a calculated mean value of 0.35 cm/s, as shown in figure 5.12.
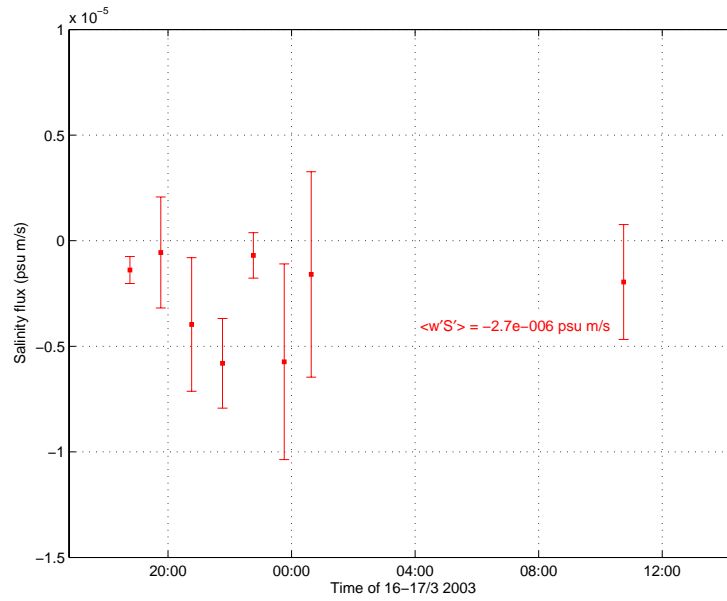
Figure 5.10 Salinity fluxes at 1 m depth, calculated from data from the turbulence mast at station 1. Values are 1 hour averages and error bars are ±1 standard deviation.

The small heat fluxes at the second station combined with a calculated salinity flux of about $-1.0 \cdot 10^{-6}$ psu m/s (figure 5.13), give hints about a similar situation as at station 1. A small salinity flux indicates a low ice formation rate, hence a small amount of latent heat is released and to conserve heat fluxes at the underside of the ice, the conductive heat flux in the ice must be small. At the station 2 location, ice and snow conditions were quite similar as at station 1, so a small heat flux in the ice can be reasonable also here.
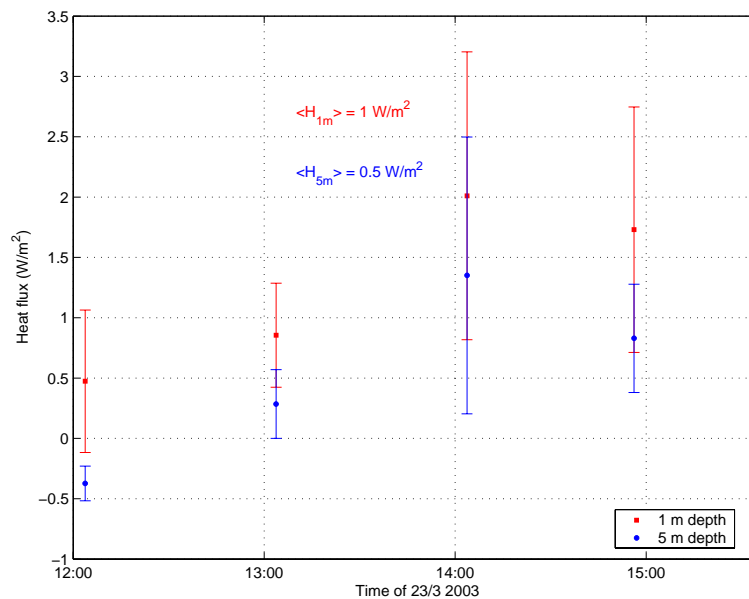

Figure 5.11 Heat fluxes at station 2, values are averaged over 1 hour. Error bars are ±1 standard deviation.
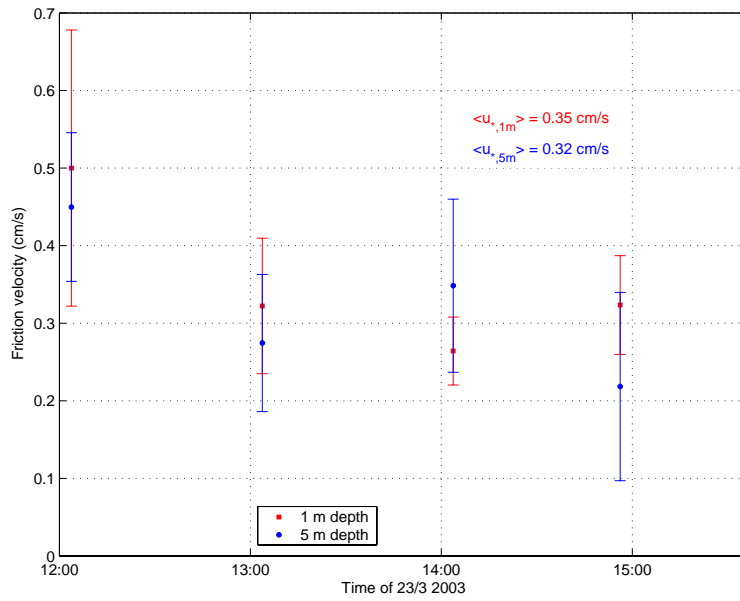
Figure 5.12 Friction velocities at two depths calculated from the turbulence mast data at station 2. Values are 1 hour averages and error bars indicate ±1 standard deviation.
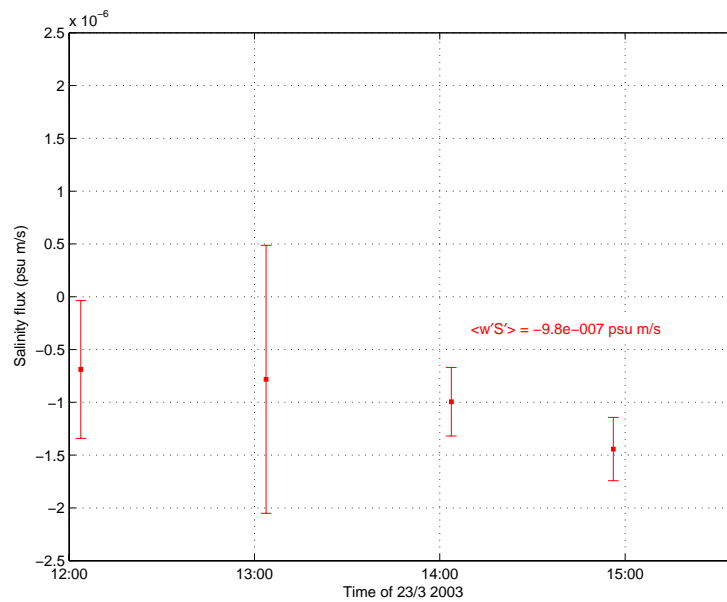

Figure 5.13 Calculated salinity fluxes at 1 m depth at station 2, data are averaged over 1 hour. Error bars are ±1 standard deviation.

Regarding the Stanton number, no such calculations are done for the Storfjorden stations. This is because the values of δT and F_w are small and close to zero and uncertainties will dominate the calculated values.

5.3 Whaler's Bay

The ice station in Whaler's Bay was carried out April 1st – April 2nd 2003. The ice in the area had a thickness of about 2 m and a lot of large ridges dominated. But in the vicinity of the ship there was an area, most likely a refrozen lead, with an ice thickness of 110 cm, in which the turbulence mast was deployed. This area had an approximate size of 100 x 50 m and was only covered by a very thin snow cover (1 – 2 cm).

In the area, the ice was drifting rapidly and the drift track during the time of the ice station is shown in figure 5.14.
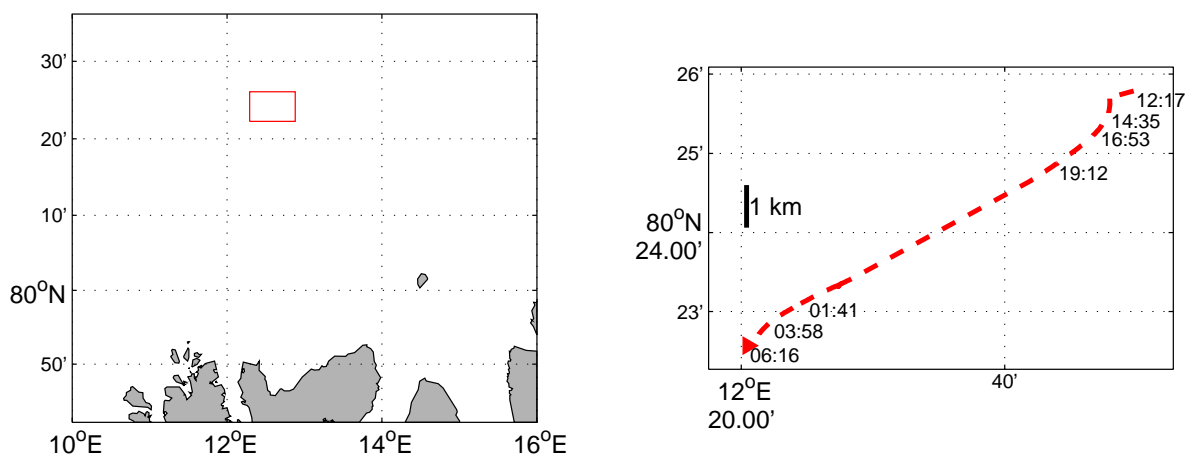

Figure 5.14 Position and drift track of the ice station in the Whaler's Bay area on April 1st and 2nd, 2003. For the location of the map section, see figure 1.1.

5.3.1 Results

A CTD profile was taken from the ship right after the end of the drift station, but the data from this profile are assumed to be representative for the area. The profile shows a 30 m thick surface layer with a mean temperature of -1.1˚C (figure 5.15). Conductivity data from the surface layer were corrupted because the conductivity sensor on the CTD was flushed with fresh water before lowered into the sea water. Salinity data are therefore not shown in figure 5.15.

Velocities and temperatures measured at this station are shown in figure 5.16 and figure 5.17. All velocity and temperature data are averaged in 15 minutes intervals and 1 hour mean values are calculated using the eddy correlation method (section 7). Mean speeds are 21.1 cm/s and 22.9 cm/s at 1 m and 5 m depth, respectively and the corresponding mean temperatures are -0.96˚C and -0.93˚C. It is worth noticing that the velocity measured at 1 m depth on March 2nd 0100 is remarkably higher than on 5 m depth. This is not corresponding to a "normal" velocity structure where the velocity is increasing from the ice boundary. It is not clear what may have caused these values.
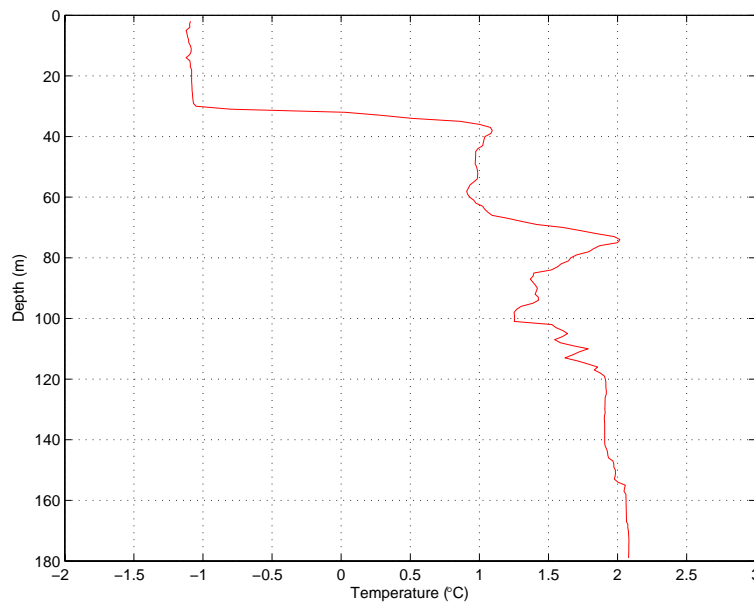
Figure 5.15 Temperature profile in the water column close to the ice station in Whaler's Bay. The CTD profile is taken on April 2nd 09:13, which is after the drift, but the data are assumed to be representative for the water column during the whole drift.

An ice core was also obtained at this station only ~5 m away from the deployment site of the turbulence mast and temperatures in the ice column were measured. Ice temperatures are shown in figure 5.18.
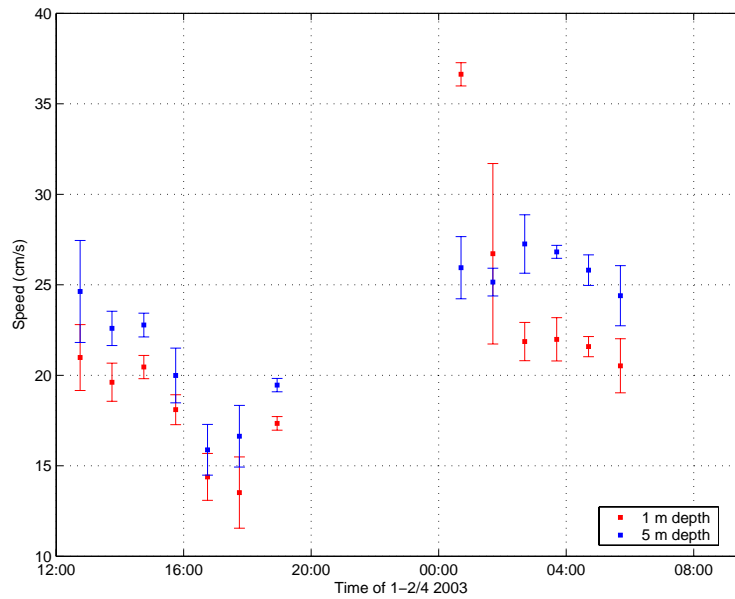
Figure 5.16 Mean horizontal speeds, measured with the turbulence mast at 1 m and 5 m depth below the ice at Whaler's Bay. Values are averaged over 1 hour and error bars indicate ±1 standard deviation.

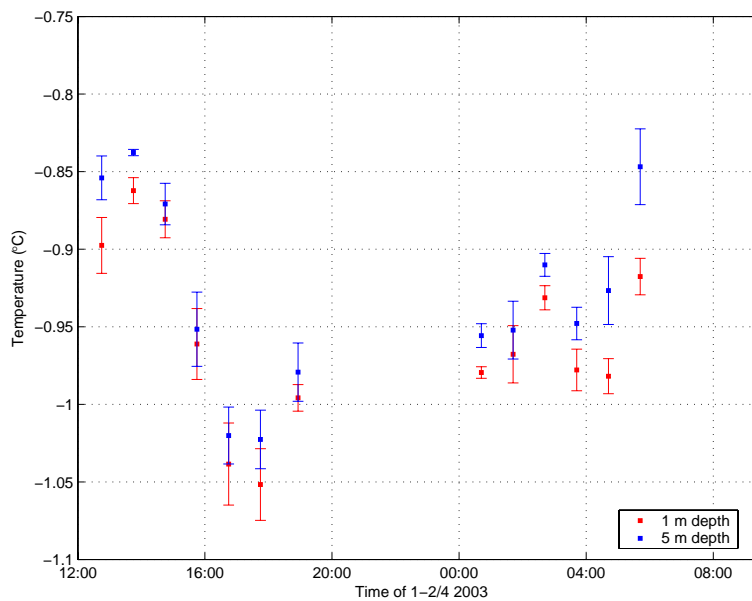**Figure 5.17** Temperatures measured with the turbulence mast in Whaler's Bay at 1 m and 5 m depth. Values are averaged over 1 hour and error bars indicate ±1 standard deviation.

5.3.2   Discussion

Data from this station differ from all the other stations in both measured velocities and temperatures. The mixed layer has a temperature about 0.8 - 1˚C above freezing which

indicates a large amount of available heat in the water column. Measurements from the turbulence mast show temperatures in the same range, but also that the measured temperatures have a standard deviation of the order 10^{-2}°C, which is for example about 50 - 100 times the standard deviations from Storfjorden and Van Mijenfjord, but of the same order as the standard deviations of the temperature measurements in Kongsfjorden.

The mixing efficiency, represented by the friction velocity, is high at the Whaler's Bay station. Calculated friction velocities have a mean value of 0.89 cm/s at 1 m depth (figure 5.19). These high values of temperature and friction velocities are also reflected in the calculated heat fluxes, as shown in figure 5.20. Mean vertical heat flux at 1 m depth is 211.9 W/m². Heat fluxes have high mean values, but also large values of standard deviations, which indicate very large fluctuations in this heat transport.

From the ice core, the temperature profile shows a more or less linear decrease in temperature towards the ice surface (figure 5.18). A linear fit to the measured temperatures results in a mean temperature gradient in the ice of -21.7°C/m which leads to a bulk conductive heat flux of 41.2 W/m², if the thermal conductivity of the ice, k_i, is set to 1.9 W /m °C. To balance these fluxes at the underside of the ice, a freezing/melting flux of -170.7 W/m² is required, which indicates a large melting rate at the underside. Using the simple formula in equation 42 with latent heat of ice calculated from ice temperature and salinity of -2°C and 4 psu, respectively, gives a melting rate of $6.2 \cdot 10^{-7}$ m/s or 5.3 cm/day.

A melting rate of this magnitude should be possible to see also in a strong positive salinity flux at the same level and calculated salinity fluxes at 1 m depth have a mean value of $1.2 \cdot 10^{-5}$ psu m/s (figure 5.21).

This magnitude is significantly larger than the salinity fluxes measured at previous stations and should come from a larger change in ice thickness. A rough calculation of melting rate from the mean salinity flux (equation 44) suggests a melting rate of $3.9 \cdot 10^{-7}$ m/s or about 3.4 cm/day. This is only a very rough calculation and the difference between the melting rate estimated from the salinity flux and the melting rate estimated from the heat budget, is quite large. But the uncertainty in both heat and salinity flux is also large, so a difference of this order is not unrealistic.
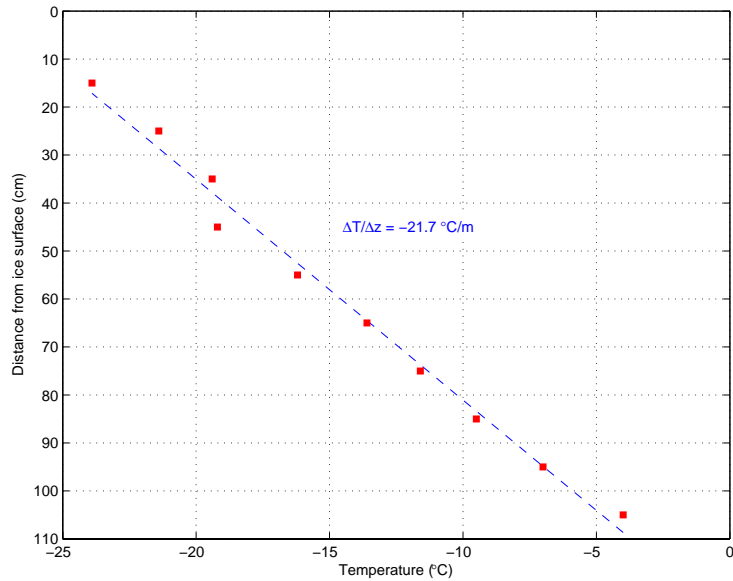
Figure 5.18 Ice temperatures at the location of the Whaler's Bay ice station, measured manually in an ice core. Red squares are measured values and the blue line is a linear fit with a mean temperature gradient of -21.7 ˚C/m.
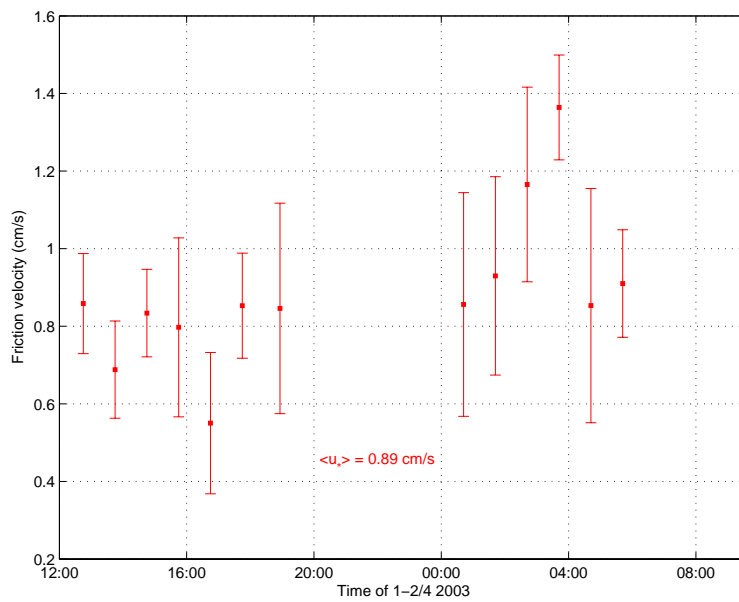
Figure 5.19 Friction velocities calculated from the data from the turbulence mast at Whaler's Bay at 1m depth. Values are averaged over 1 hour and error bars indicate ±1 standard deviation.

If temperatures and salinities from the cluster at 5 m depth on the turbulence mast are assumed to be properties of the mixed layer and the heat fluxes and friction velocities from 1 m depth are assumed to be interface values, then a Stanton number can be estimated. Using equation 19 together with the mean values at 1 m and 5 m depth, gives a mean Stanton number of 0.0061.
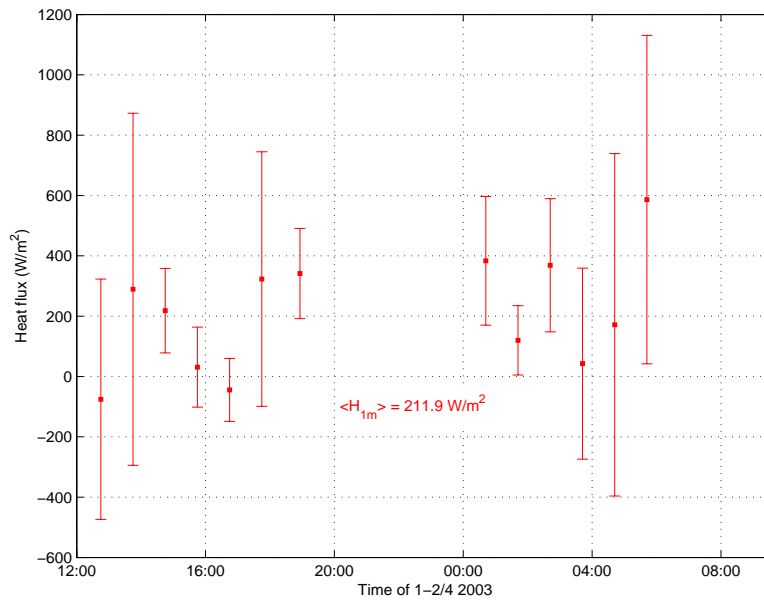
Figure 5.20 Heat fluxes calculated from the turbulence mast data at Whaler's Bay at 1 m depth. Values are averaged over 1 hour and error bars are ±1 standard deviation.
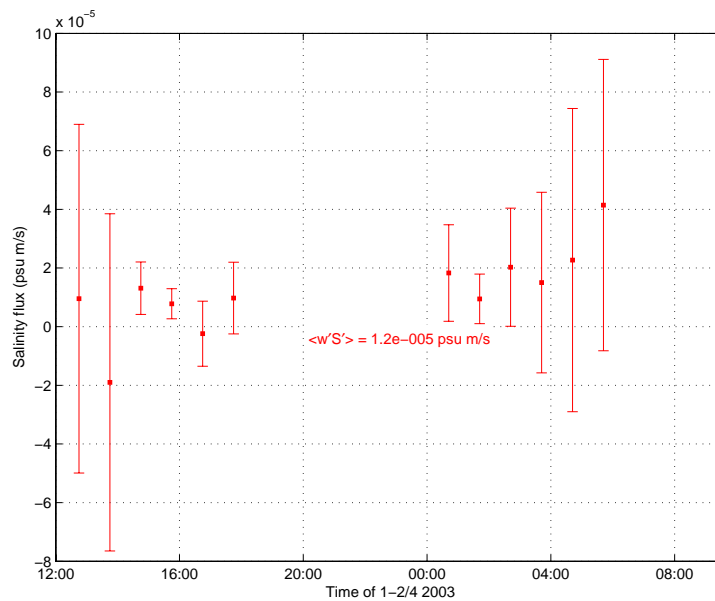
Figure 5.21 Calculated salinity fluxes at the cluster on the turbulence mast at 1 m depth. All values are averaged over 1 hour and error bars indicate ±1 standard deviation.

Compared to the fluxes presented in the previous sections from the different geographic locations, the fluxes measured at the Whaler's Bay station are extreme. But fluxes of these magnitudes are not rare; Dewey *et al.* (1999) calculated the heat loss in the WSC to be of order 100 W/m^2 due to mixing along the continental slope north-east of Spitsbergen. These

results were calculated from CTD and ADCP (Acoustic Doppler Current Profiles) measurements.

During the CEAREX (Coordinated Eastern Arctic Experiment) drift in autumn 1988 comprehensive measurements of ice properties were done (Wettlaufer, 1991). By using the residual method (section 2.2.4) in estimating the ocean heat flux, fluxes in the range $0 - 37$ W/m^2 were calculated. But these data were obtained in areas north-east of Spitsbergen, at longitudes of 30 - 35˚E.

Also Aagaard *et al.* (1987) calculated a large heat loss from the core of Atlantic Water, based on data obtained in October and November north-west of Spitsbergen. From CTD and current meter measurements they found that the vertical heat flux from the layer at $100 - 200$ m depth was 230 W/m^2, and presumably even larger from the surface layer.

Similar conditions have also been encountered in Antarctic. During some parts of the ANZFLUX experiment in 1994 (McPhee *et al.*, 1996), heat fluxes of order 100 W/m^2 were measured directly with similar TICs as on the WARPS cruise. In these periods, mixed layer temperatures of $0.4 - 0.6$˚C above freezing and friction velocities at the ice/ocean interface of $1 - 2$ cm/s were also measured and the mean Stanton number for the two drifting stations included in ANZFLUX was 0.0056 (McPhee *et al.*, 1999).

During the MIZEX (Marginal Ice Zone Experiment) drift in 1984, close to the Fram strait, the ice floe, on which the measurements were performed, drifted across a warm front in the ocean (McPhee *et al.*, 1987). During the passage of this warm front, large heat fluxes were measured with instruments similar to the WARPS turbulence mast. On one specific day in July, the mean vertical heat flux in the upper 15 m was 227 W/m^2 measured in a water column with mean temperatures about 1.5˚C above freezing (McPhee *et al.*, 1987). The mean Stanton number during MIZEX, calculated from the main part of the data, but not the periods were the temperature deviation from the freezing temperature was large, is 0.0060 (McPhee, 1992).

But McPhee *et al.* (1987) also discussed the implications of a high melt rate to the transport of heat and mass at the ice/ocean interface, and suggested that the interface transport is highly affected by the molecular exchange immediately close to the interface. Under these conditions the turbulent exchange coefficient of salt is smaller than for heat and therefore the exchange at the interface is controlled by the salt flux, not the heat flux. These effects are not discussed any further in this thesis, but they might explain some of the discrepancy between the melting rates calculated from the salinity flux and the heat flux.

80

6   Summary and conclusions

An important factor in the air/sea/ice heat budget is the ocean heat flux. In this work a complex instrumentation is used to measure these fluxes at the underside of the ice, using the ice floe itself as a stable platform for measurements. Both fjord areas and deep ocean areas have been investigated during winter, involving different conditions regarding ice and hydrography. The aim of the work has been to compare fluxes on smaller time scales and to get knowledge of the air/sea/ice interaction under different conditions.

In Kongsfjorden (section 3), where the water masses are influenced by the warm water in the WSC, ocean heat fluxes are measured in the inner part of the fjord together with other fluxes in the ice and on the upper ice surface. At the upper ice surface, heat flux comparisons show that there is a net divergence of 7.3 W/m^2 (figure 3.18). Over the whole period, this divergence in mean value is caused by inaccuracies in calculations and measurements of the atmospheric fluxes. On shorter time scales, the flux divergence/convergence at the ice surface is the result of a longer response time in the ice than in the atmosphere.

At the underside of the ice, calculated values of the conductive heat flux and ocean heat flux are used to calculate the ice growth in the field work period. From this method, the calculated ice growth was 4.4 cm, slightly larger than the measured ice growth of 3.5 cm in the same period. But the uncertainties in the measurements of the ocean heat flux and the uncertainties in the measured ice thicknesses are large, so the agreement between measured and calculated ice growth is acceptable.

In the interior of the ice, any temperature changes are determined from a divergence/convergence of conductive heat flux and absorption of short wave radiation. In Kongsfjorden, the mean temperature of the ice column is calculated from available data of ice temperatures and short wave radiation and compared with the measured temperature in the same period. The correlation between the two temperature developments is very good with a modification of the thermal conductivity of sea ice:

$$k_i = k_0 + \beta \frac{S_i}{T_i} - 0.22$$

A recent work by Trodahl *et al.* (2001) with the aim of determining the thermal conductivity of sea ice, also concluded that the calculated thermal conductivity was generally ~10% lower

than assumed by most models. This result agrees very well with the result of the temperature calculation in Kongsfjorden.

In Van Mijenfjorden (section 4), the conditions were different, with small amounts of available heat in the water column and thick, snow covered ice. Measured ocean heat fluxes here are small, but comparisons with measured salinity fluxes and other available measurements show that these heat fluxes are of the right order and that the method for heat flux measurements is reliable.

Storfjorden (section 5) can offer the same conditions as in Van Mijenfjorden, except that the ice is drifting instead of being land fast. Also here, small heat and salinity fluxes were measured, corresponding well with the "physical" environment with small amounts of heat available.

In the Whaler's Bay area (section 5), warm water enters the relatively shallow continental slope areas. This area is dominated by large amounts of heat in the water column, high current velocities and large fluxes of heat leading to large rates of ice melting. This is confirmed by the measurements in the area where the mean ocean heat flux 1 m below the ice is about 211.9 W/m^2. Comparing these measurements with measurements of the conductive heat flux in the ice and measurements of the salinity flux under the ice, show a reasonable agreement. The melting of sea ice calculated from the measured salinity flux was 3.4 cm/day, about 2 cm/day less than 5.3 cm/day as calculated from the heat budget at the ice/ocean interface. But this is within the uncertainties taking the large variability in both heat flux and salinity flux measurements into account.

Similar large values of ocean heat flux have been reported from this area before. Both Dewey *et al.* (1999) and Aagaard *et al.* (1987) calculated a heat loss in the range 100 – 200 W/m^2 from the core of Atlantic Water in the WSC north-west and north-east of Spitsbergen. Other drifting experiments such as MIZEX in the marginal ice zone in the Fram Strait (McPhee *et al.*, 1987) and ANZFLUX in Antarctic (McPhee *et al.*, 1996) where similar instrumentation as on the WARPS cruise were used, have given calculated heat fluxes similar to the results in Whaler's Bay.

The values of calculated heat fluxes from the different areas are compared to a Stanton number parameterization, which relates the turbulent heat flux to the mixed layer temperature

above freezing and the friction velocity at the ice/ocean interface. In table 6.1 these values for the work in Kongsfjorden, Van Mijenfjorden and Whaler's Bay are presented.

Table 6.1 Temperatures above freezing in the mixed layer (δT), friction velocities at the ice/ocean interface (u_*), turbulent heat flux (F_w) and the Stanton number (c_H) for three different locations around Spitsbergen.

	δT (°C)	u_* (cm/s)	F_w (W/m²)	c_H
Kongsfjorden	0.30	0.15	12.7	0.0069
Van Mijenfjorden	0.01	0.34	0.9	0.0065
Whaler's Bay	0.96	0.89	211.9	0.0061

Although the calculations presented in table 6.1 are rough, the Stanton numbers are comparable to Stanton numbers calculated for other experiments. McPhee *et al.* (1999) summarized data from the four drifting experiments MIZEX, CEAREX -88, CEAREX -89 and ANZFLUX and presented Stanton numbers in the range $0.0050 - 0.0060$. The near constant c_H presented in table 6.1 together with the magnitudes of c_H presented in McPhee *et al.* (1999) are important results for numerical models. With mixed layer temperature and friction velocity given from the model state variables, use of a constant c_H should ensure a realistic modelled ocean heat flux in a wide range of situations

The methods for measuring and calculating the turbulent heat fluxes presented in this thesis have proved to give reliable results compared to other measurements. Also the methods for calculating the heat budget of an air/sea/ice system as in Kongsfjorden give acceptable results when the fluxes at the different interfaces are compared to each other. To perform this heat flux comparison in such a system, measurements of ice temperatures, air temperature, wind and humidity and measurements of the turbulent fluctuations in temperature and velocity at the ice underside are necessary. If, in addition, direct measurements of short wave and long wave radiation are available, it is possible to set up a reliable budget for the heat exchange between ocean, ice and atmosphere.

Future work
For future work, longer time series of the measured turbulent fluxes would be an advantage. This is first of all to even out some of the events which occur on shorter time scales, but also

to get more statistically "solid" results. Longer time series with more representative mean values would also be interesting in other aspects, such as numerical modelling. To improve the calculated heat budgets, more comprehensive data are needed and especially a more thorough investigation of ice properties and time series of ice temperatures are important. These investigations would be helpful, not only in setting up a heat budget at a given location, but also as a validation of the measured turbulent fluxes.

Heat fluxes included in the air/sea/ice budget vary over a wide range during the winter season, from early winter freezing conditions to late spring melting. If the measurements done in Kongsfjorden were performed at different stages in the seasonal cycle, it would give valuable insight in how the ratio between the fluxes and the importance of each flux, change during winter.

7   Appendix: Eddy correlation method

Velocity data from the turbulent masts are grouped in 15 minutes long intervals. The 15 minutes interval is longer than the typical time scale of the energy containing eddies, which is typically $1 - 5$ minutes (McPhee *et al.*, 1987), and smaller than other phenomena with longer time scales/lower wave numbers (McPhee, 1992).

Within each 15 minutes interval, the velocities are rotated into a moving reference frame so that the mean vertical velocity and mean cross-stream velocity vanishes, $\langle \vec{v} \rangle = \langle \vec{w} \rangle = \vec{0}$. In the 15 minutes interval, also the mean values of temperature and salinity are removed and the covariances of w'T' and w'S' are calculated. The 15 minutes values are then averaged over a time period of 1 hour or more to get representative values of the turbulent fluxes.

A sample of the method is shown in figure 7.1 where 15 minutes intervals of vertical velocity and temperature from the field work in Kongsfjorden are shown together with the calculation of the w'T' covariance.
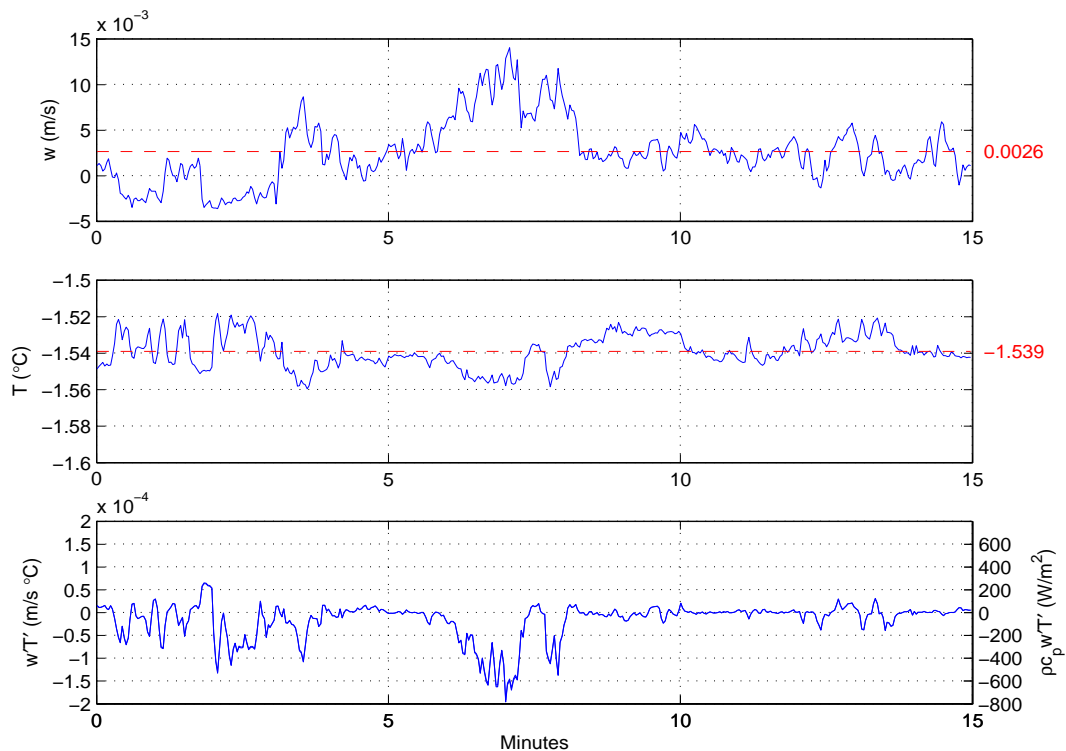

Figure 7.1 A 15 min data sample from the field work in Kongsfjorden. The two upper most panels show the turbulent fluctuations of vertical velocity and temperature 1 m below the ice. The lower panel shows the covariance of w'T' and the heat flux.

Bibliography

Andreas, E.L., A Theory for the Scalar Roughness and the Scalar Transfer- Coefficients over Snow and Sea Ice, *Boundary-Layer Meteorology*, *38* (1-2), 159-184, 1987.

Coachman, L.K., and C.A. Barnes, The movement of Atlantic Water in the Arctic Ocean, *Arctic*, *16*, 8-16, 1963.

Dewey, R., R. Muench, and J. Gunn, Mixing and vertical heat flux estimates in the Arctic Eurasian Basin, *Journal of Marine Systems*, *21* (1-4), 199-205, 1999.

Doronin, Y.P., and D.E. Kheisin, *Sea Ice*, 323 pp., Amerind Publ. Co., New Dehli, 1977.

Ebert, E.E., and J.A. Curry, An Intermediate One-Dimensional Thermodynamic Sea-Ice Model for Investigating Ice-Atmosphere Interactions, *Journal of Geophysical Research-Oceans*, *98* (C6), 10085-10109, 1993.

Ebert, E.E., J.L. Schramm, and J.A. Curry, Disposition of Solar-Radiation in Sea-Ice and the Upper Ocean, *Journal of Geophysical Research-Oceans*, *100* (C8), 15965-15975, 1995.

Førland, E.J., I. Hansen-Bauer, and P.Ø. Nordli, Climate statistics & longterm series of temperature and precipitation at Svalbard and Jan Mayen, *DNMI report, 21/97 klima*, 1997.

Gade, H.G., *Turbulens og turbulent diffusjon i sjø og hav*, Geophysical Institute, University of Bergen, 1996.

Gade, H.G., and A. Edwards, Deep water renewal in fjords, in *Fjord Oceanography*, edited by H.J. Freeland, D.M. Farmer, and C.D. Levings, 1980.

Gerland, S., J.G. Winther, J.B. Orbaek, and B.V. Ivanov, Physical properties, spectral reflectance and thickness development of first year fast ice in Kongsfjorden, Svalbard, *Polar Research*, *18* (2), 275-282, 1999.

Grenfell, T.C., The effects of ice thickness on the exchange of solar radiation over the polar oceans, *Journal of Glaciology*, *22* (87), 305-320, 1979.

Hinze, J.O., *Turbulence*, 586 pp., McGraw-Hill, New York, 1959.

Holland, M.M., J.A. Curry, and J.L. Schramm, Modeling the thermodynamics of a sea ice thickness distribution 2. Sea ice/ocean interactions, *Journal of Geophysical Research-Oceans*, *102* (C10), 23093-23107, 1997.

Haarpaintner, J., J.C. Gascard, and P.M. Haugan, Ice production and brine formation in Storfjorden, Svalbard, *Journal of Geophysical Research-Oceans*, *106* (C7), 14001-14013, 2001.

Kangas, T.-V., Thermohaline sesongvariasjoner i Van Mijenfjorden, Master thesis, University of Bergen, 2000.

Kolmogorov, A.N., On degeneration (decay) of isotropic turbulence in an incompressible viscous liquid., *Dokl. Nauk. SSSR*, *31*, 538-540, 1941.

Leavitt, E., Surface Drag Coefficient Dependence on Aerodynamic Roughness of Sea - Reply, *Journal of Geophysical Research-Oceans and Atmospheres*, *81* (27), 4995-4995, 1976.

Loeng, H., Features of the Physical Oceanographic Conditions of the Barents Sea, *Polar Research*, *10* (1), 5-18, 1991.

Louis, J.F., Parametric Model of Vertical Eddy Fluxes in the Atmosphere, *Boundary-Layer Meteorology*, *17* (2), 187-202, 1979.

Massom, R.A., H. Eicken, C. Haas, M.O. Jeffries, M.R. Drinkwater, M. Sturm, A.P. Worby, X.R. Wu, V.I. Lytle, S. Ushio, K. Morris, P.A. Reid, S.G. Warren, and I. Allison, Snow on Antarctic Sea ice, *Reviews of Geophysics*, *39* (3), 413-445, 2001.

Maykut, G.A., The surface heat and mass balance, in *The geophysics of sea ice*, edited by N. Untersteiner, pp. 395-463, Plenum press, New York, 1986.

Maykut, G.A., and P.E. Church, Radiation Climate of Barrow, Alaska, 1962-66, *Journal of Applied Meteorology*, *12*, 620-628, 1973.

Maykut, G.A., and N. Untersteiner, Some Results from a Time-Dependent Thermodynamic Model of Sea Ice, *Journal of Geophysical Research*, *76* (6), 1550-1575, 1971.

McClimans, T.A., Energetics of Tidal Inlets to Landlocked Fjords, *Marine Science Communications*, *4* (2), 121-137, 1978.

McGuinness, M.J., H.J. Trodahl, K. Collins, and T.G. Haskell, Non-linear thermal transport and brine convection in first-year sea ice, in *Annals of Glaciology, Vol 27, 1998*, pp. 471-476, 1998.

McPhee, M., Small-scale processes, in *Polar Oceanography*, edited by W. Smith, pp. 287-334, Academic Press, San Diego, 1990.

McPhee, M.G., A Time-Dependent Model for Turbulent Transfer in a Stratified Oceanic Boundary-Layer, *Journal of Geophysical Research-Oceans*, *92* (C7), 6977-6986, 1987.

McPhee, M.G., Turbulent Heat-Flux in the Upper Ocean under Sea Ice, *Journal of Geophysical Research-Oceans*, *97* (C4), 5365-5379, 1992.

McPhee, M.G., S.F. Ackley, P. Guest, B.A. Huber, D.G. Martinson, J.H. Morison, R.D. Muench, L. Padman, and T.P. Stanton, The Antarctic Zone Flux Experiment, *Bulletin of the American Meteorological Society*, *77* (6), 1221-1232, 1996.

McPhee, M.G., C. Kottmeier, and J.H. Morison, Ocean heat flux in the central Weddell Sea during winter, *Journal of Physical Oceanography*, *29* (6), 1166-1179, 1999.

McPhee, M.G., G.A. Maykut, and J.H. Morison, Dynamics and Thermodynamics of the Ice Upper Ocean System in the Marginal Ice-Zone of the Greenland Sea, *Journal of Geophysical Research-Oceans*, *92* (C7), 7017-7031, 1987.

McPhee, M.G., and T.P. Stanton, Turbulence in the statically unstable oceanic boundary layer under Arctic leads, *Journal of Geophysical Research-Oceans*, *101* (C3), 6409-6428, 1996.

Meincke, J., B. Rudels, and H.J. Friedrich, The Arctic ocean Nordic seas thermohaline system, *Ices Journal of Marine Science*, *54* (3), 283-299, 1997.

Midttun, L., Formation of Dense Bottom Water in the Barents Sea, *Deep-Sea Research Part a-Oceanographic Research Papers*, *32* (10), 1233-1241, 1985.

Nilsen, F., Measurements in Van Mijenfjorden March-April 2001, Student report AGF-211, Air-Sea-Ice interaction, University Courses on Svalbard, 2001.

Nilsen, F., Measurements in Van Mijenfjorden March-April 2002, Student report AGF-211, Air-Sea-Ice Interaction, University Courses on Svalbard, 2002.

Omstedt, A., and J.S. Wettlaufer, Ice Growth and Oceanic Heat-Flux - Models and Measurements, *Journal of Geophysical Research-Oceans*, *97* (C6), 9383-9390, 1992.

Ono, N., Thermal properties of sea ice. II. A method for determining the K/c value of a non-homogeneous ice sheet, *Low Temp. Sci. J.*, *A23*, 177-183, 1965.

Ono, N., Specific Heat and Heat of Fusion of Sea Ice, in *Physics of Snow and Ice*, edited by H. Oura, pp. 599-610, Inst. Low Temp. Sci., Hokkaido Univ., Sapporo, 1967.

Ono, N., Thermal properties of sea ice. IV. Thermal constants of sea ice., *Low Temp. Sci. J.*, *A26*, 329-349, 1968.

Perovich, D.K., C.S. Roesler, and W.S. Pegau, Variability in Arctic sea ice optical properties, *Journal of Geophysical Research*, *103* (C1), 1193-1208, 1998.

Quadfasel, D., B. Rudels, and K. Kurz, Outflow of Dense Water from a Svalbard Fjord into the Fram Strait, *Deep-Sea Research Part a-Oceanographic Research Papers*, *35* (7), 1143-1150, 1988.

Schauer, U., and E. Fahrbach, A dense bottom water plume in the western Barents Sea: downstream modification and interannual variability, *Deep-Sea Research Part I-Oceanographic Research Papers*, *46* (12), 2095-2108, 1999.

Shirasawa, K., and R.G. Ingram, Currents and turbulent fluxes under the first-year sea ice in Resolute Passage, Northwest Territories, Canada, *Journal of Marine Systems*, *11* (1-2), 21-32, 1997.

Shirasawa, K., R.G. Ingram, and E.J.J. Hudier, Oceanic heat fluxes under thin sea ice in Saroma-ko Lagoon, Hokkaido, Japan, *Journal of Marine Systems*, *11* (1-2), 9-19, 1997.

Sirevaag, A., Report from field work in Kongsfjorden, West Spitsbergen 9th to 18th March 2002, Geophysical Institute, University of Bergen, 2002.

Svendsen, H., A. Beszczynska-Moller, J.O. Hagen, B. Lefauconnier, V. Tverberg, S. Gerland, J.B. Orbaek, K. Bischof, C. Papucci, M. Zajaczkowski, R. Azzolini, O. Bruland, C. Wiencke, J.G. Winther, and W. Dallmann, The physical environment of Kongsfjorden-Krossfjorden, an Arctic fjord system in Svalbard, *Polar Research*, *21* (1), 133-166, 2002.

Tennekes, H., and J.L. Lumley, *A first course in turbulence*, MIT press, 1972.

Trodahl, H.J., S.O.F. Wilkinson, M.J. McGuinnes, and T.G. Haskell, Thermal Conductivity of Sea Ice; Dependence on Temperature and Depth, *Geophysical Research Letters*, *28* (7), 1279-1282, 2001.

Untersteiner, N., On the mass and heat budget of arctic sea ice, *Arch. Met. Geophys. Bioklim.*, *A* (12), 151-182, 1961.

Wadhams, P., *Ice in the ocean*, 351 pp., Gordon and breach science publishers, 2000.

Weeks, W.F., and S.F. Ackley, The growth, structure and properties of sea ice, in *The geophysics of sea ice*, edited by N. Untersteiner, pp. 9-164, Plenum, New York, 1986.

Wettlaufer, J.S., Heat Flux at the Ice-Ocean Interface, *Journal of Geophysical Research*, *96* (C4), 7215-7236, 1991.

Wettlaufer, J.S., N. Untersteiner, and R. Colony, Estimating oceanic heat flux from sea-ice thickness and temperature data, *Annals of Glaciology*, *14*, 315-318, 1990.

Yaglom, A.M., and B.A. Kader, Heat and Mass-Transfer between a Rough Wall and Turbulent Fluid-Flow at High Reynolds and Peclet Numbers, *Journal of Fluid Mechanics*, *62* (FEB11), 601-623, 1974.

Yen, Y.C., Review of thermal properties of snow, ice and sea ice, pp. 27, US Army Cold Regions Res. & Engng. Lab., Hanover N.H., 1981.

Aagaard, K., A. Foldvik, and S.R. Hillman, The West Spitsbergen Current - Disposition and Water Mass Transformation, *Journal of Geophysical Research-Oceans*, *92* (C4), 3778-3784, 1987.